Development of a Finite Element Based Nominal Stress Extraction Procedure for Fatigue Analysis of Welded Structures

Alewyn Petrus Grové

Submitted in partial fulfilment of the requirements for the degree:

Master of Engineering

Department of Mechanical and Aeronautical Engineering

University of Pretoria

September 2006

Development of a Finite Element Based Nominal Stress Extraction Procedure for Fatigue Analysis of Welded Structures

Alewyn Petrus Grové

Department of Mechanical and Aeronautical Engineering, University of Pretoria

Study Leaders: Mr. F. van Tonder
Prof. P.S. Heyns

Degree: Master of Engineering

Abstract

The implementation of finite element methods (FEM) for fatigue analysis of complex structures in industry are becoming an increasingly effective and accepted practice. In the case of large plate-like structures, such as Load Haul Dumper (LHD) equipment, constructional frames and supports in plants and heavy vehicle trailers to name but a few, modeling can take place by implementation of either two dimensional shell elements or three dimensional solid elements.

It is, however, not clear which shell element modeling procedure is the most realistic. Solid elements are accepted to give the closest resemblance since the element itself is the closest to reality in terms of geometry and also due to the fact that it is a three dimensional element. Due to economical and practical considerations, however, shell elements are used in industry - especially in large, plate-like structures. Another primary source of uncertainty lies with the definition of nominal stress in complex structures and the correct determination and extraction thereof from finite element obtained stress distributions. This situation occurs as a consequence of the absence of clear and distinct guidelines in the nominal stress based fatigue design codes such as BS 7608:1993; ECCS 6: 1985 and IIW XIII-1965-03 on weld modeling and nominal stress extraction procedures in conjunction with FEM. Explicit guidelines for finite element modeling and fatigue relevant stress determination do exist in the IIW fatigue

design recommendations on top of the nominal stress guidelines, but focus primarily on the implementation of the hot spot stress fatigue assessment procedures.

This dissertation consequently entails the development of a nominal stress extraction procedure for fatigue design and analysis of plate-like structures, utilizing shell elements. Firstly, the integrity of shell elements as concerned with the accurate capturing of the stiffness properties and stress distribution in the vicinity of welds are investigated, with the aim of establishing a set of guidelines and recommendations for the correct meshing and modeling procedure of welds in plate-like structures. Secondly, an extensive numerical investigation into the stress concentration characteristics of various T-piece and stiffener configurations is performed, resulting in a nominal stress extraction procedure.

The developed methodology is applied on a complex plate-like structure for verification purposes. The structure is modeled by means of a finite element model, compiled according to the meshing recommendations developed. The stress distribution due to static loading is investigated and compared with measured values. Furthermore, the stress response of the structure due to stochastic dynamic loading is investigated and also validated in terms of the suitability for assessment by static equivalent design criteria, in particular the Fatigue Equivalent Static Load (FESL) methodology. A nominal stress and hot spot stress fatigue life prediction under stochastic loading is made, based on measured stresses in conjunction with the developed stress extraction methodology and the IIW guidelines respectively. Furthermore the finite element stresses are implemented in conjunction with the FESL procedure to repeat the nominal stress and hot spot stress life predictions. The viability and integrity of the FESL methodology is also critically assessed. The actual fatigue life of the structure under the particular loading characteristics is then determined and compared to the predicted lives.

Ontwikkeling van ’n Eindige Element Gebaseerde Nominale Spanningsonttrekkingsprosedure vir Vermoeidheidsanalise van Gesweisde Strukture

Alewyn Petrus Grové

Departement Meganiese en Lugvaartkundige Ingenieurswese,
Universiteit van Pretoria

Studieleiers: Mnr. F. van Tonder
Prof. P.S. Heyns

Graad: Magister in Ingenieurswese

Opsomming

Die implementering van eindige element metodes (EEM) vir vermoeidheidsanalise van komplekse strukture in die industrie is besig om ’n toenemend effektiewe en aanvaarde praktyk te word. In die geval van groot plaatagtige strukture, soos laaigrawe, skeptoerusting, strukture en installasies in aanlegte en swaarvoertuigsleepwaens, kan modellering in die vorm van twee-dimensionele dopelemente of drie-dimensionele soliede elemente geskied.

Dit is egter nie duidelik watter tipe dopelement modelleringsprosedure die mees realistiese resultate gee nie. Soliede elemente word algemeen aanvaar om die beste ooreenkoms met die werklike spanningsvelde te gee aangesien dit die mees realistiese element in terme van geometrie is en ook a.g.v. die feit dat dit drie-dimensioneel van aard is. As gevolg van ekonomiese en praktiese oorwegings word dopelemente egter meer algemeen in die industrie gebruik, vernaam in groot, plaatagtige strukture. ’n Verdere prominente bron van onsekerheid berus by die definisie van nominale spanning in komplekse strukture en die korrekte bepaling en onttrekking daarvan vanuit spanningsvelde wat d.m.v die eindige element metode bepaal is. Die situasie is ’n direkte gevolg van die afwesigheid van duidelike en spesifieke riglyne in die nominale spannings-gebaseerde vermoeidheids-ontwerpkodes soos BS 7608:1993; ECCS 6: 1985 en IIW XIII-1965-03 oor sweisnaatmodellering en nominale spannings

onttrekkingsprosedures, in aansluiting met EEM. Eksplisiete riglyne vir eindige element modellering en die bepaling van vermoeidheidsrelevante spannings bestaan egter in die IIW vermoeidheidsontwerpriglyne, afgesien van die normale nominale spanningsriglyne. Dit fokus egter primêr op die implementering van die sogenaamde "hot spot" spanning vermoeidheidsassessering prosedures.

Hierdie verhandeling handel vervolgens oor die ontwikkeling van 'n nominale spanningsbepalingsprosedure vir vermoeidheidsontwerp en analise van plaatagtige strukture deur die implementering van dopelemente. Eerstens word die integriteit van dopelemente met betrekking tot akkurate bepaling van die styfheidseienskappe en spanningsverdelings in die omgewing van sweisnate ondersoek, met die doel om 'n versameling riglyne en aanbevelings vir die korrekte modellering en maasimplementering van sweisnate in plaatagtige strukture daar te stel. Tweedens word 'n breedvoerige numeriese ondersoek na die spanningskonsentrasie eienskappe van verskeie T-stuk en plaatverstywer konfigurasies geloods. Die gevolg daarvan is 'n nominale spanningsonttrekingsprosedure.

Die gevolglike metodologie vind dan toepassing op 'n komplekse plaatagtige struktuur vir verifiëringsdoeleindes. Die struktuur word vervolgens gemodelleer met behulp van 'n eindige element model wat saamgestel is volgens die ontwikkelde maastegniek en aanbevelings. Die spanningsverdeling as gevolg van statiese belasting word ondersoek en vergelyk met gemete waardes. Verder word die spanningsresponsie van die struktuur as gevolg van stogastiese dinamiese belasting ondersoek in terme van die geldigheid vir assesering deur middel van staties ekwivalente ontwerpskriteria; in besonder die Vermoeidheids Ekwivalente Statiese Belasting (VESB) metodologie. 'n Nominale spanning en kritieke punt (*hot spot*) spanning vermoeidheidslewe voorspelling onder stogastiese balasting word gemaak na aanleideing van gemete spannings, die implementering van die spanningsbepalings metodologie en die IIW riglyne onderskeidelik. Verder word die EEM spannings, in aansluiting met die VESB prosedure gebruik om die leeftydsvoorspellings te herhaal. Die geldigheid en integriteit van die VESB metodologie word ook krities geassesseer. Die werklike vermoeidheidslewe van die struktuur onder die spesifieke belastingstoestande word dan bepaal en vergelyk met die voorspelde leeftye.

Erkennings

Ek betuig graag my dank aan die volgende persone en instansies vir hulle insette in hierdie verhandeling:

- My direkte studieleier, Mnr. Francois Van Tonder vir die akademiese en tegniese leiding en ondersteuning wat hy deurgaans aan my verleen het.

- My oorhoofse studieleier, Prof. P.S. Heyns vir die oorhoofse leiding en korrespondensie met die belanghebbende partye.

- Mnr. Frans Windell vir tegniese hulp in die SASOL Laboratorium vir Struktuurmeganika met toetswerk en instrumentasie.

- Mnr. Danie Drent vir tegniese raad en advies met toetswerk en prosedures in die SASOL Laboratorium vir Struktuurmeganika.

- Mnre. Jan Brand, Willem Ras en At du Preez vir hulp en bystand met die vervaardiging van toetsmonsters.

- Mnr. Jimmy Mokhafela vir diverse hulp in die SASOL Laboratorium.

- Die NRF vir gedeeltelike befondsing van die projek.

- Anglo Gold vir gedeeltelike befondsing van die projek.

- My ouers, Alewyn en Christilda Grové vir hulle deurlopende ondersteuning en liefde.

Contents

List of Symbols

A	Cross sectional area
C_0	Constant relating to average logS_r - log$N$ curve
C_d	Constant relating to design logS_r - log$N$ curve
D	Fatigue damage parameter
D_e	Damage caused by an equivalent stress range
$D_{longitudinal}$	Damage caused by a longitudinal stress range
$D_{principal}$	Damage caused by a principal stress range
E	Young's modulus
F_b	Bending force
F_t	Tensile force
K	Gauge factor
L	Weld leg length
l	Length
m	Inverse slope of logS_r - log$N$ curve
N	Number of cycles to failure
N_e	Number of cycles to failure under equivalent stress range
N_i	No. of cycles to failure for a discrete stress range
n_i	No. of cycles completed under a discrete stress range
R	Strain gauge resistance
R_p	Shunt resistance
t	Plate thickness
V_{shunt}	Voltage disturbance due to shunt resistor
x	Distance from weld toe
$\varepsilon_{measured}$	Total measured strain
ε_x	Strain in x-direction
ε_y	Strain in y-direction
ε_z	Strain in z-direction
$\varepsilon_{1\text{-}4}$	Strain contribution of particular measuring grid
ε^*	Theoretical total bridge strain
σ_{hs}	Hot spot stress
σ_{gload}	Stress due to an inertial load of 1g

σ_{hs_prins}	Hot spot stress based on principal stress
σ_n	Nominal stress, general
σ_{nom}	Calculated nominal stress
σ_{nom_prins}	Nominal stress based on principal stress
σ_x	Stress in x-direction
σ_{x_nom}	Nominal longitudinal stress
σ_y	Stress in y-direction
σ_z	Stress in z-direction
σ_1	First principal stress
σ_2	Second principal stress
$\Delta\sigma_e$	Fatigue equivalent stress range
$\Delta\sigma_i$	Discrete stress range
$\Delta\sigma_{measured\_e}$	Fatigue equivalent measured stress range
τ_{xz}	Shear stress in x-z plane
υ	Poisson's ratio

List of abbreviations

AM	Area Method
ANSI	American National Standards Institute
AWS	American Welding Society
BEM	Boundary Element Method
BSI	British Standards Institute
CMM	Crack Modeling Method
CEN	European Committee for Standardization
DOT	Degree of Tension
ECCS	European Convention for Structural Steelwork
FAT	Fatigue Class
FEA	Finite Element Analysis
FEM	Finite Element Method
FESL	Fatigue Equivalent Static Load
HAZ	Heat Affected Zone
IIW	International Institute of Welding
ISO	International Standards Organization
ISSC	International Ships & Offshore Struct. Congress
MPC	Multi Point Constraint
N-LSP	Non-Linear Stress Peak
N-LSR	Non-Linear Stress Rise
NSCF	Notch Stress Concentration Factor
N-SIF	Notch-Stress Intensity Factor
PSD	Power Spectral Density
S-N	Stress-Life

Chapter 1

1. Introduction and literature survey

1.1 Introduction

Fatigue of metals is a very complex phenomenon, which is still not fully understood and is also the topic of much active research. It can be defined as the failure of a component or material subjected to cyclic loads of which the resulting stresses are well under the yield or tensile strength of the particular material. There are mainly three stages in normal fatigue failure namely crack initiation, crack propagation and instantaneous failure. The damage of the material starts in the crystalline structure and becomes visible in a later stage by plastic deformation, formation of micro cracks on slip bands, coalescence of micro cracks and finally propagation of a main crack. Many influence factors complicate the process while the effect of these influence factors and the behavior of different materials under these factors has been and still is extensively studied.

The fatigue failure of welded joints are even more complicated. Welding is defined by the American Welding Society as a localized coalescence of metals or non-metals produced by either heating the materials to a suitable temperature with or without the application of pressure, or by the application of pressure alone, with or without the use of filler metal. As can be deduced by contemplation of the welding process, welding strongly affects the material by the process of heating and subsequent cooling as well as by the fusion process with additional filler material. This results in inhomogeneous material properties in the vicinity of the weld, which is termed the heat-affected zone (HAZ). The other influence factors result from the inclusions, pores and cavities in the weld, since no weld can be perfect. Furthermore the effect of residual stresses and varying geometrical parameters also play a big role in complicating welding fatigue. In view of the complexity and importance of the subject a great amount of effort is put into research and testing of welded joints and the fatigue characteristics thereof as well as the development and evaluation of new and existing approaches for fatigue analysis. Several organizations and research groups are dedicated to such research, amongst others the International Institute of Welding (IIW) and the International Ships and Offshore Structures Congress (ISSC). A few major journals which include the topic, are, amongst others, the International Journal of Fatigue, Fatigue and Fracture of Engineering Materials and Structures,

Welding in the World and the Journal of Constructional Steel Research. Several code making and standard enforcing bodies also give guidelines for the constructional use and design of fatigue resistant welded joints such as the ISO, BSI, IIW and ECCS to name but a few.

Over the years five basic approaches to fatigue assessment of welded joints evolved namely the nominal stress approach, the structural or hot spot stress approach, notch stress and notch intensity factor approach (N-SIF), the notch strain approach and the crack propagation approach (fracture mechanics approach). The differences, properties, advantages and application of each approach will be discussed in the subsequent sections. The basis of the nominal stress and hot spot stress approaches is experimental determination of stress-life curves for certain detail classes or categories of components, materials and geometries from which the fatigue life could be determined for similar cases for design purposes. Although the hot spot stress method is more refined than the nominal stress approach, it still relies to a great extent on experimental results. Stress determination is, however, critical to the application of any procedure. Although experimental assessment thereof is widely employed in designing, especially in the commercial vehicle sector, time and cost considerations do not always allow it.

In view of the above points, it becomes clear that there exists a need for computer aided methods for stress determination for fatigue assessment, especially when it comes to short production runs, special designs or the analysis of complex structures. The technique currently employed is the Finite Element Method (FEM). Its application becomes very prominent especially in the hot spot and notch stress methods since the effect of geometrical stress concentrations due to structural discontinuities and notch effects can be effectively modeled. It is also widely employed in industry for stress determination where complex structures are assessed by the nominal stress method. The physical modeling of the weld itself by means of finite elements is, however, not yet clearly established and there still exists some uncertainty and discrepancy about it. The way in which the weld should be modeled is also dependent on the type of fatigue analysis that will be performed. This is because different stress parameters are needed for different assessment procedures. For nominal and hot spot techniques the requirement is simply that the elements representing the weld should impose the correct stiffness characteristics in the part of the structure containing the weld in order to transfer the geometrical or macro stresses and stress gradients, which form the basis of the nominal and hot spot methodologies, correctly. The local approaches such as notch strain and N-SIF, however, requires knowledge of the exact local stress distribution and stress concentrating effects in the weld. Since the determination of the stresses due to applied loading at certain points in the vicinity of welds forms the basis of fatigue assessment, the correct determination of such stresses is crucial for correct life estimation.

The aim of this study is therefore to investigate and validate existing techniques for numerical stress determination for the nominal stress and hot spot stress fatigue assessment procedures in particular, since they are the most widely used in especially the automotive and mining industries. The focus will mainly be on factors such as element type, meshing considerations and the position where stresses should be extracted. Once the aforementioned factors are clarified, recommendations concerning the application of FEM for the stress determination of plate like structures will be

made, based on experimental and numerical comparisons of simple constructional details. The proposed technique will then be applied to a complex structure for validation purposes. This will include a detailed finite element analysis of the structure as well as actual strain measurements for comparison. A fatigue life prediction, based on the stress extraction recommendations that will be developed in this study will also be made and experimentally verified. The fatigue life prediction will be for loading modes such as are typically encountered by similar structures under operating conditions. This implies that variable amplitude loading will be included in the analysis. Finally the fatigue equivalent static load (FESL) methodology, which is a quasi-static technique that allows variable amplitude loading to be assessed numerically by means of limited measurements and linear static finite element analysis, will be investigated and applied on the structure.

1.2 Background on the nature of welded joints and welding fatigue

The influence factors that complicate welding fatigue analysis can be subdivided into the following: inhomogeneous material, geometrical variations and welding residual stresses. According to Radaj (1995:159), variations in the above parameters generally remain unconsidered in global approaches for welding fatigue. In general, the material characteristics of the base material are used, the effect of residual stresses is only taken roughly into account while the worst case of geometrical notch parameters is considered. The following is a short summary of the nature of the different complicating factors as stipulated by Radaj (1995:159):

1.2.1 Inhomogeneous material

The filler material that is added to the base material during the welding process is of a similar type in general, but especially alloyed in order to achieve a high quality of manufacture, e.g. the weld pool shape, the transfer of droplets and the suppression of hot cracking. The filler material mixes with the base material in the weld pool while individual alloying elements may be burnt or evaporated and other elements may intrude from the ambient atmosphere or materials. Micro pores may occur if the evaporation is impeded, micro separations are fostered if the material is susceptible to hot cracking. The micro inclusions may be changed in respect of type and number. Such irregularities may especially occur in the area of the toe groove and weld root. Due to the different thermal cycles experienced, the heat-affected zone adjacent to the weld pool shows different microstructures and grain sizes, which are accompanied by different hardness values, yield strengths and crack propagation resistances. This problem is only partially reduced by welding without filler material. Furthermore, the following imperfections are also typical of welded joints as a result of the welding process: cracks, pores, cavities, lack of fusion, overlap and inadequate penetration.

1.2.2 Residual stresses

The general process of welding is done by joining adjacent members together by the application of a concentrated heat source to their surfaces, which results in melting and fusion. The subsequent rapid cooling process produces large residual stresses due

to the relaxation of thermal strains and micro structural transformation. These stresses may reach yield limits locally and is also responsible for local stress concentrations at notches. The welding residual stresses are reduced or redistributed by cyclic loading if the alternating amplitudes are sufficiently severe and the ductility of the material is sufficiently high, as shown by Sarkani et al. (2001). Since fatigue and crack propagation is actually a local phenomenon, governed by local stresses, it does not come as a surprise that the high cycle fatigue strength and endurance limit is influenced by the effect of residual stresses. Sarkani et al. (2001) also showed that the presence of residual stresses significantly altered the accumulation of fatigue damage on a T-welded joint.

1.2.3 Geometrical parameters

The exact geometrical characteristics of fillet and butt-welded joints, such as toe angle, notch radius and slope of the weld contour near the weld toe and base plate are highly variable and scattering. These geometrical data depend on the type and parameters of the welding process, on the welding materials and also on the margin of tolerance when positioning the structural elements to be joined. They are also difficult and expensive to measure and to determine by means of notch-mechanical analysis or external casting techniques. The local stress distribution under external loading is as a matter of fact also highly dependent on these geometrical characteristics. These parameter variations are automatically accommodated in the nominal methods by means of the S-N curves as will be discussed subsequently, but have to be taken into account when more specialized local approaches are applied for fatigue life evaluation. The influence of some of these parameters on fatigue resistance of welded joints have been studied by amongst others: Hobbacher (2003); Taylor et al. (2003); Li et al. (2001); Gurney (1991) and Kihl et al. (1997).

1.3 Overview of the different approaches for fatigue assessment of welded joints

The different fatigue assessment procedures are all based on different stress parameters, ranging from very basic linear elastic far field stresses for the traditional application of the nominal stress method to detailed local stresses including non-linear components and welding residual stresses in the case of local methods such as the notch strain approach. According to the IIW the stress response through the plate thickness of a structural member at the weld toe can be divided into three basic components as shown in figure 1.1. The first component is the membrane stress which is constant through the thickness of the plate and is calculated as an average stress – typically due to uni-axial loading. The second component is shell bending stress, which vary linearly through the plate thickness as is characteristic of bending stress distributions. The non-linear stress peak is then the remaining component of stress and is a result of geometrical stress raisers such as the notch caused by the weld toe in this case. The relevance of this differentiation will become clear when the philosophy and stress definition of the different fatigue assessment procedures are discussed in the following paragraphs.

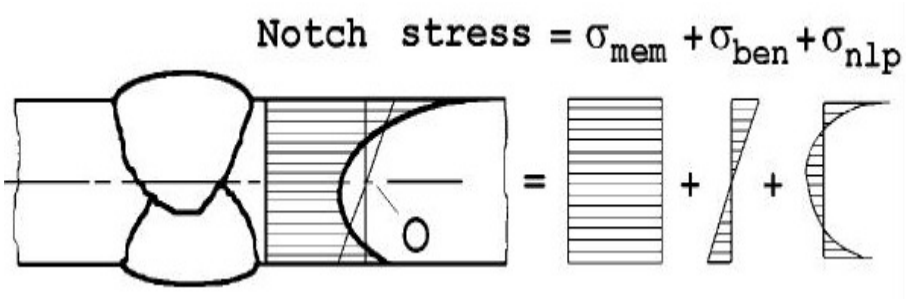

Figure 1.1: Non-linear stress distribution in the vicinity of a weld broken down to stress components. (IIW, 2004).

1.3.1 Nominal stress approach

The fatigue strength assessment of welded structures is in most cases based on the nominal stress, σ_n , which is defined in terms of sectional forces and moments in the structure at some distance away from the welding joint, based on simple linear elastic theory. A nominal stress range versus fatigue life curve (S-N curve) is then determined experimentally for a given weld and structural geometry. The nominal stress S-N curve comprises the influence of material, geometry (inclusive of notch and size effect) and surface (inclusive of residual stresses). It is thus clear that the approach is not suited for the evaluation of differences in welding parameters such as size, geometrical and stress concentration effects since it is implicitly included in the experimentally determined S-N curve, which is adjusted to include the effect of the statistical scatter due to parameter variations. Since the welded component to be evaluated should be similar to the component for which the S-N curve is determined, the nominal approach is also not suited for the evaluation of new details or geometries. The advantages of the approach lie in the fact that the results are reliable, given that the nature of the welded joint under consideration correlates closely to the given class of joint for which the curve is established in terms of welding process, weld quality and geometry. The method also requires very little computational effort in the case of simple geometries. In most cases there is no adjustment for mean stresses, based on the assumption that there exist large residual tensile stresses in the weld, close to the yield stress of the material, which will decrease with cyclic loading due to plastic flow (Dowling, 1999:460). The applicability of such an assumption was verified also by Fayard et al. (1996), amongst others, when they found that mean stress effects had very little influence on the S-N curves that they were generating.

The nominal stress approach is also the method used and applied in industrial standards and design codes which contain standard S-N curves and detail classes of basic welded joints, mainly based on the statistical evaluation of relevant fatigue tests that were performed in the 1970s by Gurney and Maddox (1973) as well a catalogue by Olivier and Ritter (1979). A few of the most prominent codes are among others: BSI.1993: BS 7608, AWS.1996: ANSI/AWS D1.1-96, IIW: Doc. XIII-XV, ECCS comm. 6 1985. The IIW document was internationally agreed on in 1996 to provide a harmonized set of S-N curves and an associated catalogue of details containing joints of aluminum and steel.

1.3.2 Hot spot / structural stress approach

The structural stress in a component is defined as the stress at some distance away from the weld toe or at the toe itself due to the structural configuration or macro geometry. It is linearly distributed across the plate or shell thickness. An adjacent structural discontinuity enhances the structural stress in two ways namely redistribution of the membrane stress due to added stiffness of the attachment and secondary shell bending stresses due to eccentricity of the attachment. The hot spot stress is the value of the structural stress in a component or structure at the point where a crack is expected to initiate (normally the weld toe) and is computed as the sum of the membrane stress and the local bending stress, excluding the non-linear stress peak due to the weld notch (see figure 1.1). The actual local stress at the hot spot, in conjunction with the welding residual stresses and material characteristics, governs the fatigue life of the weld, in particular the crack initiation period. The determination thereof, however, is very difficult due to the stochastic nature of weld bead geometry, to name but one influence factor. This led to the idea of defining the hot spot design stress as the structural stress at the weld toe excluding the local stress peak.

Figure 1.2 illustrates the difference between actual notch stress and structural hot spot stress more clearly. The assessment of fatigue strength and service life proceeds from a comparison of the structural hot spot stress amplitudes in a component or structure with a structural hot spot stress S-N curve obtained in a similar manner as the nominal stress S-N curves. Since the hot spot stress is defined at the weld toe as seen in figure 1.2, the measurement of stress amplitudes was firstly proposed to be measured by strain gauges as near as possible to the weld toe, at locations where cracks are expected. The proposal was a measurement at a distance of 3 mm from the weld toe (Haibach, 1968). The method was later refined by measuring the stress at two locations, a small distance away from the weld toe and then determining the stress at the toe by means of an extrapolation procedure which can also be seen in figure 1.2. The approach was developed in the 1970s in a combined effort by classification societies and operators of offshore installations together with research institutes, such as the American Petroleum Institute, the American Welding Society and the UK DEN. The main objective was the fatigue strength assessment of tubular joints. The development is reviewed and summarized by amongst others: Almar-Naes (1985); Huther and Lieurade (1997:332-8); Marshall (1992); van Wingerde et al. (1995:35:71-115), Fayard & Bignonnet (1996) and Niemi & Partanen (1996). The last two also provided fatigue test data based on hot spot stresses for various configurations, including C-Mn and stainless steel.

The procedure was later standardized for better results. Various codes and recommendations aimed at tubular joints exist for load assumptions, stress evaluation and extrapolation as well as parametric formulae of hot spot stress concentration factors and definitions of appropriate S-N curves (Zhao et al., 2000). There has been an increasing demand to extend the approach to plate-like structures, which resulted in the European pre-standard Eurocode 3 (CEN 1992). According to Niemi and Marquis (2003:39), this document gave only limited guidance. Thereafter, a background document focusing on definitions and the determination of stresses were published in 1995 by the IIW, edited by Niemi. Since 1996 Commission XIII of the

IIW had an active working group for the development of guidelines for the determination of hot spot stresses. The result was a designer's guide approved for publication in 2001. Detailed guidance on the determination of hot spot stresses as well as fatigue data and hot spot S-N curves are also provided in the IIW recommendations for fatigue design of welded joints and components, edited by Hobbacher, 1996 and last revised in 2004. The document also contains detailed guidance on the use of the nominal, notch stress and fracture mechanics approach for weld analysis.

As already mentioned, the local stress concentration due to the weld notch is excluded from the analysis but is implicitly included in the S-N curve. The implication thereof is similar to the nominal approach in the sense that the influence of the actual local geometry of the weld toe on fatigue resistance cannot be evaluated by the hot spot stress method. The effect of dimensional variations of structural details as well as loading condition can, however, be successfully investigated and incorporated. Scatter in fatigue life predictions of a structure containing stress concentrations (welds) is also much smaller than the widely used nominal stress approach since the stress state is defined much more accurately. One limitation of the hot spot method is that it is only applicable for the evaluation of failure by toe cracking. However, this is not a severe drawback since structures with a possibility of root cracking is commonly viewed as bad design practice. There also exist basic design principles in which the possibility of root cracking is eliminated.

Another positive aspect of the hot spot stress approach is its compatibility with the finite element method, which provides a powerful tool for the computation of stresses, especially in complex structures. A few different approaches exist for the finite element modeling of welded structures, the main differences between the techniques being element types, meshing and mesh sensitivity of stress concentrations. Applications of these variations will be discussed subsequently together with measuring and extrapolation considerations. Concluding, it should be true to state that structural stress analysis is always important since notch stresses and stress intensity factors depend on structural stress. This statement was supported by Radaj (1995), when he compared different techniques for fatigue assessment of welded joints.

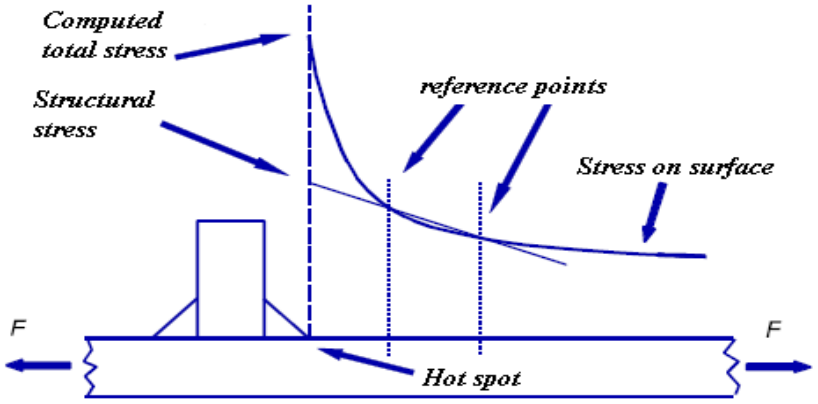

Figure 1.2: Measurement and definition of hot spot stresses at the weld toe (IIW, 2004).

1.3.3 Notch stress/strain approach

The notch strain approach is based on the stress / strain state at the notch directly, taking into account all stress raisers, including the local stress peak due to the geometry of the notch itself. The approach has its foundations in the so-called notch root approach, which is valid for notched members in general and can be summarized as follows (Radaj, 1995). The notch root approach is applied for assessing fatigue strength and service life up to crack initiation and proceeds from elastic / plastic strain amplitudes at the notch root, which are compared to the strain-life (ε-N) curve of the same material in an unnotched test specimen. The philosophy behind it is that the mechanical behavior of the material in the notch root and in the test specimen are the same with respect to stress-strain characteristics and damage accumulation. The stresses and strains at the notch root of the structural component are calculated according to the cyclic stress-strain curve and the macro structural support formula of Neuber together with the micro structural support effect in the case of sharp notches. The strain-life curves of the comparison specimen, which are dependent on mean stress, can be represented by a single damage parameter ε-N curve that comprises the effect of mean stress. The damage contributions from the stress-strain path are determined cycle by cycle, added up and then assessed relative to the damage parameter ε-N curve. This procedure can be seen in figure 1.3 as outlined by Kloos (1989:7-40) and portrayed by Radaj (1995). The stress-strain history can also be numerically evaluated by means of non-linear finite element analysis. The approach described above as a whole is essentially strain based and consequently requires high expenditure and computational effort.

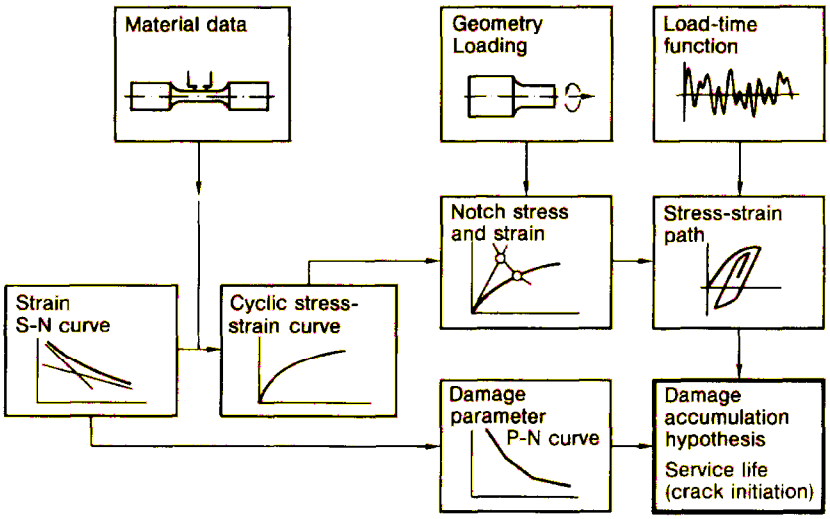

Figure 1.3: Notch root approach for assessing the fatigue strength and service life of non-welded components (Radaj, 1995).

This strain-based approach is well suited also for welded joints especially in low cycle (N less than 10^5) fatigue were local plasticity effects are more prominent. Lawrence and co-workers performed the first numerically supported analysis based on the notch strain approach during the period of 1977-1981 on butt-welded joints with crack

initiation at the weld toe. The crack initiation phase was covered by the notch strain approach, while the remaining life was assessed by means of the fracture mechanics approach. The fatigue notch factor of the welded joint characterizing the endurance limit was determined first by means of the radius of curvature of the notch taken as a worst case, and finite element analyses. The notch factor was then implemented to determine the fatigue strength by means of the cyclic stress-strain curve and the macro support formula of Neuber as well as the strain-life curve. The material characteristics were taken as those of the unaffected base metal in all cases. The procedure is illustrated in figure 1.4 as outlined by Radaj (1995:164). Sonsino & Radaj (1998) gave an outline of the application of strain-based methods based on the more classical elements in connection with the base metal, i.e. the stress strain relation by Ramberg and Osgood, Neuber's support effect, the stress-strain path according to Masing and strain-life (ε-N) curve according to Manson, Coffin and Morrow, or alternatively a damage parameter P-N curve where Smith, Watson and Topper's stress-strain function is preferred. One disadvantage of the strain-based approach is that it is rather sensitive to assumed mean stresses in the process zone at the notch root and it is thus extremely important to estimate the welding residual stresses and their possible relaxation effects correctly (Niemi, 1995). This becomes very clear from investigations such as those performed by Teng et al. (2002); Radaj et al. (1998) and Sonsino et al.(1999). Various examples of the application of the notch strain approach in especially the offshore and vehicle industries exist and will be outlined in the following sections.

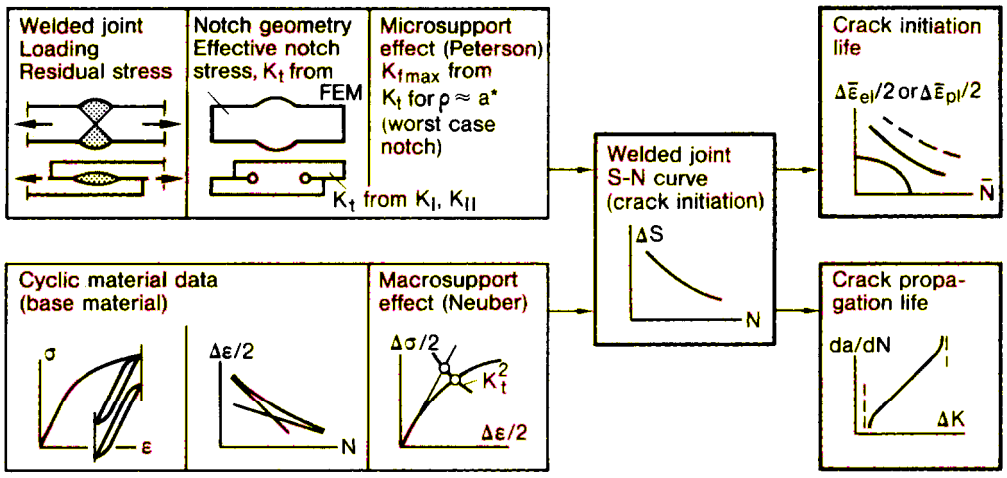

Figure 1.4: Notch strain approach for welds according to Lawrence (Radaj, 1995).

The notch stress approach is a simplification of the strain-based approach focusing on the determination of residual stresses and based on the assumption that no appreciable plastic deformation occurs at the notch and that the notch effect can be described as linear elastic and set against the endurance limit of the material. The fatigue notch factor is derived from the elastic stress concentration factor, which is dependent on the shape, dimensions and loading of the component. The Von Mises strength hypothesis is introduced in the case of ductile materials with multi-axial loading, while the endurance limit of the material is taken from an amplitude mean diagram, taking into account the effects of surface roughness and residual stresses.

The notch stress approach for welded joints was developed, refined and applied by Radaj in particular. It is restricted to the determination of the endurance limit of the welded joint with possible extensions into the medium cycle fatigue range. A prominent feature of this approach is the incorporation of the micro support effect at the most sharply notched toes and roots of the different welded joints according to the Neuber hypothesis as well as the fictitious rounding of the notches to obtain the fatigue-relevant uni-axial notch stress. This results in a fatigue notch factor of the weld relevant to the nominal stress. The approach is applicable for any radius of notch curvature. An alternative form of this method is also described by Hobbacher (1996).

The procedure for the fatigue life assessment by means of the notch stress according to Radaj can be summarized as follows. Firstly, the structural stresses at the weld notches (toe, root etc.) are determined by means of analytical formulas, strain gauges or the finite element method, neglecting the notch effect. Secondly, the structural stresses or internal forces are transferred as external forces to the cross sectional model of the welded joint with fictitiously rounded notches in order to determine the fatigue notch factors by applying notch stress theory and the boundary element or finite element method. The multi-axiality of the stress state at the notch as well as mean stress effects are taken into account by means of the von Mises hypothesis and a relevant Haigh diagram as far as ductile materials are considered. The result of the notch stress procedure described above is the endurance limit of the considered welded joint in terms of nominal stress. It is, however, recommended to correct the results in respect of residual stresses, which are not taken into account (Radaj, 1995:165).

The notch stress approach as described by Radaj is claimed to be particularly well suited to determine the influence of local geometrical parameters of welded joints (such as radius of notch curvature, slope angle at the weld toe, penetration depth and plate thickness) on their fatigue strength. Sonsino (1998) also summarizes and applies the procedure. It has been checked whether the notch stress approach as described above accurately and correctly classifies simple welded joints in respect of the standardized notch case scheme in terms of the nominal stress approach. The comparative investigation was initiated by the IIW and successfully completed by Petershagen in 1986. Another comparison with standard S-N data by Olivier et al. (1994) delivered convincing results in respect of mean values and scattering widths.

The method as prescribed by the IIW is slightly simpler although the principles are the same. The procedure basically consists of determining the effective notch stress, defined as the total stress at the root of a notch, obtained assuming linear elastic material behavior by means of finite or boundary element analysis and the modeling of the notch root by a radius of 1mm. The exact geometry of the weld bead is otherwise kept the same. The resulting notch root stress is then entered into a notch stress S-N curve for life prediction. Note that the S-N curves include the effect of residual stresses. This method is recommended for situations where nominal and hot spot methods are not applicable e.g. where the weld geometry or the influence thereof needs to be assessed or where a total absence of test results or possibility of comparison with a detailed weld category exists.

1.3.4 General

Hobbacher (2003) conducted fatigue tests on cruciform, load carrying, fillet welded joints using all of the three techniques as described above as well as the fracture mechanics approach. The test results led him to the following conclusions. The nominal stress method required the least expenditure, with very effective application but deviations from existing data occurred due to the effect of dimensional variations and misalignment, which could not be covered. The printed fatigue classes in the tables of structural details as well as the clear FAT (fatigue strength at 10^6 cycles) values created the illusion that these numbers were accurate and clear cut. He also found that the definition of nominal stress under certain loading conditions were difficult or questionable, especially in the case of tubular structures.

The application of the structural hot spot stress method circumvented most of the drawbacks of the nominal stress method since macro-structural effects, wall thickness and misalignment were automatically considered. The drawbacks were found to be the incertitudes of the extrapolation procedure and the fact that different executions of fillet welds and weld angles at the throat section were not completely covered by the method. One of the advantages of the method is the fact that relatively coarse and economic meshing is possible, which is favorable when large structures are analyzed.

The notch stress method was found to be the most accurate since it refers directly to the notch at which the actual crack initiation is expected. The procedure is numerically more expensive since a very fine mesh is required to accurately capture the stress peaks at the notch. This also indicates the implementation of substructure techniques when large structures are analyzed. The method becomes indispensable when new or critical structural details are developed and assessed, for which no nominal stress fatigue data exists.

Various examples of the application of the different techniques for fatigue assessment of different structural components, especially in the shipbuilding and vehicle industry are available in the literature. To name but a few: Fricke & Paetzhold (1994) investigated and tested the fatigue strength of scallops (small cut-outs in ship structural members) by the application of the hot spot stress approach at the welds. Li et al. (2001), investigated lap joints by means of the fracture mechanics approach. Savaides & Vormwald, (1999) also did a hot spot stress analysis of certain welded structural elements in the vehicle sector (floor structures of city buses in particular). Sarkani et al. (2001) investigated the influence of residual stress and loading characteristics on stochastic fatigue damage accumulation by means of an elastic, perfectly plastic material model supported by a nominal stress approach. Lie and Lan (1997) performed a boundary element analysis of misaligned load carrying cruciform fillet welded joints to establish the notch stress concentration factors due to the root gap and the misalignment. The life assessment was done by means of the fracture mechanics approach. Some examples of the application of local approaches include the following: Teng et al. (2002) performed a local stress analysis by means of linear elastic finite element analysis of butt welded joints and investigated the effect of residual stresses and geometrical factors such as notch radius and flank angle on the fatigue life by means of the strain-life approach. Radaj and Sonsino (1998) assessed the fatigue strength and service life of K-shaped tubular joints by the same approach.

The local stress-strain approach supported by elastic finite element analysis is also implemented by the Ford Motor Company. The basic principles and application of the procedure are outlined by Conle & Chu (1998).

Issues concerning stress determination and life assessment of the mentioned applications will be discussed in more detail in the subsequent sections. All of the abovementioned investigations were supported by finite element analyses to determine relevant stresses, which indicate the applicability and importance thereof.

Tovo & Lazzarin (1998,1999) developed an analytical mathematical relationship between the local stress at the weld toe and the structural stress some distance away from the weld toe, obtained by thin shell finite element analyses. The basic philosophy was to compare the weld geometry to an open V-shaped notch for which there exists analytical solutions for stress field distributions due to external loading. The definition and mathematical principles are quite complex, but also very thorough, taking into account factors such as overall loading distribution, geometry of the weld, and notch opening angle and stress gradients. The method is, however still dependent on the availability of accurate notch stress concentration factors, which can also be determined analytically, but still has to be obtained through finite element analyses in certain cases. The appeal of the method lies in the fact that local stress distributions can be determined analytically and with low computational effort, taking the abovementioned parameters (geometry etc.) into account. This gave rise to the notion of relating the fatigue strength of fillet-welded joints to a so-called notch-stress intensity factor (N-SIF), which is calculated by parameters obtained from the local stress distribution around the weld toe as well as main geometrical parameters. The approach is, however, still in its developing phase and very little experimental verification of such correlations is available. Verreman & Nie (1996) obtained such a correlation. The method is, however, viewed in a very optimistic manner since the influence of asymmetric stress fields will also be included in the procedure.

Another new approach was developed by Taylor et al. (2001), the so-called critical distance and crack modeling methods. These methods use a simplified description of weld geometry, excluding the modeling of toe radii and can be supported by a low-density finite element mesh. The crack modeling method (CMM) finds an equivalent stress intensity range for notches instead of cracks by using stress data from the FEA after which a line is drawn from the point of highest stress in a direction perpendicular to the direction of the local maximum principal stress. The stresses along this line are then compared to stresses that would occur ahead of a crack. The critical distance method or area method (AM) uses the average stress in an area of circular shape surrounding the point of maximum stress. The methods are claimed to be able to accommodate stress singularities, since they are based on a fracture mechanics approach as well as low mesh densities, especially in the case of the CMM. The approaches were compared with tests results for a T-shaped fillet weld and a butt weld and good results were obtained (within a scatter band of 20%). The results also indicated that the techniques were able to account for the effect of reinforcement shape on butt welds and the thickness effect of non-load carrying cruciform welds on fatigue life.

1.4 Implementation of finite element methods (FEM) and in stress determination of welded joints for fatigue analysis.

The emergence of numerical methods such as the finite element method allows a detailed analysis of even very complex structures and is nowadays widely applied in stress determination and analysis of welded structures as well as the welds itself. Two approaches, which rely strongly on good finite element modeling, are in particular the hot spot and notch stress-strain approach. The implementation of finite element methods requires a good understanding of the principles and the philosophy behind it. Further important aspects are careful consideration of boundary conditions, mesh properties, size dependency and element capabilities to capture relevant stresses. Careful consideration should also be given to proper modeling of the welding zone, which is also the aim of the following discussion.

Another numerical method, the boundary element method complements the finite element method when analyzing welded joints and structures. Its main area of application is the analysis of notch stresses and the determination of stress intensity factors. The method is based on the discretization of the boundary of the structural element to be analyzed. 2D problems are subsequently reduced to boundary lines and 3D problems to surfaces. The computational results are thus also available only on the boundary lines and surfaces but for the application to welded joints, which are characterized as notches, this is acceptable, since the maximum stresses, which govern fatigue life, occur on the surfaces. The boundary method is claimed to be best used in combination with the finite element method where the global structure is analyzed to determine the structural stresses, which can then be used as an input to the boundary element model of the weld itself to determine notch stresses. This procedure was suggested by Radaj (1995) and implemented by, among others, Lie and Lan (1997).

1.4.1 Different element types and application

The following is a summary of elements commonly used in the modeling of welded structures and welds as stipulated by Niemi (1995). Beam elements are mainly used in the determination of nominal stresses in frames, trusses and similar structures containing beam like structural elements. The analysis is restricted to bending and torsional stresses in the absence of warping. Membrane elements are applied in the modeling of plate-like structures with in plane loading. Thin shell elements are suitable for solving the elastic structural stresses, based on the theory of shells and can only model the mid-planes of plates since the actual plate thickness is a property of the element. Another drawback is their inability to model the real stiffness and stress distribution in and around the welding zone of intersecting shells. Solid elements (20-noded, curved, isoparametric) are suited for modeling three-dimensional stress and deformation fields. They are sometimes implemented in welded joints for modeling the intersection of plates and shells. A single layer of 20-noded solid elements instead of shell elements can also be used to model plate-like structures. The generation of a too coarse mesh can also exaggerate the bending stiffness in the case of plates. Niemi

(1995:31) also states that the use of 20-noded solid elements with 3-point integration to model non-linear stress distribution across plate thickness gives poor results. One element across the plate thickness with 2-point integration should be used instead. Two dimensional plane strain models are implemented to study local stress fields around notches where the notch is modeled as a two-dimensional cross sectional model with unit thickness. Transition elements are used to connect two element types with different numbers of nodes and degrees of freedom as for example a solid and shell element. The last element type that has significance in weld modeling is multi point constraints (MPCs). The rigid link MPC is commonly implemented to imitate weld stiffness when shell elements are used. It is basically a mathematical constraint that imposes the displacement of one node onto another, which effectively makes it a rigid link, thus creating artificial stiffness.

1.4.2 Application of different finite element meshing and resolution considerations as well as examples of the application of different techniques in fatigue investigations

The hot spot method, as already stated, excludes the non-linear stress peak caused by the notch of the weld toe. This has to be conformed to in the finite element procedure as well. In order to meet this requirement, the stresses have to be extracted at the integration points of elements adjacent to the weld toe (i.e. within the element at the element's integration points) or at nodal points some distance away from the hot spot (i.e. at the element closest to the hot spot's node the furthest away from the hot spot). The mesh has to be refined in such a way that the stress gradients in the vicinity of the hot spot can be accurately extrapolated and correlated to the stresses used to determine the hot spot S-N curve. The mesh should also be refined in such a way that further refinement will not influence the stress distribution inside the area between the extrapolation points. Niemi (1995:35) found that the non-linear stress peak is still included within a distance of 0.4t of the local notches (t = plate thickness) when plates are modeled with a multi layer of solid elements through the thickness. Consequently the stress results should be read outside the area containing the non-linear stress peak (0.4t) and extrapolated to the weld toe or linearized through the thickness of the plate when in the region of 0.4t such as will later be illustrated through Dong's work (2001). A single layer of elements with reduced integration could be used instead, as previously mentioned.

Commission XII of the IIW (Niemi, 2002) basically defines two types of hot spots for plate like structures as shown in figure 1.5: type 'a' hot spots, which are located on the plate surface and type 'b', which are located on the plate edge. The shipbuilding industry has developed specific guidelines for type 'a' hot spots which comprise a relatively coarse meshing with element sizes in the vicinity of $t \times t$ where t is the plate thickness. Eight-node shell elements or twenty-node solid elements with reduced integration are recommended. Figure 1.6 shows an example of the detail in figure 1.5 modeled with shell and solid elements respectively. For more general cases a finer element mesh is implemented which uses an extrapolation technique similar to the one shown in figure 1.2.

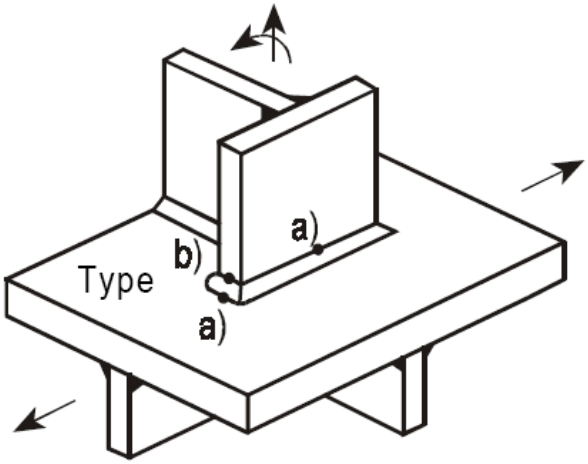

Figure 1.5: Two types of hot spots. (IIW, 2003).

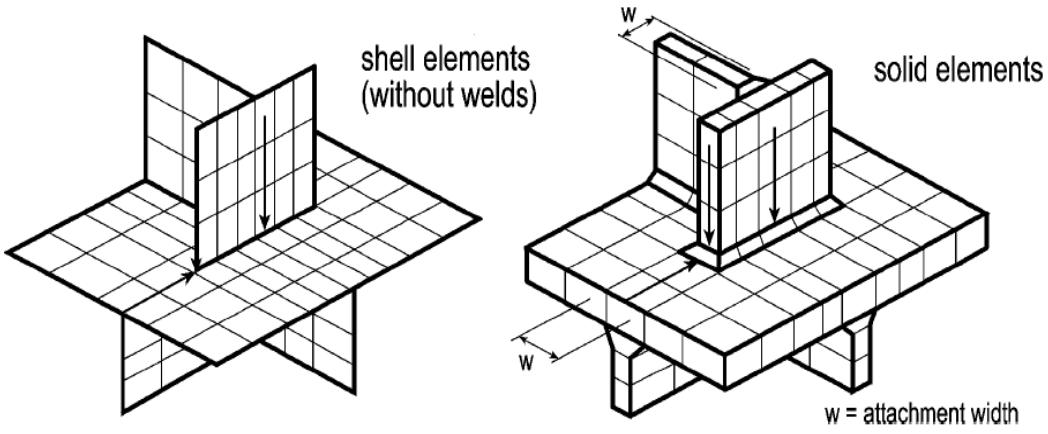

Figure 1.6: An example of a shell and solid element model for hot spot stress determination. Linear extrapolation is performed from the midside nodes adjacent to the weld toe (Niemi, 2003).

Figure 1.7 shows an example of a solid element mesh of a gusset edge. Note that the extrapolation points are located at $0.4t$ and $1.0t$ respectively and that 20-node elements with reduced integration are used. Niemi (2002) further stipulates that the element and meshing as shown in figure 1.7 is not suitable if the gusset is loaded under bending, since the actual hot spot stress is then directed towards the corner. He also gives conceptual guidelines as to how the gusset should be modeled in such a case. Type 'b' hot spots have stress gradients that are independent on plate thickness. Consequently fixed element sizes of either 10×10 mm or 4×4 mm are prescribed. The element types are the same as with type 'a' hot spots but extrapolation is performed from mid-side nodes adjacent to the element representing the weld bead.

Fayard & Bignonnet (1996), proposed similar meshing guidelines in 1996 aimed at capturing hot spot stresses. They claimed that modeling with shell elements were

sufficient to capture hot spot stresses in plate like structures and that no additional information could be gained by the use of solid elements.

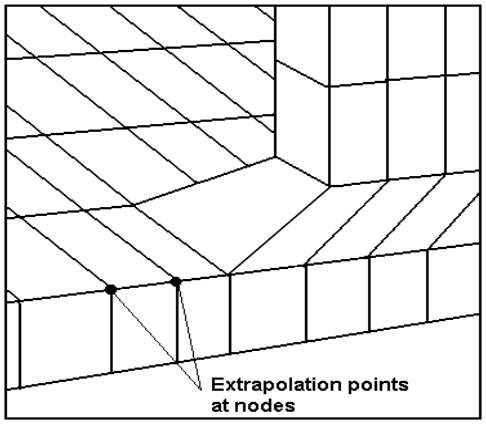

Figure 1.7: Gusset detail modeled with solid elements.
(adapted from: Niemi, 2003).

They made this statement due to the fact that the weld are modeled by means of rigid elements (multi-point constraints) which link the two shells together. Their basic meshing philosophy is summarized in the following points (see figure 1.8): The first two elements adjacent to the intersection line have lengths approximately equal to the weld leg length and arranged in such proportions that the connecting node between the two elements coincide with the centre of the weld leg. The rigid element is connected between these two nodes. Note that the plate and the attachment are not otherwise connected, thus nodes n1 (a) and n1 (p) are not connected. The highest stress value approaching the intersection line is found at the centre of gravity of E2, which represents the weld toe.

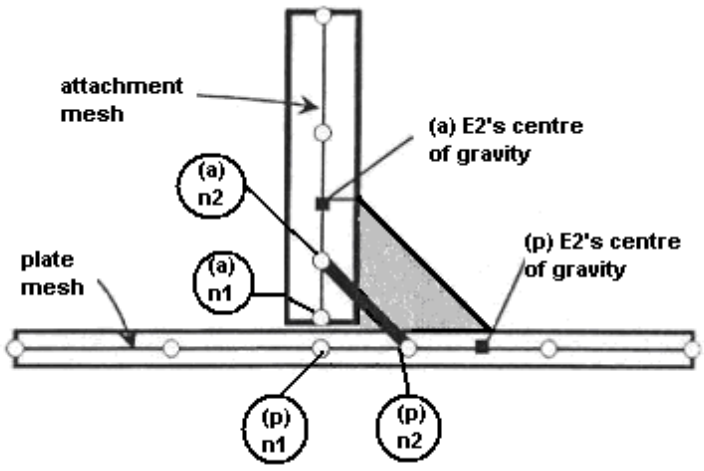

Figure 1.8: Modeling of the weld by means of solid rigid links as well as an indication of element size and connectivity
(Fayard & Bignonet, 1996).

In view of the above meshing considerations, Dong (2001) proposed a post processing procedure for the finite element results to obtain a structural stress parameter, which includes the effect of geometric stress concentration factors in a mesh size insensitive manner. This procedure was mainly motivated by his opinion that the linear extrapolation scheme, as discussed above, lacks the ability of capturing the structural or hot spot stress correctly due to the exclusion of local stress concentration effects at the weld toe as well as the mesh dependency of stress values obtained by finite element analysis in the vicinity of the weld toe.

The theory behind the procedure is mainly based on the postulate that there exists a corresponding linear structural stress distribution that is equivalent to the actual local stress distribution near the weld toe by satisfying elementary structural mechanics theory such as force and moment balance through the thickness of the plate. He also suggested the use of element nodal forces instead of the converged element stresses in the vicinity of the weld toe in the cases of shell or plate models since shell or plate element solutions at structural discontinuities converge only to solutions prescribed by shell theory. The equivalent structural stress are basically determined by using sectional forces and moments some distance away from the weld toe to calculate the corresponding structural stress at the weld toe. Figure 1.9 (c) shows the mesh insensitivity of the procedure as obtained for a single plate lap joint modeled with eight-node plane strain elements while (b) and (a) shows one of the finite element models and the model definition respectively

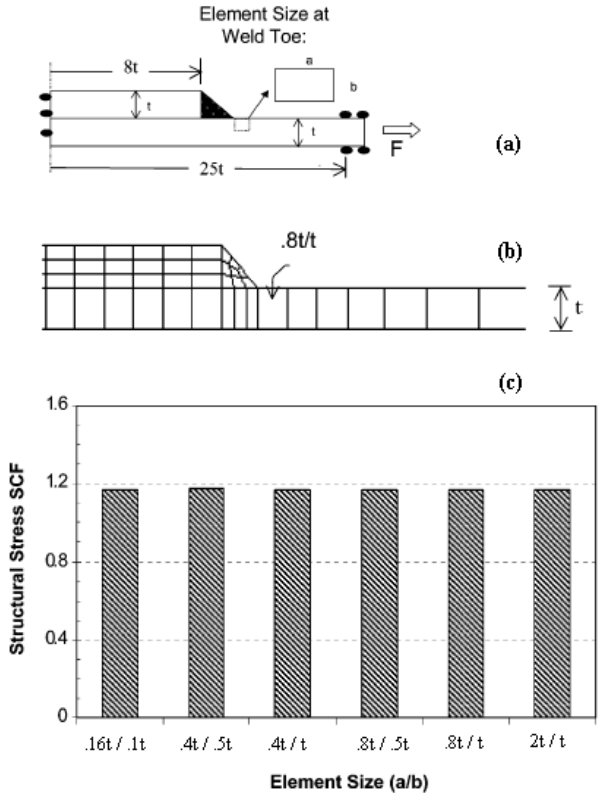

Figure 1.9: Structural stress and mesh insensitivity for a single plate lap joint (Dong, 2001).

Similar results were obtained with solid and shell elements. For further investigation into the possibilities of the procedure Dong (2001) took standard nominal stress fatigue data for a few welded details and performed both a structural stress (according to his proposed procedure) and a hot spot stress evaluation of the different details. Apart from the mesh size sensitivity of the hot spot stresses he also identified the possibility of transferring S-N data between different joint types by plotting the structural stress based S-N curves for different weld details on the same graph and noting that the data points lie much closer together than the nominal or hot spot points. This approach was further refined together with Hong (2004) and led to the development and proposal of a master S-N curve for pipe and vessel welds.

Fricke & Paetzhold (1994) investigated the fatigue strength of scallops as previously mentioned in section 1.3.4 by the application of the hot spot stress method. Scallops may be subjected to high stresses. Under axial loading the rounded corners and the ends of the fillet welds between the web and the flanges are points of increased stress and are subsequently prone to fatigue failure. Figure 1.10 shows the typical geometry (one half due to symmetry) and meshing of scallops. Note the presence of both type 'a' and type 'b' hot spots. Fricke & Paetzhold also states that the increase in structural stress in the scallop is highly non-linear, depending on geometric parameters. They proposed non-linear extrapolation, also in view of the fact that there exist two hot spots which could affect the stress values of each other. The finite element modeling was done by means of plate elements or three-dimensional elements while the following considerations were taken into account.

A fairly fine mesh was used in the vicinity of the rounded plate edge and the hot spots while the elements used had to be able to model the local bending occurring particularly under shear and local pressure loads. The meshing was done with plate and twenty-node solid elements respectively as can be seen in figure 1.10.

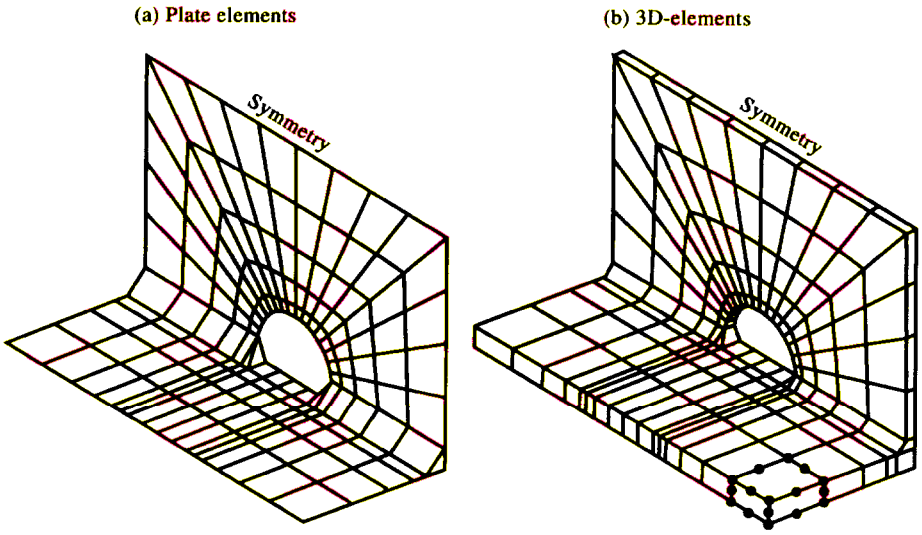

Figure 1.10: Finite element modeling of scallops
(Fricke & Paetzhold, 1994).

Plate elements created some problems when modeling the fillet weld since elements representing the weld should be sufficiently stiff to clamp the adjacent plates while the axial stiffness, governed by the cross section of the elements, should not be enlarged in order to avoid overstressing of the plate below the scallop under axial loads. They also found that the actual stiffness properties of the weld are better modeled by the three-dimensional elements. By following the definition of the hot spot stress as a plate or shell stress, a stress linearization in the direction of the plate thickness is required. They obtained this by using three-dimensional elements, arranging only one layer of elements with two integration points in the thickness direction. This method is also prescribed by Niemi (1995). By modeling the half-round scallop with plate elements, good results, which correlated well with measured values, were obtained. By using the design S-N curve based on hot spot values for 45° welds as well as the hot spot stress concentration factor a corresponding value for the allowable nominal stress were obtained. Good correlation with the detail classification given in the design rules was obtained if the non-linear extrapolation was taken into account.

In further work by Fricke & Doerk (2004), the fatigue resistances of bracket toes with stiffeners were investigated. It was found that the hot spot stress procedure gave conservative but rather unexpected results. The specimens failed at the centre of the weld from the root instead of the weld toe at the stiffener end, which had much higher predicted stresses. The reason for this was due to beneficial residual stresses at the stiffener toe and tensile residual stresses at the centre of the weld. The existence of these stresses was numerically and experimentally verified. The fatigue test results, however corresponded with the predicted lives when the specimens were stress relieved. One can deduce from this that a possible pitfall of the hot spot method as applied to non-categorized details is the omission of residual stresses since it is not included in the S-N curve in such an explicit manner as is the case with the nominal approach. This may lead to non-conservative results.

Savaidis & Vormwald (1999) investigated various welded joints from the floor structure of city buses by means of the hot spot stress approach using a single hot spot stress-life curve for different details and the IIW recommendations for finite element modeling of welds (Niemi, 1995). All of the welds consisted of butt and fillet welds between webs and flanges while being subjected to bending and normal force. The structures were modeled by four node shell elements at the centre plane of the plates. The welds were modeled as an intermediate shell, which can be seen as variant (a) in figure 1.11 since it was the easiest to implement. The thickness assigned to the intermediate shell was equal to the distance between the plane sections in the middle of the plates (after their own discretion). This thickness was lesser than that of a real weld. The reason for modeling a thinner weld was to exclude the excessive rise in structural stress that was calculated when greater thicknesses were assigned. Clear guidelines as to the thickness of the weld elements were, however not available to them and in certain cases, depending on the geometry, the weld was not modeled at all at the plate intersections (after the IIW recommendations). Element sizes in the vicinity of the hot spot were such that the centre of the first element was no more than 0.4t from the highest hot spot stress (where t is the thickness of the plate). They found, however that the element sizes did not influence the values of the hot spot stresses for certain variants of the structures that they investigated. The hot spot stresses were taken from the finite element calculation as nodal stresses at the point of

the weld root, since the weld was modeled by an intermediate shell, which actually had the same location for the toe and the root.

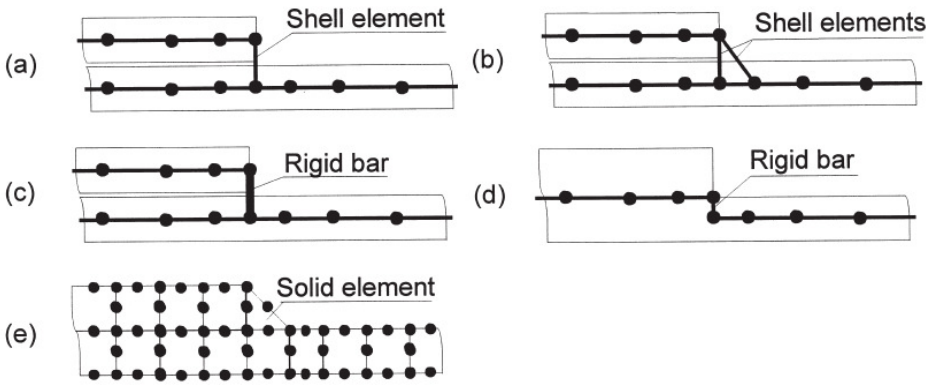

Figure 1.11: Alternatives for modeling welds with shell elements (Niemi, 1995).

It had to be ensured, however, that the postprocessor of the finite element package did not take the nodal forces of the adjacent elements into account. The wider aim of the study was also to determine failure critical locations for the different design variations and details proposed for the floor structure of the buses. They had good correlation between numerical results and test results regarding the failure locations, as well as actual fatigue lives determined through tests and as calculated from the hot spot curve as recommended by the IIW (Hobbacher, 1996). They also found that many failures actually originated from the weld root instead of the toe, but those failures also occurred at lives similar to the failures originating from the weld toe.

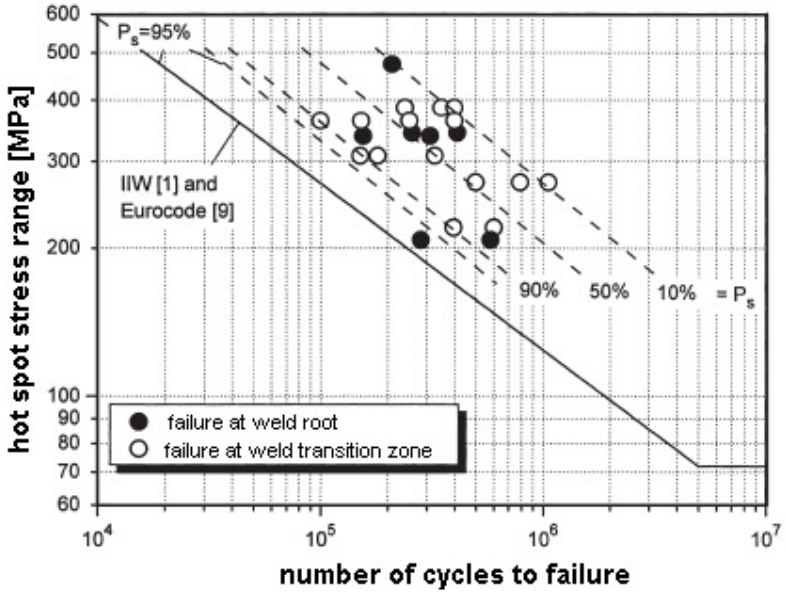

Figure 1.12: Fatigue test results obtained by Vormwald & Savaidis compared with the hot spot stress curve of the IIW (Vormwald & Savaidis, 1999).

This gave rise to the notion that the hot spot approach could be extended to failure of welds at the root also. Figure 1.12 summarizes their results quite clearly as compared to the prescribed hot spot S-N curve.

Doerk et al. (2002) performed investigations into the different methods for structural hot spot stress evaluation of welded joints with the aim to investigate mesh insensitivity in particular. The analysis procedures used consisted of finite element analysis with surface stress extrapolation as well as implementation of the post processing procedure proposed by Dong (2001), which was previously discussed. Finite element modeling was once again done by means of eight-node plate and twenty-node solid elements. The surface stress extrapolation was subdivided into the different prescribed procedures, according to the mesh size and type of weld toe, as stipulated by the IIW (Niemi, 2001 and Hobbacher, 2004) The procedure by Dong (2001) computes the linearized membrane and shell bending stress at the weld toe by imposing equilibrium between the axial and shear stresses acting on the far side of the element closest to the weld and the stresses at the weld toe. For the shell model, the structural stress can be directly evaluated at the hot spot, since a linear stress distribution is already assumed in the element. The above procedures were applied to four different structural details which included a plate lap fillet weld (similar to the one shown in figure 1.8), a one sided doubling plate, which is three-dimensional in nature, and a flat bar welded to an I-beam by means of a fillet weld around the plate edge. The plate lap fillet weld gave the same results for Dong's approach and the extrapolation approach, as well as mesh insensitivity, since the problem could be reduced to an entirely two-dimensional problem. The same could not be said, however, for the one-sided doubling plate which were modeled with twenty-node solid elements, especially concerning mesh insensitivity when implementing Dong's approach. The reason for this is the fact that vertical shear stresses acting on the element sides are not considered in Dong's approach.

The scatter was considerably smaller for the results obtained from the linear extrapolation technique. The flat bar and I-beam setup was modeled by eight node shell elements. The stress extrapolation yielded similar results for coarse and finer meshes, but were influenced by the element sizes at the bracket toe of another component, which was similarly modeled. Doerk et al. (2001) consequently arrived at the following conclusions: Dong's approach became questionable in three-dimensional problems but gave good compliance with test results and claimed mesh insensitivity in two-dimensional cases. Mesh insensitivity when using shell elements could not generally be assumed.

In the work done by Li et al., the effect of weld geometry, penetration and load condition on the fatigue strength of a lap welded joint was investigated. Finite element modeling and linear elastic fracture mechanics were implemented. The approach were used since lap joints are commonly encountered with defects such as toe cracks and lack of penetration, which is easily modeled by the fracture mechanics approach, since it is based on the assumption of pre-existing cracks. The crack propagation life was calculated by means of the Paris-Erdogan relationship while the initial crack lengths were assumed to be 0.2mm. Figure 1.13 shows the geometry and loading of the lap joint under investigation. It was found that an increase in the lack of penetration, the ratio w/t and a decrease in the ratio h/t, the weld leg length, reduced the fatigue strength for all load cases.

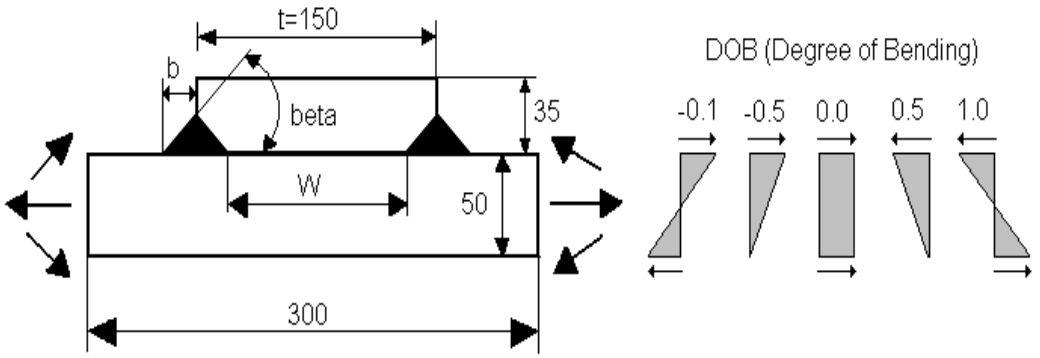

Figure 1.13: Dimensions and loading on the lap joint (Li et al., 2001).

It was also found that smaller flank angles (beta in figure 1.13) gave higher fatigue strengths except in the case where the h/t ratios were very small and the loading purely tensile. The joint was also analyzed under pure axial loading with a main plate constraint in the vertical direction. Strangely enough the effects of lack of penetration and weld leg length were found to be contrary to the results obtained with the model in figure 1.13.

Thirdly the finite element model was reduced to one tenth of its original size with similar geometry and loading conditions to investigate the effect of size reduction on the FEM model, but very non-conservative results were obtained with regards to fatigue life. The precise modeling with regards to the finite element method was not discussed and the numerical results were not supported by laboratory tests so the integrity of the results remains unclear. The exercise did, however, demonstrate the possible effect of parameters such as weld geometry and loading conditions on the fatigue characteristics of welded joints and the effective manner in which it could be assessed by means of numerical aid. The possibilities of the fracture mechanics approach for assessing manufacture related imperfections such as introduced cracks and lack of penetration was also illustrated.

The structural or hot spot approach was so far only applied to thick plate structures but developments for the application to thin plate structures have also emerged - especially in the automotive industry. Fermer et al. (1998) developed a FE based method for predicting the fatigue life of MAG welded thin sheet structures which comprises a specific experimentally determined structural S-N curve together with structural stresses analytically calculated along the weld line from nodal forces and moments obtained from the FEM. Two different S-N curves are used depending on the degree of bending in the load case. The usage of a rather course mesh is implemented without too much loss of accuracy. The modeling of the weld is the same as stipulated by the IIW except for the use of 4-node shell elements instead of 8-node shell elements. Figure 1.14 shows an example of the meshing of the connection between two thin sheets. Another important aspect of the weld element is that its thickness is prescribed as being equal to the weld throat length, a. The analytically calculated stresses are mesh insensitive to a large extend while poor results are obtained from the nodal stresses. The use of the analytical stresses is thus recommended for the specific application of the abovementioned meshing and S-N curve to thin sheet structures.

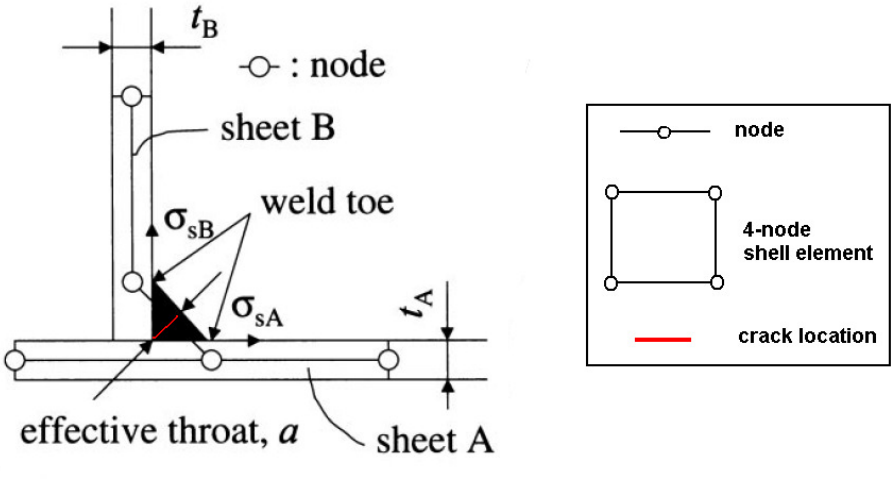

Figure 1.14: Modeling of the weld in thin sheet structures for structural stress determination according to the Volvo Car Corporation (Fermér et al., 1998).

Petterson (2002) performed fatigue analyses on a component (an A-stay from an articulated hauler) by means of different assessment procedures, based on results from finite element analyses. He found that the boundary conditions, manufacturing tolerances and accuracy of the finite element model had a huge impact on the stresses that were determined, especially in the case were fasteners were involved. For the hot spot stress approach in particular solid92 elements (ANSYS) were used in the sub model representing the weld area. The sub modeling technique is based on the transfer of nodal displacements from a more global model to a local one.

In almost all of the above cases the numerical fatigue assessment was done by means of the structural hot spot stress approach, which did not require detail analysis of the stress intensity at the notch caused by the weld toe. The notch stress approach, as described by Radaj (1998), needs a detailed finite element analysis of the fatigue prone location such as the weld toe. The IIW (Niemi, 1995) recommend the use of a very fine two-dimensional mesh with plane strain elements such as shown in figure 1.15. The results obtained by extrapolating structural stress values or nodal forces into the refined mesh as was suggested by Radaj (1995) is claimed to give good correlation with analytical solutions obtained from the literature (Niemi, 1995).

Radaj et al. (1998) applied the local notch strain approach on a welded tubular joint. The aim of their investigation was to clarify certain conceptual questions regarding the approach. The first part of the numerical procedure consisted of the determination of the structural stresses in the vicinity of the critical fatigue endangered locations. This was done by linear static analysis with curved 4-node ‘thick’ shell elements and meshing as shown in figure 1.16. The calculated stresses were lower than the measured ones due to the three dimensional behavior of the structure in the weld area which was not captured by the finite element analysis. The weld was not specifically modeled and consequently its stiffening effect on the chord wall bending was not correctly captured. The structural stresses were then converted to constraint forces and moments to serve as an input to a localized plane strain model of the weld area.

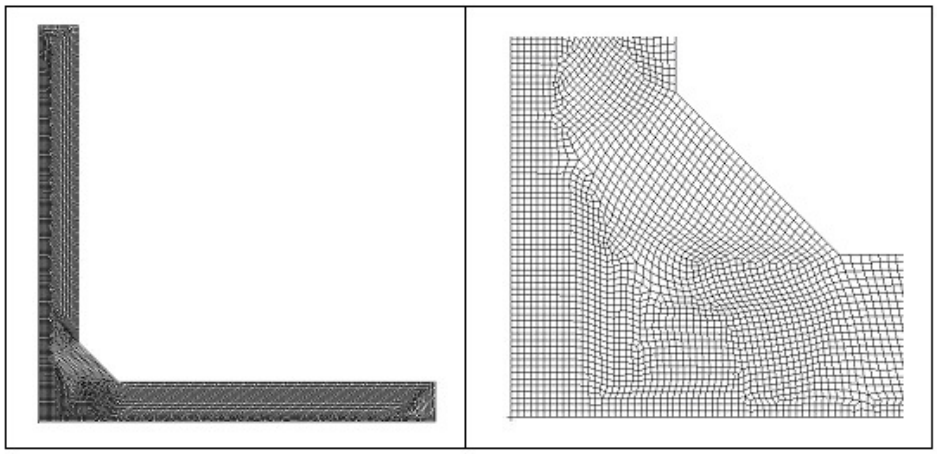

Figure 1.15: Finite element meshes for determination of the stress concentration factor at a weld toe (Niemi, 1995).

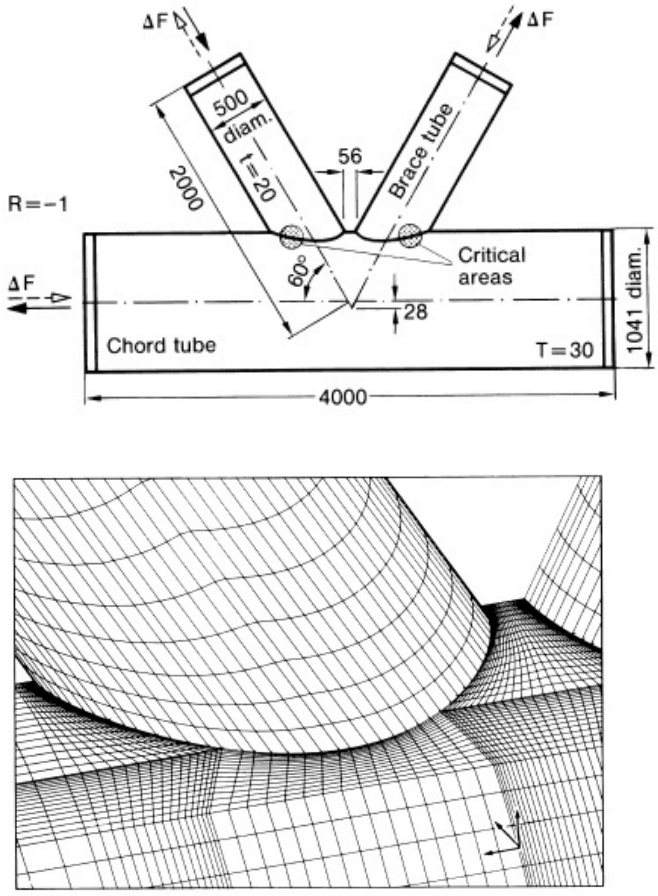

Figure 1.16: Details of the K-joint as well as the 3D finite element mesh (Radaj et al. 2001).

The structural stress and the plane strain model stresses were in good agreement in areas adjacent to the weld toe but not at the toe itself since the stress concentration

was captured by the localized plane strain model. Once the stress concentration factor and the cyclic material data of the heat affected zone (HAZ) and base material was known the life predictions were made according to the notch-strain approach. Drawbacks of the approach were, however, found in the uncertainty of the local geometrical parameters, such as toe radius and notch geometry. The local hardness distribution and the cyclic material properties of the HAZ are also irregular and scattering. A further problem occurred due to the absence of proper knowledge concerning the residual stresses at the weld toe. This is crucial since the strain-life approach is based by definition on the exact local stress state at the location under consideration. The abovementioned uncertainties were indicated by occurrence of non-reproducible crack initiation and propagation modes and positions.

Teng et al. (2002) investigated the effect of residual stresses and geometrical parameters on the fatigue life of butt-welded joints by means of the notch strain approach. A numerical prediction of the residual stresses was made. The method, however, is beyond the scope of this research. The notch stresses were once again determined with a 2D plane strain finite element mesh similar to those shown in figure 1.15 and 1.16. The residual stresses were used as an input for the life determination by simply adding it to the mean stress in the life equation. This procedure is quite simple and tests results confirm it to be effective. They had, however, accurate knowledge of the cyclic material data in the vicinity of the weld toe. On the grounds of the good correlation of numerical and experimental results they used their numerical procedure to investigate the geometrical parameters of the weld bead and to make certain recommendations.

1.5 Quasi-static approach to fatigue stress determination under dynamic loading

As mentioned in the introduction, the fatigue analysis of the test structure in this study will be performed under variable amplitude loading. The assessment procedure will include the fatigue equivalent static load (FESL) methodology which is a quasi-static technique. The following paragraphs will consequently serve to illustrate the philosophy and limitations of stress determination and fatigue assessment by means of quasi-static analysis.

The quasi-static approach can be defined as a method by which input loads on a structure of dynamic nature can be approximately simulated and quantified in a static manner. The incentive behind such an approach is cost and time saving. This is necessary due to the large computational expenditure and expertise required by transient or dynamic finite element analysis as well as the restriction regarding the accessibility of critical positions on a structure for direct measurements.

The basic principle of the technique, as outlined by Haiba et al. (2002) encompasses linear static analyses associated with the variation in external loads and the replacement of such external load histories with a static unit load acting in the same location and direction as the specific external load history. A static stress analysis is then performed for each individual load history from where the dynamic stress response due to the various individual load histories are determined by multiplying

the history by the static stress influence coefficients resulting from the corresponding unit load. The total dynamic stress history within the structure is then calculated by means of the principle of superposition.

The imposition of such a unit load on a structure is often done by means of an inertial or g-load. As explained by Xu (1998), the g-load is implemented in the form of a uniform acceleration applied to the whole structure. Due to the acceleration the mass of the structure produce a distributed load applied throughout the entire structure. Such a g-load effectively deforms the structure, resulting in strains and stresses throughout the structure, similar as would be obtained by imposing a unit static force through the centroid of the structure.

The fundamental assumption of the quasi-static method with application of a g-load is that the stress response and deflection throughout the structure due to the inertial load correspond to that caused by the actual dynamic loading. This implies that the ratios of the stresses relative to each other due to the inertial load are the same as the ratios resulting from the dynamic loading. Should this be the case for a specific structure, it follows automatically that the magnitude and distribution of the fatigue relevant stress response can be simulated by imposition of an appropriately scaled g-load on the structure. In such a way the structure can be assessed solely by means of linear static analysis supported by experimental measurements of the actual input loading or stress response for scaling purposes.

Wannenburg (1998) illustrated the application of a quasi-static methodology referred to as the fatigue equivalent static load (FESL) methodology on tankers, implementing inertial finite element analysis. The dynamic loading is replicated by imposition of a g-load that is scaled by means of experimental strain gauge measurements. The measured stress response for a typical load cycle at a position sensitive to global bending, tensile and shear stressing is processed by means of Rainflow cycle counting from which a fatigue damage equivalent sinusoidal stress range is determined. The g-load is then scaled according to this stress parameter. Since it is assumed that the relative stress ratios due to the g-loading corresponds to the ratios due to the measured dynamic loading, the fatigue resistance of the structure under consideration can now be assessed by considering only the static stresses obtained from the g-load. A detailed outline of the procedure is presented later in this study. Wannenburg also presents a comparison between results obtained from a case study where the specific technique is applied as opposed to formal design codes which specify allowed structural stresses under prescribed inertial loads. He also stresses the importance that the requirements concerning relative stress ratios should be met. According to Wannenburg a vehicle would typically be excited in its first global bending mode under vertical loading, which would yield stress responses similar to the static inertial load response. The excitation of higher bending modes or twisting modes, however, would not be considered by static analysis although they could yield considerably higher stresses in different areas.

Other examples of the application of quasi-static methods in the vehicle industry are presented by Conle & Mousseau (1991), Tebbe & Mathers (1995) and Shrikantan et al. (2000). Sanders and Tesar (1978) also illustrated that the quasi-static approach is viable for most industrial mechanisms that are stiff (and consequently possess high natural frequencies) and operate well underneath their natural frequencies. They also

stated that this, however, is not true when resonant dynamics participated in the response of the structure.

Xu (1998) discussed the shortcomings of the quasi-static method by means of relevant examples and past experience. He mentioned a few cases were the stress response obtained from quasi-static analyses failed to correlate with either tests or reality and that significantly lower fatigue relevant stresses were predicted at failure critical locations. He mainly blames the fact that additional modes other than the static deflection mode takes part in the response as well the occurrence of non-uniform accelerations due to the nature of dynamic resonant modes. In addition he discusses a modal scaling technique that utilizes the results obtained from modal analyses in conjunction with measured reaction forces. The technique is said to be more accurate for two reasons: firstly the exact mode shapes in which the structure will respond is determined and utilized as opposed to the assumed deformation due to the inertial load. Secondly, as many modes as are prominently participating in the structural response can be included in the analysis, thus increasing the accuracy of the approximation.

Various techniques and discussions aimed at the improvement of dynamic stress computation by utilizing modal analysis are presented in the literature. Van Tonder et al. (2006) presented a dynamic fatigue design methodology that accounts for the effect of dynamic modes on the stress response of a complex structure. Ryu et al. (1997) illustrated how the accuracy of dynamic stresses could be improved by a technique referred to as the modal superposition technique while Dickens et al. (1995) gave a detailed review of the mode acceleration and modal truncation augmentation methods used in modal response analyses. A more detailed discussion of these techniques is, however, beyond the scope of this report due to the fact that the fatigue analyses that will be performed will be limited to the quasi-static method.

1.6 Scope of research

From the literature survey it becomes clear that most case studies and analyses implementing the finite element method was done by means of the hot spot stress method. This is due to the clear and explicit guidelines concerning weld modeling, meshing and stress extraction. Such guidelines as supplied by the IIW are currently not available for implementation with the nominal stress method.

The aim of this research is consequently to develop and verify a finite element supported nominal stress determination methodology for welded structures. Cruciform joints and plate-stiffener configurations will be investigated in particular with the possibility of expansion to other details. As mentioned in the introduction, there exists a fair amount of uncertainty around the finite element modeling of welds by means of conventional shell elements in particular. The main issues are meshing and element configuration in the vicinity of the weld and the representation of the weld itself in such a manner that the correct stiffness properties of the connection are obtained. This is important since the stiffness of the weld in the finite element model strongly influences the values of the structural stress distribution in the vicinity of the weld as well as the stresses that are nominally obtained. For the application of the

nominal stress approach the extraction of correct nominal stress values is of utmost importance in fatigue life determination.

As already mentioned, the hot spot stress procedure as stipulated by the IIW gives explicit guidelines for correct meshing and stress extraction from finite element methods for implementation with the hot spot S-N curve. Such guidelines are not established for the nominal stress approach as covered by the BS 7608, ECCS and IIW (nominal stress) structural design codes. The reason is that the stress parameter is classically defined as the far field stress that could be determined from simple elementary linear-elastic structural mechanics. The finite element modeling and stress extraction procedures, however, does not always present a clear transition from local weld induced stresses to nominal far field stresses due to the strong influence of the weld discontinuity and load related stress gradients (particularly in the case of bending). The position in terms of element lengths or real distances from the weld toe for the stress extraction is consequently uncertain - especially in complex models.

In order to clarify the two abovementioned issues (correct modeling and nominal stress extraction) the procedure as outlined in the following paragraphs will be followed in order to develop clear, explicit and verified guidelines for the application of the nominal stress fatigue assessment procedure for plate like structures using finite element methods.

1. Determination of actual stresses and stress gradients on a T-piece (viewed as a variant of a cruciform joint) with full penetration welds.

This will be done by means of axial loading together with the use of multiple, closely spaced strain gauges. Once the actual stress distribution due to a known loading is obtained multiple finite element analyses of the joints and loading conditions will be done with the applications of different configurations of shell, solid and rigid elements. The aim is to determine which element and mesh configuration resembles the stress state in the most realistic manner and to investigate the related mesh sensitivity of such a configuration. The achievement of coarse and economic meshing will be pursued as well as a recommendation as to the correct meshing procedure, specifically for butt welded T-pieces (T-joints).

2. Establishment of a nominal stress extraction procedure

Once the correct modeling procedure is determined the nominal stresses in the T-piece specimens will be calculated from elementary structural mechanics. This will be done for various load conditions applied to the specimen. This is required since the nominal S-N curves are determined for stresses deduced from elementary analytical structural mechanics. This will be compared with the finite element results obtained by means of the correct meshing procedure in order to establish at what position stresses should be extracted from the finite element model. The extracted stresses must represent the correct stress value (far field nominal stress excluding stress concentrations due plate intersections formed by the joint and the weld discontinuity) for implementation with the relevant nominal S-N curve.

3. Verification of the stress extraction procedure on an actual structure

The following step will be to validate the obtained nominal stress determination methodology considering an actual structure containing T-joints and stiffeners. The hot spot stress method will also be applied to the structure for the purpose of comparing actual and predicted fatigue lives obtained from the two methods (nominal and hot spot stress) since clear and distinct guidelines for the application of the hot spot method in conjunction with FEM are available in the IIW fatigue design recommendations.

The structure will be plate like in order to be compatible with the hot spot assessment procedure as well as the determined meshing methodology, which relates to plate-like structures. Strain gauges will be positioned in the vicinity of the welds at the critical points according to the developed methodology. The relevant stresses for fatigue life determination by means of the nominal and hot spot methods will be determined through measurements. The applied loading on the structure will be dynamic and stochastic in nature while the induced stresses will be due to the inertial effects of the mass of the structure.

The verification procedure will consequently be twofold: Firstly to verify that the stress distribution and values at certain points on the structure due to static loading corresponds to the measured values at the same points, obtained from the strain gauge measurements. This will confirm the integrity of the developed weld stiffness representation and meshing scheme when applied to a more complex structure.

Secondly the structure will be dynamically loaded and the response of the structure with respect to resonance and compatibility with equivalent static fatigue life assessment procedures will be assessed. A quasi static analysis procedure, known as the Fatigue Equivalent Static Load (FESL) methodology will be implemented in order to predict the fatigue life of the structure under consideration. The FESL methodology was chosen since it requires finite element analyses as well as experimental strain measurements. A life prediction of the structure will thus be made by means of actual strain gauge measurements in failure critical locations on the structure as well as the implementation of the fatigue equivalent static load methodology in conjunction with strain gauge measurements on non-critical locations. The application of the FESL methodology, which relies strongly on good finite element modeling, will thus serve to augment the physical life prediction. In this manner comparative predictions on the same structure can be obtained while the effectiveness of the FESL methodology is being critically assessed. The implementation and efficiency of the hot spot method as prescribed by the IIW will also be investigated through the fatigue evaluation of the structure since it will also be applied, together with the developed nominal stress methodology. The life predictions based on the nominal and hot spot methods can thus be compared to each other and to the actual obtained fatigue lives, once the fatigue test results of the structure becomes available.

Since all of the above analyses and investigations rely strongly on accurate strain gauge measurements, the processing of measured data into correct stresses and the logical interpretation thereof will also receive attention - especially when the static assessment of the structure is done.

Chapter 2

2. Experimental and numerical investigation of the stress distribution in a welded T-piece

2.1 Aim of the procedure

From chapter 1 it becomes clear that there are basically four ways to model a weld in a plate-like structure, three of which are shown in figure 1.11. The four techniques include modeling by means of shell elements only, shell elements with rigid links to imitate the weld stiffness, shells with adjacent inclined elements to resemble the weld and solid elements. It is, however, not clear which modeling procedure is the most realistic. Solid elements are accepted to give the closest resemblance since the element itself is the closest to reality in terms of geometry and also due to the fact that it is a three dimensional element.

The reason for not using solid elements by default in all cases lies in the fact that the analysis time and required computing capability is considerably more in the case of solids. This is due to the greater number of degrees of freedom per element and the fact that several elements are required through the thickness of a plate to capture bending stress distribution accurately if solid elements with a lesser amount of degrees of freedom than 20 nodes per element are used. Consequently shell elements are used in industry - especially in large, plate-like structures, due to economical and practical considerations.

The aim of this experimental analysis is to obtain the actual stress distribution in the vicinity of the weld of a but-welded T-piece due to static loading. This is done by means of multiple, closely spaced strain gauges. The results will establish a basis for comparison and validation of the finite element results obtained from analyses with the different representations of the weld as noted in the first paragraph of this section.

2.2 Experimental setup

2.2.1 The T-piece specimen

The specimen on which the static load test was performed is a simple T-piece as shown in figure 2.1. A full penetration weld conforming to the AWS D1.1 structural welding code was used for the attachment. The specimen was manufactured by firstly welding two larger 10mm plates to each other and then machining the specimen to size in order to eliminate welding end effects such as undercut. Only two specimens were manufactured - one for the actual test as well as an additional specimen, should further tests be required later on. The material was 300W mild steel with the following properties as provided by the supplier:

Yield strength: 300 MPa.
Elastic modulus: 206 GPa.
Poisson ratio: 0.33.

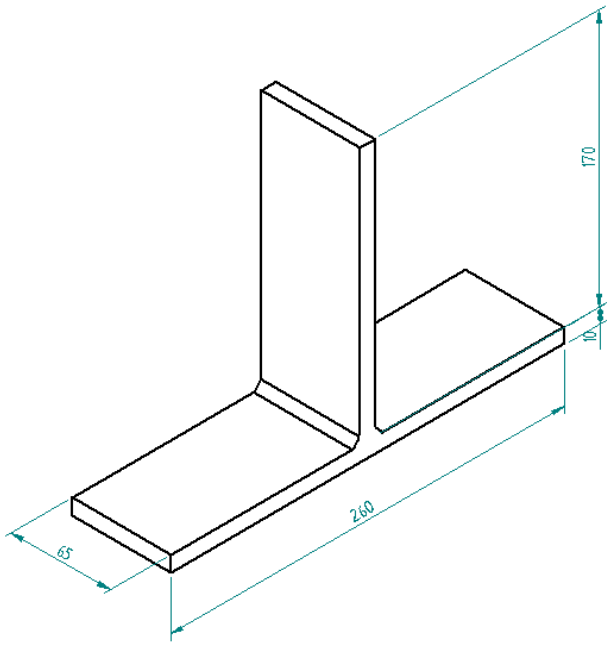

Figure 2.1: Geometry and dimensions of the test specimen (dimensions in mm).

2.2.2 Test setup and procedure

For the first round of testing the test specimen was equipped with 0º-90º strain gauges, with a 2mm grid length. This enabled easy connection into a Wheatstone bridge configuration with the two strain gauges forming one half of the bridge. The completion circuit was formed by means of a Spider 8 bridge connector while the data acquisitioning was done by means of the Catman Express software package, both supplied by Hottinger Baldwin Messtechnik (HBM). Loading was applied by means of a Schenk 630 kN Hydropuls actuator.

The strain gauges were positioned as close as possible to one another and to the toe of the weld on the upright member of the test piece. This was done in order to capture the stress concentration as well as the stress gradient in tension. The upright leg of the test specimen contained five strain gauges, i.e. five gauges on the tensile leg. The distances of the strain gauge measuring grid centre points from the weld toe were as follows: 5mm, 14mm, 23mm, 32mm and 40mm. Strain gauge 1 on figure 2.2 was thus placed at a distance of 5 mm from the weld toe etc. The test piece was bolted onto a rigid bracket, which, in turn, was clamped into the base of the actuator. The setup was of such nature that a beam with fixed ends could be simulated. The loading was applied on the vertical member, thus creating tension vertically and bending in the horizontal member. Figure 2.2 schematically shows the test setup (loading, clamping and the 5 strain gauge positions) while figure 2.3 shows an images of the actual setup.

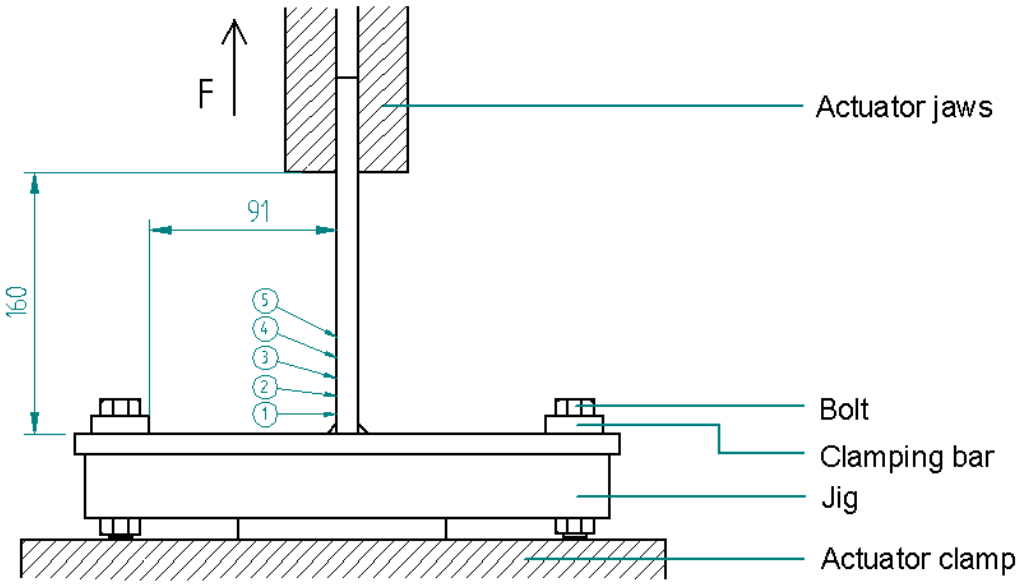

Figure 2.2: Test specimen/actuator assembly and strain gauge positions (dimensions in mm).

The testing procedure was as follows:

- Secure the test specimen in the jig and fix the jig in the bottom jaws of the actuator. Ensure that the centre of the weld is aligned with the centre of the top jaws of the actuator to avoid possible eccentricity
- Ensure that the loading on the T-piece is equal to zero while the actuator is set to load control
- At this point all five strain gauge channels can be zeroed. This is done before the drive signal is imposed on the actuator to ensure that the final strain gauge readings do not contain the strains caused by the clamping procedure
- Ensure that all 5 channels are set to the half bridge configuration and start measuring. Impose the drive signal on the actuator shortly after the strain gauge data acquisition system was enabled.
- Record the strain gauge measurements for the duration of the drive signal.

The drive signal imposed a linearly increasing force, starting at 0, peaking at 6.3 kN and ending at 0. The strain gauge measurements were extracted as bridge unbalances in mV/V.

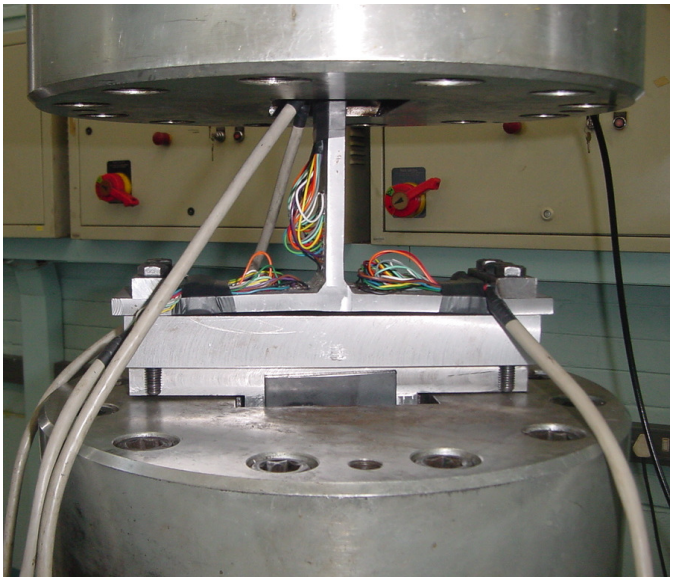

Figure 2.3: Overall view of the test specimen/actuator setup (under loading).

2.2.3 Test results and data processing

Figure 2.4 shows the recorded strain gauge and actuator load cell data for the vertical member of the test specimen. The units are mV/V for the strain gauge readings and volts for the load cell readings. The calibration of the load cell was set at 63 kN/volt. It is thus clear from the graph that the maximum force on the specimen was set at 6300 N (6.3 kN). This extreme was selected as such to stay clear of the yielding point of the steel with a safety factor of 3 and thus operate well within the linear elastic range. The numbers on the graph legend correspond to the positions of the strain gauges as shown in figure 2.2. The force data and the strain gauge data had to be synchronized on the graph since the strain gauge data acquisitioning system started recording before the drive signal was imposed on the actuator as mentioned previously. This was simply done to ensure that the force peak and the strain peak coincide as can be seen on the graph. It should also be noted that the strain gauge readings all returned to zero as the force returned to zero. This is an important factor concerning the integrity of the measurements since it confirms that the strain gauges were correctly applied and also stayed in the linear elastic range.

The calibration of the strain gauges was done by the direct shunt method. A shunt resistor of 119.8 kΩ was connected over each strain gauge respectively and the disturbance voltage change due to the bridge unbalance, as given by the data acquisitioning system, noted. These results, along with the gauge factors, which characterizes the strain – resistance change relationship of the measuring grid, could then be manipulated to give a direct correlation between the measured mV/V values and the actual strains on the 0º-90º grids. This could, in turn, by implementation of Poisson's ratio be converted to the actual strain on the specimen in a certain direction.

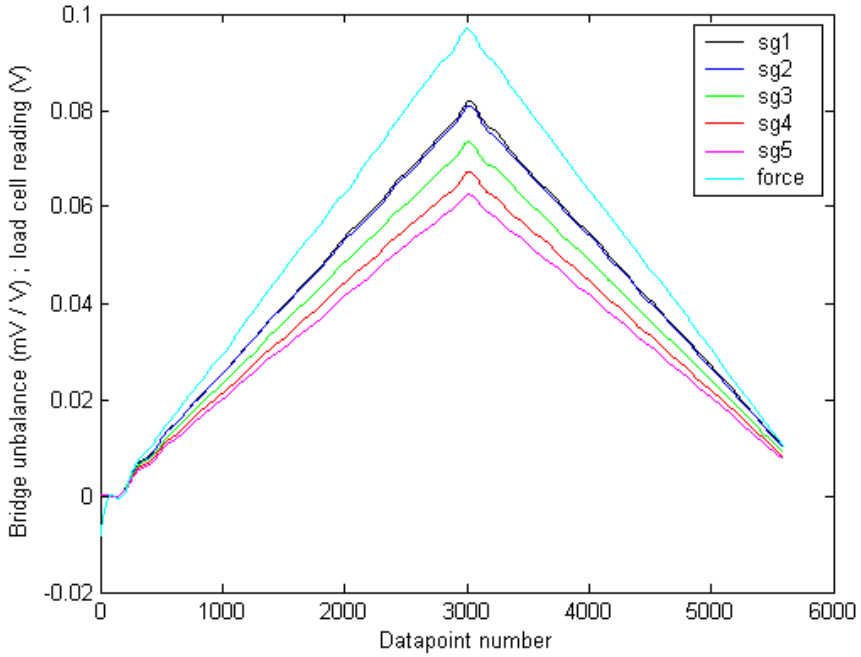

Figure 2.4: Strain gauge and load cell measurements for the vertical leg of the test specimen.

The calibration procedure is as follows:

- Connect the shunt resistor in parallel over one of the strain gauge grids in the half-bridge configuration.
- Repeat the procedure for all 5 channels and note the disturbance voltage change V_{shunt} due to the bridge unbalance on each channel respectively.
- The equation stipulating the amount of strain due to a known change of resistance in the bridge can now be implemented to determine the calibration values and conversion factors:

$$\varepsilon^* = \frac{1}{k}\frac{\Delta R}{R} = \frac{1}{k}\left(\frac{R_p}{R+R_p} - 1\right) \qquad [2.1]$$

Where ε^* = Theoretical total bridge strain that would cause the same bridge unbalance than the applied shunt resistor
k = Gauge factor of the measuring grid
R_p = Shunt resistance
R = Measuring grid resistance

- Once the ε^* values for each of the channels has been calculated the calibration factors can be determined by dividing the disturbance voltage change V_{shunt} by

the ε^* values for each channel respectively. The units of the calibration factors is thus ε V/mV.

- The total measured strain, $\varepsilon_{measured}$ due to the combined strain of the measuring grids making up the bridge can now be determined by multiplying the measured disturbance voltage changes, i.e. the data plotted in figure 2.4, by the calibration factors for all 5 channels.
- Determine the strain in the longitudinal axis of the two legs of the T-piece. This is done by noting that

$$\varepsilon_{measured} = \varepsilon_1 - \varepsilon_2 + \varepsilon_3 - \varepsilon_4 \qquad [2.2]$$

where $\varepsilon_{1\text{-}4}$ are the strains due to the four measuring grids in the full bridge configuration. By denoting ε_x as the strain in the longitudinal axis of the vertical leg of the T-piece and ε_y as the strain perpendicular to ε_x and noting that ε_3 and ε_4 is zero due to the half bridge configuration equation 2.2 can be written as:

$$\varepsilon_{measured} = \varepsilon_x - \varepsilon_y \qquad [2.3]$$

Since $\varepsilon_y = -\upsilon\varepsilon_x$ it can then be shown that:

$$\varepsilon_x = \varepsilon_{measured}/(1+\upsilon) \qquad [2.4]$$

where υ = Poisson's ratio.

- The stresses along the longitudinal axis can now easily be determined by multiplying the strains with Young's modulus, E since the Poisson effect was accounted for in the measuring grid.

$$\sigma_x = E\varepsilon_x \qquad [2.5]$$

The stresses obtained by the above procedure as well as the theoretical uni-axial stress obtained from hand calculations for the vertical leg of the test specimen are shown in figure 2.5.

Once the strain gauge measurements were calibrated and converted to actual strains and stresses the next step was to perform the relevant finite element analyses on the T-piece for comparison with the measured results and validation of the different modeling techniques.

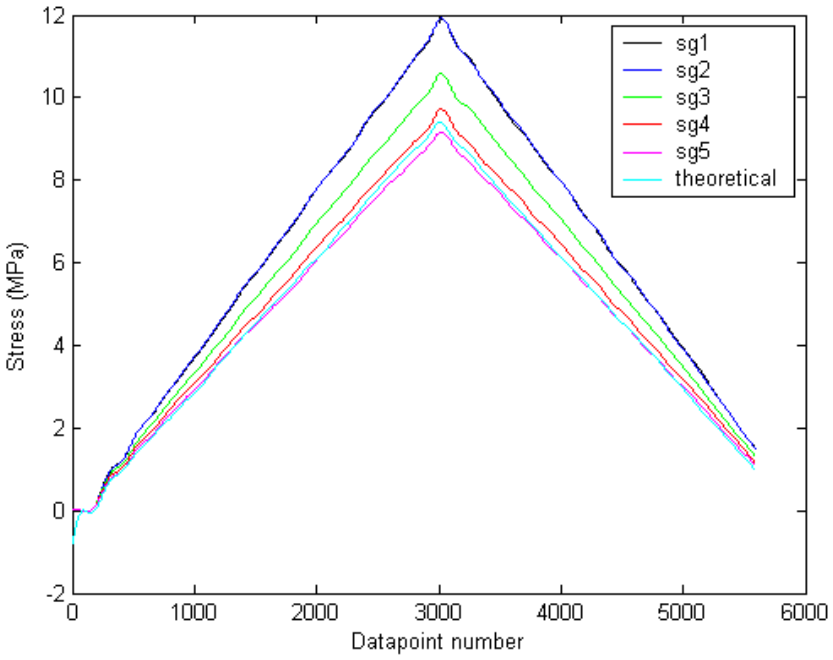

Figure 2.5: Strain gauge measurements and theoretical stress for the vertical member of the test specimen.

2.3 Finite element analysis and comparison with test results

For the numerical investigation four finite element models of the T-piece were created with the weld modeled in the four different ways, as stated in section 2.1. The boundary conditions conformed to the constraints of the actual test setup, namely clamped ends (i.e. fixed in all six degrees of freedom) and a vertical tensile load applied to the upright member of the T-piece. Figures 2.6 to 2.9 illustrate the different finite element models. The sizes of the elements in the models are all equal to 0.5t where t equals the plate thickness. A sensitivity analysis verified that convergence was reached at this element size for the particular geometry in all of the models. A typical contour plot of the results for the 20-noded solid element model for a load of 3.535 kN is shown in figure 2.10. The stresses in the Y-direction as well as the deformation mode are shown.

With the experimental and finite element stresses available a comparison of both results are possible. Figure 2.11 illustrates the strain gauge results and finite element results for a load of 3.535 kN. The origin of the x-axis is positioned at the toe of the weld while the units on the x-axis correspond to the spatial dimensions of the vertical leg. Note that the finite element stresses converge to the analytical uni-axial tensile stress of 5.44 MPa, a certain distance away from the weld toe. This is also the theoretical stress featuring in figure 2.5.

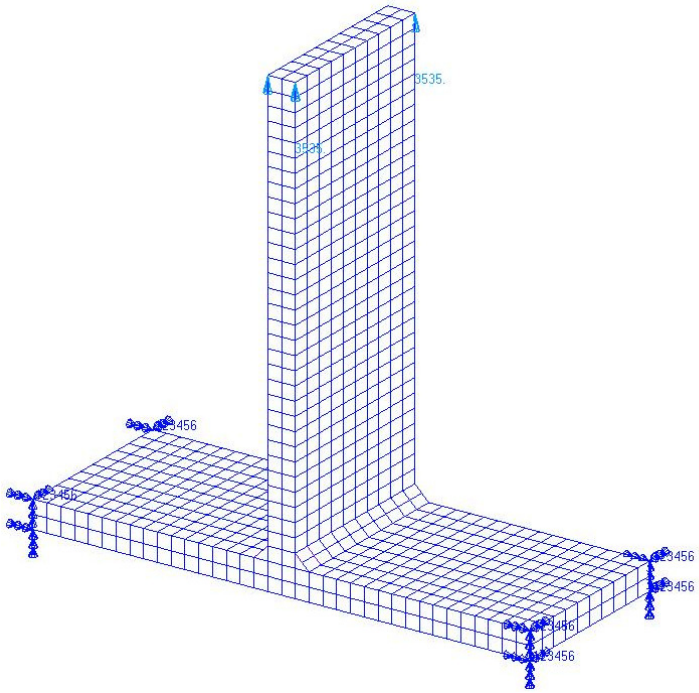

Figure 2.6: Solid 20-node finite element model of the test specimen.

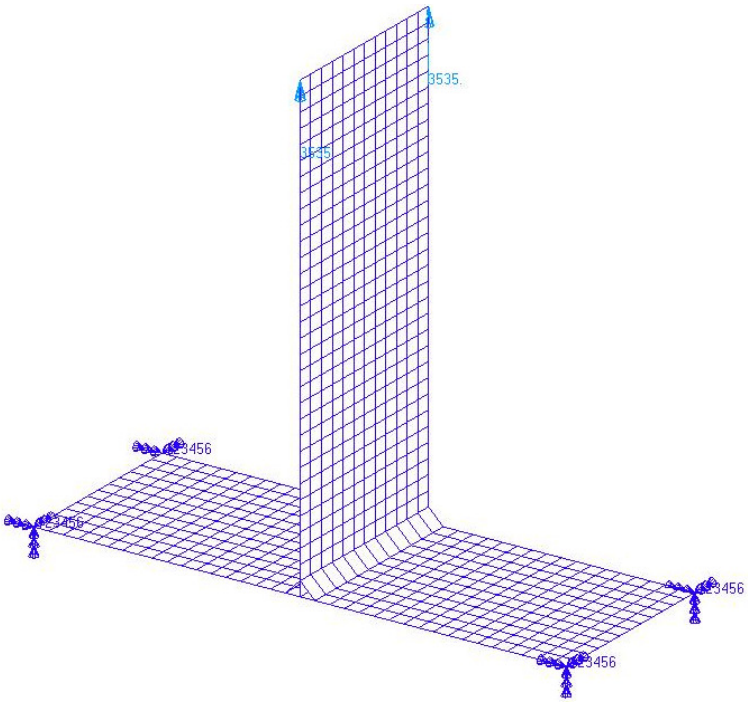

Figure 2.7: 4-noded shell element model with explicit weld modeling by means of inclined elements.

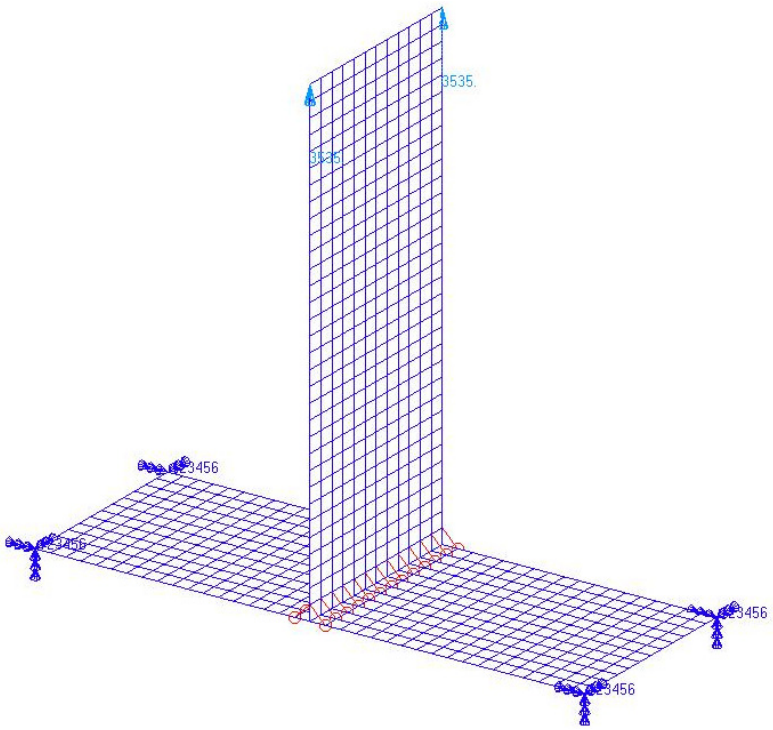

Figure 2.8: 4-noded shell element model with explicit weld modeling by means of rigid links (multi-point constraints).

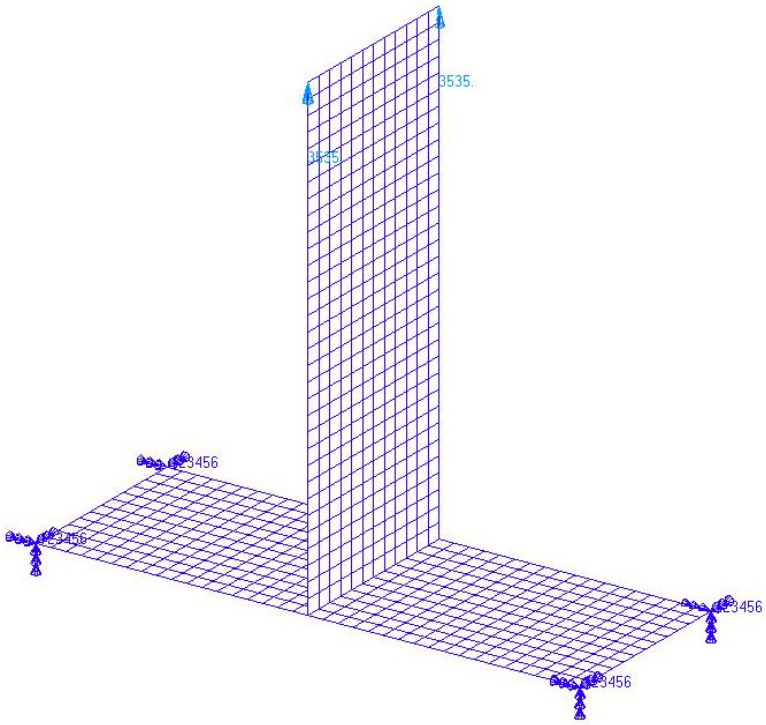

Figure 2.9: 4-noded shell element model with no weld modeling except equivalencing of the nodes at the intersection of the two plates.

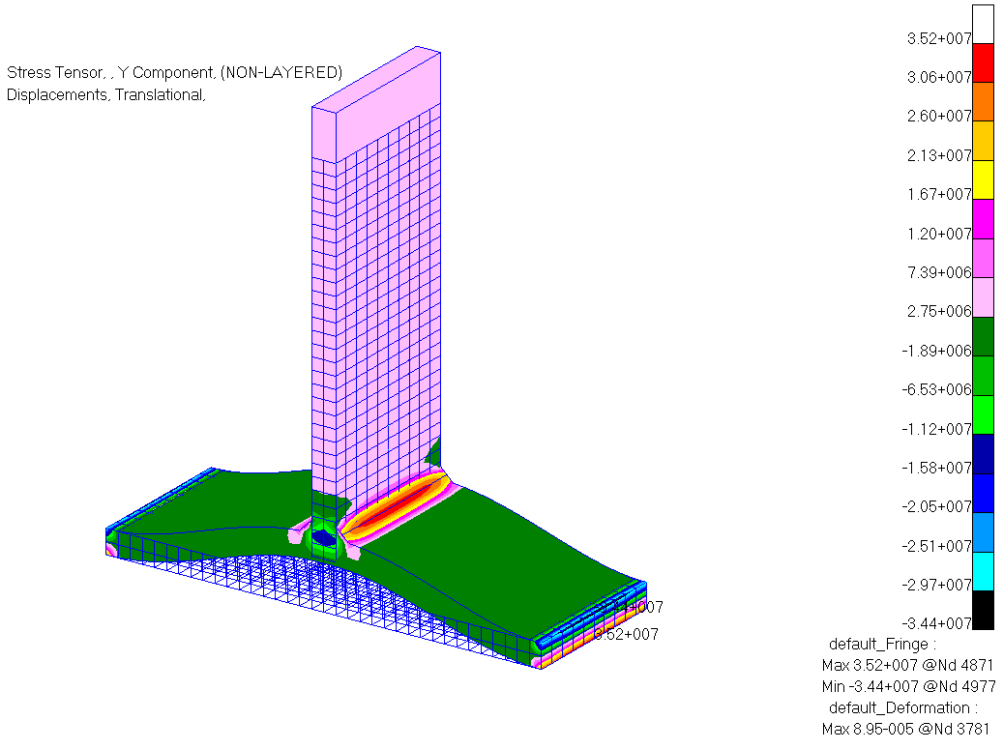

Figure 2.10: Contour plot of the stresses in the Y-direction obtained from the solid element model.

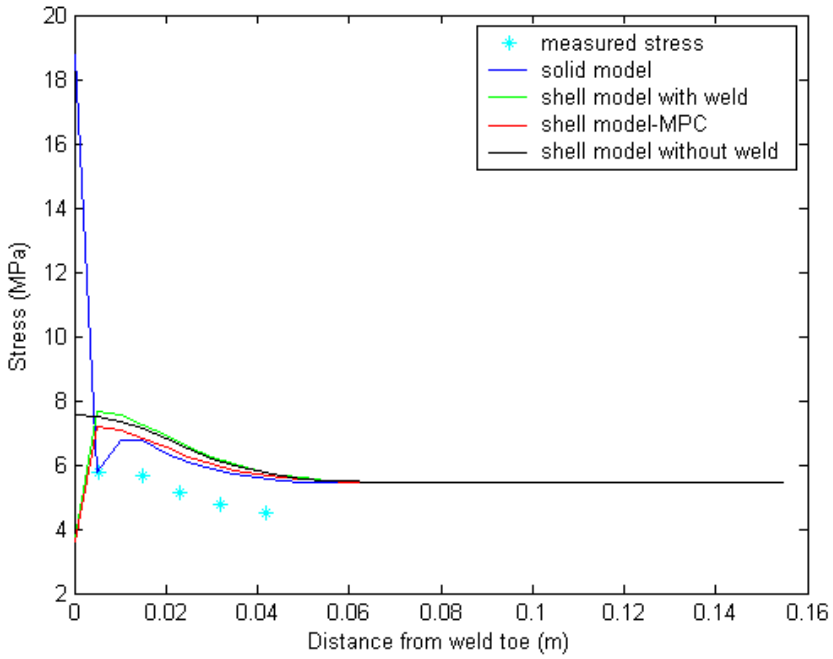

Figure 2.11: Comparison between the finite element stresses and the half bridge strain gauge readings for a load of 3.535kN.

From figures 2.5 and 2.11 it becomes clear that the theoretical and the measured stresses do not correlate at all. This is due to possible misalignment in the fixing procedure, which in turn causes secondary bending stresses in the member due to eccentricity, i.e. the working line of the actuator force does not coincide the centre of the member's base. Another influence factor, essentially causing eccentricity and thus secondary bending stresses, could also be the initial deviation from the ideal perpendicular geometry of the T-piece due to the welding process. The deviation from the theoretical and finite element stress is thus suspected to be caused by the superposition of these secondary bending stresses on the uni-axial stress.

To eliminate the effect of secondary bending a full bridge configuration had to be set up since it is possible to configure a full bridge setup in such a way that only uni-axial, tensile stress is measured. This implied that another set of 0º-90º strain gauges had to be positioned on the opposite face of the vertical member of the test specimen. It had to be ensured that their positions matched up with their original counterparts in order to measure correctly.

The testing procedure and data processing otherwise stayed exactly the same as outlined previously. Figure 2.12 shows the stress results obtained from the full bridge measurements plotted against the same finite element results as in figure 2.11.

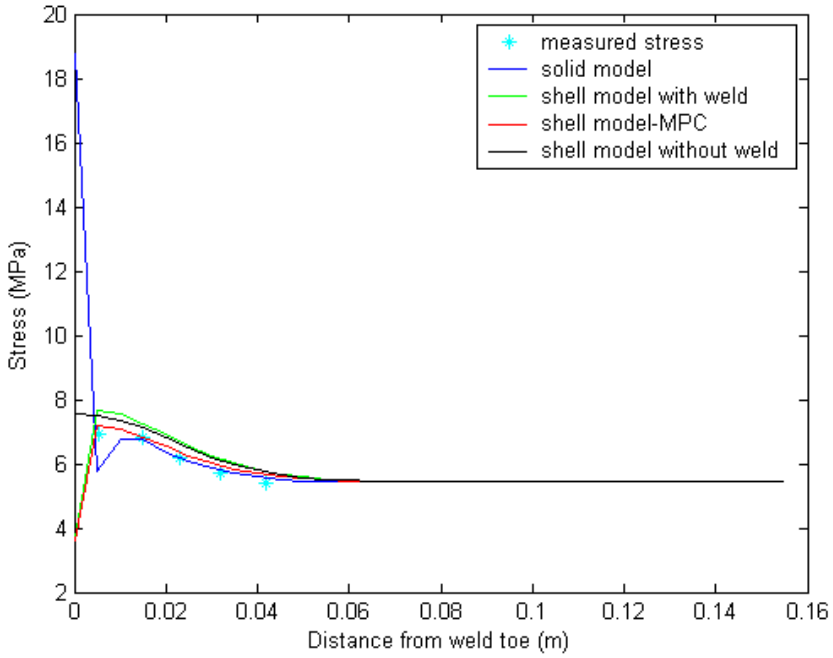

Figure 2.12: Comparison between the experimental and finite element stresses and of the various models.

The importance of eliminating eccentricity and misalignment from experimental work of this nature becomes clear since an almost exact correlation of the numerical and experimental work now exists. This also serves to verify the integrity of the 20-noded solid elements used in the finite element model since it gave the most accurate results. The aim of the experiment, namely to establish that the 20-noded solid element with

explicit modeling of the weld can be used as a benchmark for assessing the accuracy of other element configurations such as shells and multipoint constraints has thus been reached. The development of a finite element modeling methodology, using shell elements with the correct weld modeling procedure can thus commence on a purely numerical manner since the solid element can be used as a reference as will indeed be done in the following section.

2.4 Development of a finite element meshing and stress extraction procedure for nominal stress

2.4.1 Finite element analyses and results of load carrying and non-load carrying cruciform joints under bending and tensile loads

The following step was to determine which shell element configuration gave the closest resemblance to the solid element solution when imposing different load cases and boundary conditions on the finite element models of figures 2.6-2.9. The following load cases were consequently created and analyzed:

Load case 1: Full penetration T-piece with fixed ends and vertical loading corresponding to the test piece setup as shown in figure 2.2. The stresses in the horizontal member (bending stresses) and the vertical member (tensile stresses) were analyzed.

Load case 2: Full penetration T-piece with tensile loading on the horizontal member. The other end was clamped in. Tensile stresses in the horizontal member were analyzed.

Load case 3: Full penetration T-joint with a bending load on the horizontal member. The other end was clamped in. Bending stresses in the horizontal member were analyzed.

Load case 4: Symmetrical full penetration cruciform joint with tensile loading on the horizontal members and one end fixed. Tensile stresses in the horizontal member were analyzed. The loading and boundary conditions are shown in figure 2.13.

Load case 5: Full penetration T-piece with a fixed base and a combination of vertical and horizontal loading on the vertical member as shown in figure 2.14. The combined effect in the vertical member was analyzed.

Load case 6: Full penetration T-piece with a fixed base and a horizontal loading on the vertical member similar to that shown in figure 2.14. The bending stresses in the vertical member were analyzed.

Load case 7: Full penetration cruciform joint with fixed ends and horizontal loading on the vertical member. The bending stresses in the vertical member were analyzed.

Load case 8: Full penetration cruciform joint with fixed ends and a combination of vertical and horizontal loading on the vertical member. The loading is similar to that

shown in figure 2.14 while the boundary conditions corresponds to those shown in figure 2.7

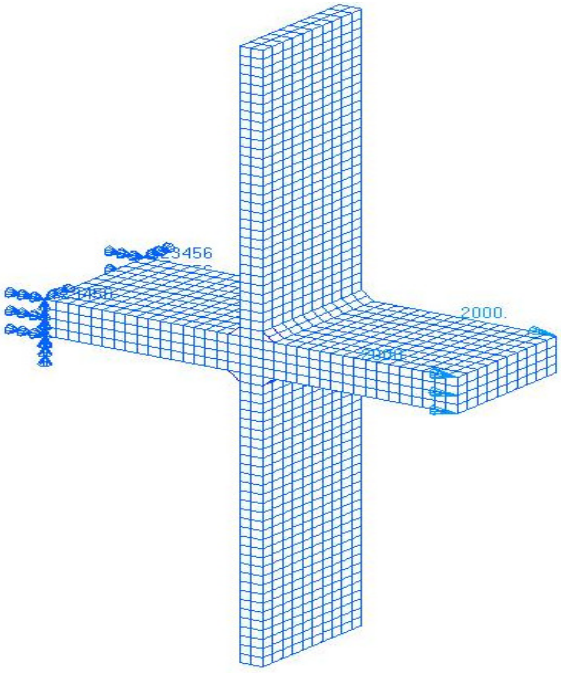

Figure 2.13: Symmetric cruciform solid element model with horizontal loading.

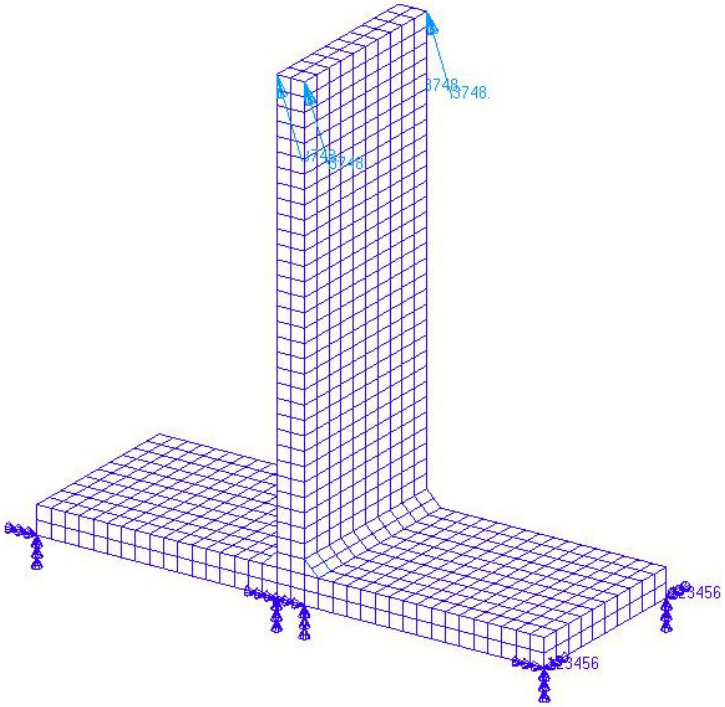

Figure 2.14: Solid element, 20-noded model with fixed base and combined loading.

The numerical results are summarized in the figures that follow. The origin of the x-axis represents the weld toe while the units on the x-axis correspond to the spatial dimensions of the vertical or horizontal leg of the specimen. It can be seen throughout figures 2.15 to 2.26 that explicit modeling of the weld by means of inclined shell elements give either the closest resemblance to the solid element models or at least, conservative results i.e. a higher stress response than the solid model. In some cases the differences in the stress distribution obtained from the various models are not clear due to the discontinuity of the finite element results at the weld toe causing large stresses and thus corrupting the scale of the graph (e.g. figure 2.16). Additional graphs showing a closer view of the stress response in the vicinity of the weld are included in such cases.

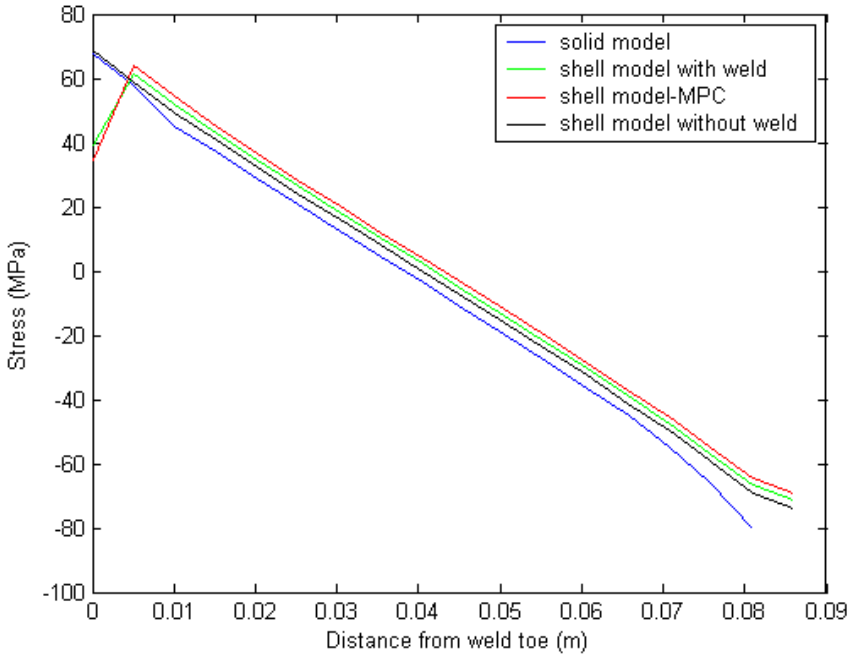

Figure 2.15: Finite element bending stress results for load case 1 (3.535 kN).

As can be seen from figure 2.15, the solid elements predict the lowest bending stress value throughout the horizontal member, except in the vicinity of the weld. This is due to the sensitivity of the solid elements towards the stress concentration at the weld toe while the shell elements experience a discontinuity at the weld toe. Thus in order for equilibrium to be established, the remaining stress distribution in the solid model has to be a bit lower than the shell elements since the integral of the moments around the weld toe for both the solid and shell models has to be equal to F*l* /2 where F is the vertical force and *l* the length of the specimen, i.e. *l*/2 is the distance from the point of application of the force to the weld toe. The following relationship should thus hold:

$$\int_0^l \sigma_x A x dx = F\frac{l}{2} \qquad [2.6]$$

where σ_x is equal to bending stress in the horizontal member and A is the sectional area of the horizontal member

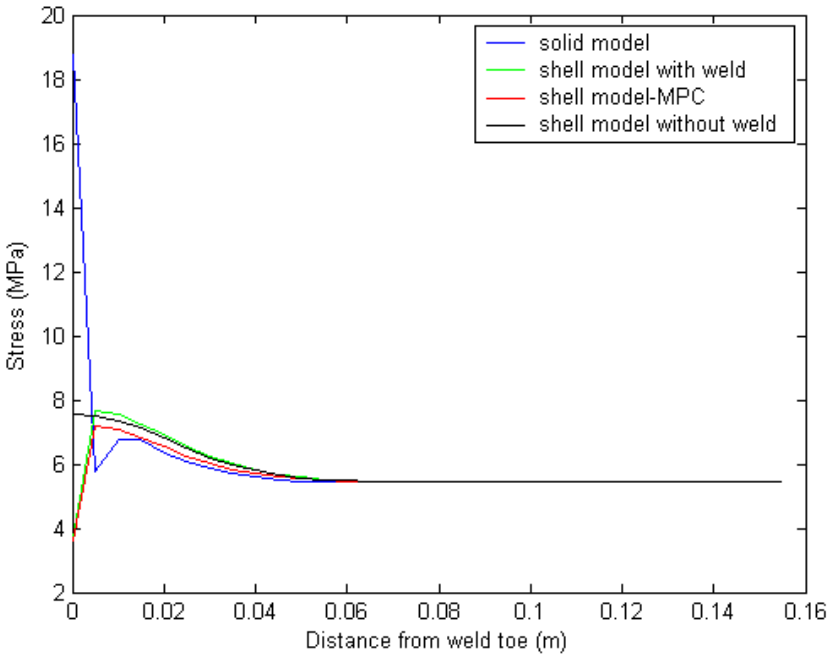

Figure 2.16: Finite element tensile stress results for load case 1 (3.535 kN).

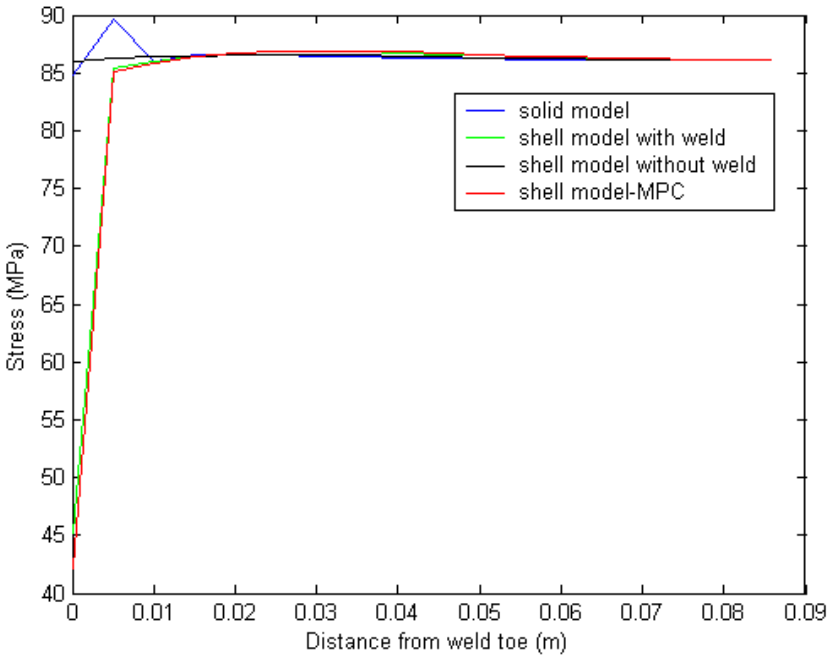

Figure 2.17: finite element tensile stress results for load case 2 (56 kN).

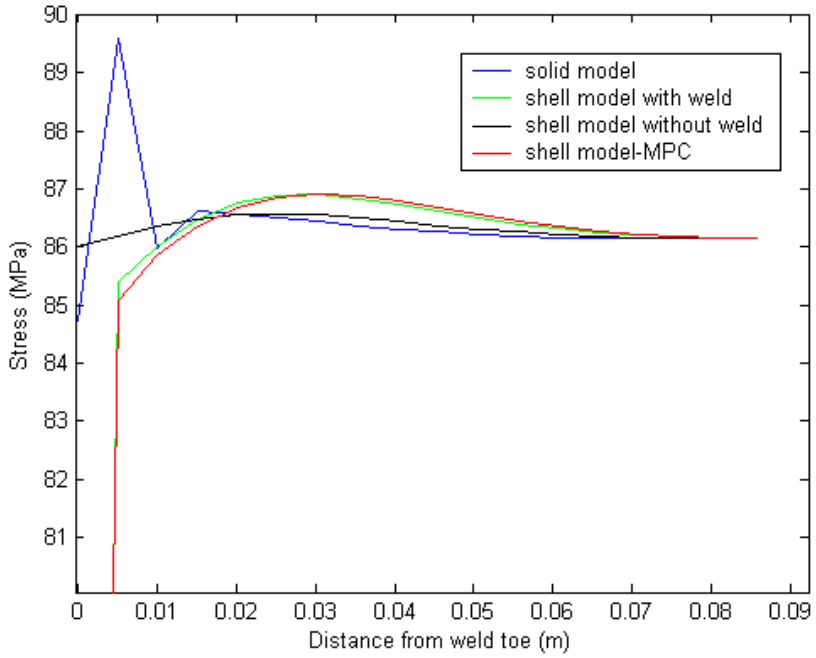

Figure 2.18: Finite element tensile stress results close up view for load case 2 (56 kN).

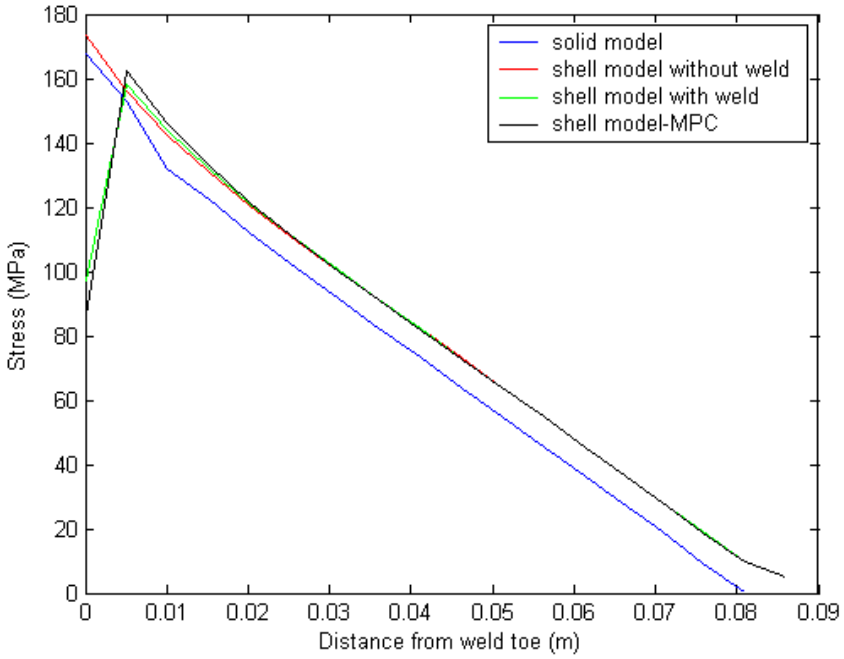

Figure 2.19: Finite element bending stress results for load case 3 (2 kN).

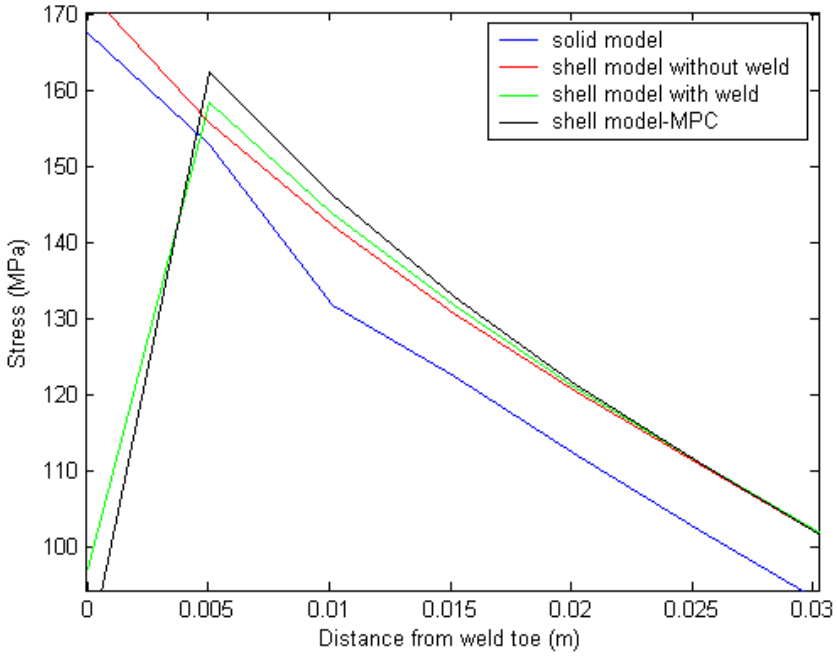

Figure 2.20: Finite element bending stress results close up view for load case 3 (2 kN).

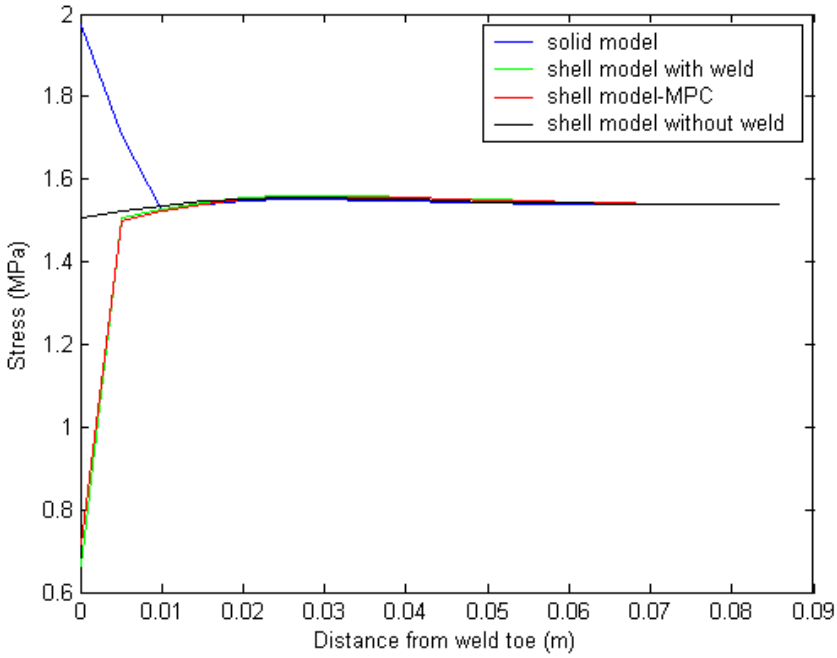

Figure 2.21: Finite element tensile stress results for load case 4 (2 kN).

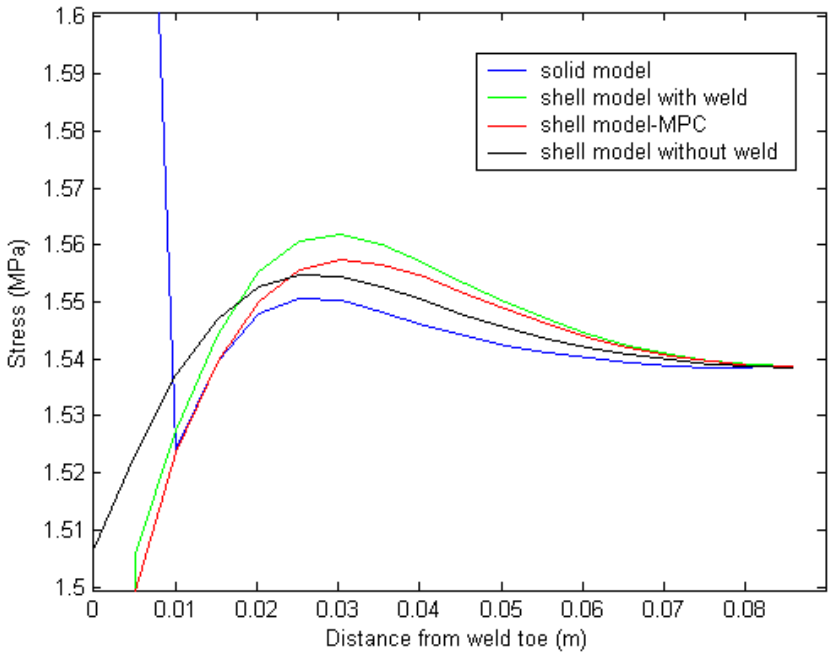

Figure 2.22: Finite element tensile stress results close up view for load case 4 (2 kN).

Note that figures 2.23 and 2.24 contain no results for the multi-point constraint (MPC) mesh, since the MPC and the fixed base boundary condition clash due to the fact that two different displacement constraints are imposed on the same nodes. This is a shortcoming of the MPC technique although it is not considered a serious one since constraints of the nature encountered in load case 5 and load case 6 are not very common in practice. It should, however be noted by the analyst in the event of similar constraints occurring in practice. The results for load case 6 corresponded exactly with load case 5 (figures 2.23 and 2.24) except for a constant offset in the stress values caused by the tensile stress in the vertical member.

From closer inspection of figures 2.15 to 2.26 it can be noted that the representation of the weld by means of inclined shell elements as portrayed in figure 2.7 gave the closest resemblance to the solid element solution. In cases where a better correlation was achieved with other configurations, the shell representation of the weld still gave conservative results as for example in figures 2.16 and 2.18. The use of MPCs often gave non-conservative results as can be seen in figures 2.25 and 2.26. This also holds for shell models with no weld representation in certain cases such as can be seen in figure 2.26. These considerations led to the conclusion that the representation of the weld by means of inclined shell elements gives the best results, since you will either achieve reality (which is approximated by the solid elements) or be conservative in terms of the cases considered.

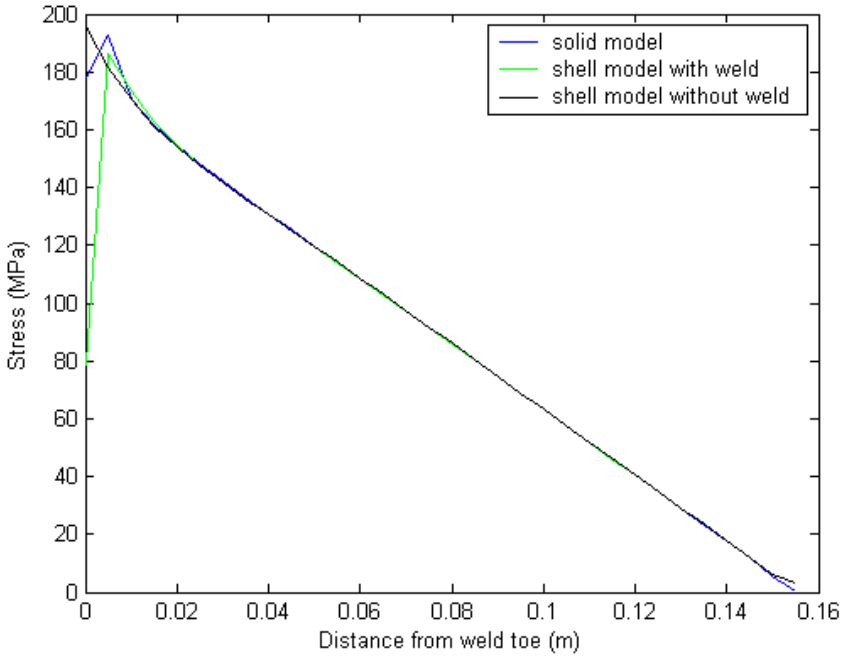

Figure 2.23: Finite element combined stress results for load case 5 (3.535 kN, y-direction and 1.246 kN, x-direction).

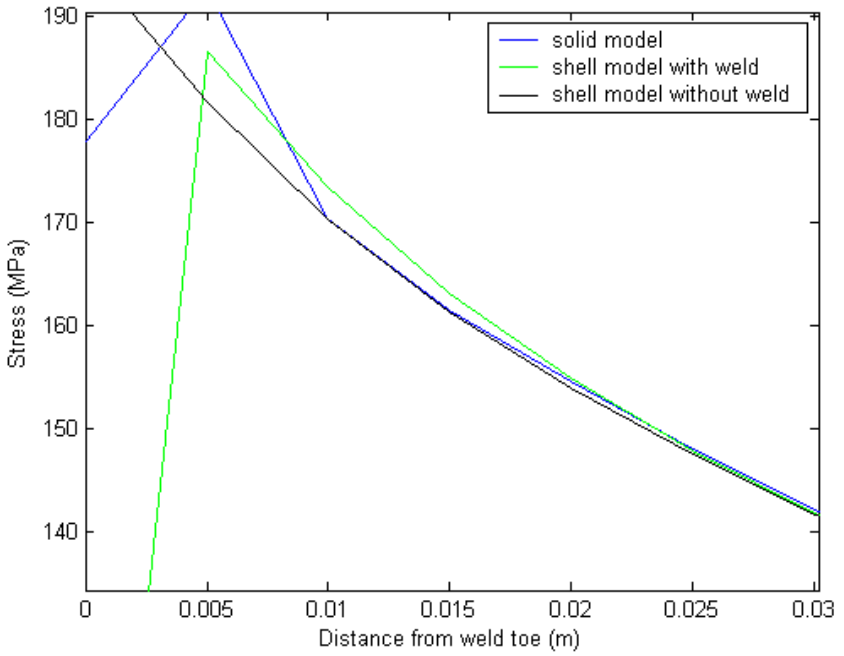

Figure 2.24: Finite element combined stress results close up view for load case 5 (3.535 kN, y-direction and 1.246 kN, x-direction).

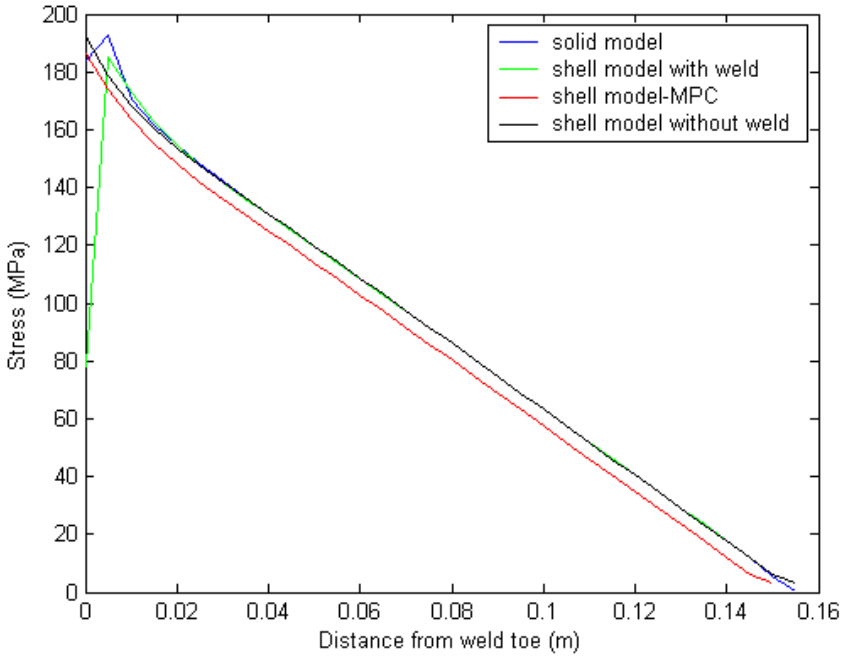

Figure 2.25: Finite element bending stresses results for load case 7 (1.246 kN).

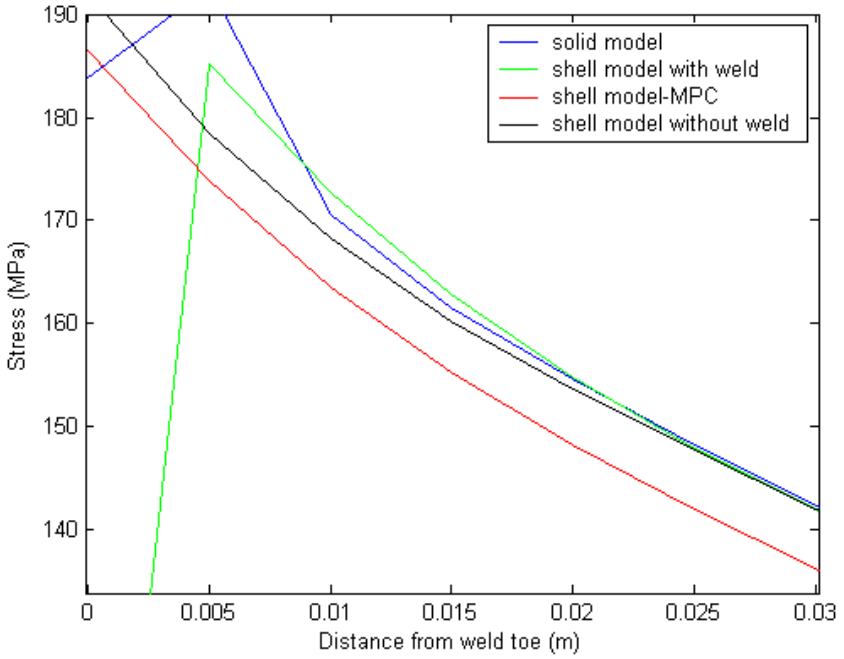

Figure 2.26: Finite element bending stresses results close up view for load case 7 (1.246 kN).

It is also noted that the difference in stress response between the various configurations lies primarily in the vicinity of the weld toe, i.e. in the region affected by the stress rise due to the weld toe and the plate intersection or structural discontinuity. The differences in stress values in these zones vary from 1% to 2% in the case of tensile stress distributions such as load case 4 and load case 2. In the case of bending stress distributions the differences between the weld modeling with shell elements and ordinary equivalencing can be up to 5% while the differences between inclined elements and MPCs can be as large as 13% for the load cases considered. In almost all of the load cases the solutions obtained by the various configurations converged once the effect of the stress concentration/raise is eliminated (for example load case 1 (tensile) to 6. In some cases the solutions obtained from the MPC configurations never converged to the other solutions but stayed non-conservative. Load case 7 serves as an example. Typical differences between the stress values obtained in these converged regions were in the order of 0.1% of which load case 5 is an example. The bending stresses in load case 1, however, never converged and the difference between the model with weld modeling and the model with ordinary equivalencing remained up to 6%. In view of the above findings the following conclusions emerge:

1. Modeling by means of MPCs should be avoided where possible since significant errors (on the unsafe side) and modeling difficulties (such as was encountered in load case 5 and 6) can arise.
2. In most cases the difference between the results obtained with weld modeling and those without weld modeling (ordinary equivalencing) were very small resulting in the notion that explicit weld modeling were superflous. There were cases, however where the results obtained from the equivalenced models, i.e. no weld modeling, differed from the results obtained through weld modeling with up to 6%. Such an error in stress could result in a significant error in predicted fatigue life due to the highly non-linear nature of the S-N relation.

It is thus concluded (from the investigated geometries and load cases) that modeling by means of inclined shell elements will always give safe results. Stress extraction, as will be seen in the next section is also simplified since the geometrical position of the weld is better highlighted in the finite element model. In view of the marginal additional effort connected to the application of inclined shell elements in the weld modeling of plate-like configurations it is recommended that inclined elements are implemented in practice since the analyst will be able to apply it with confidence.

2.4.2 Finite element mesh and nominal stress extraction

The exact configuration of the recommended shell element mesh is shown in figure 2.27. Note that t represents the plate thickness. The inclined elements representing the weld also have a thickness of t. All the nodes in the vicinity of the weld are equivalenced. L is the weld leg length (usually 0.5 to 0.7 times the plate thickness). It was further found that in order to achieve convergence of stresses, the first ten elements adjacent to the weld element must have a length of 0.5t. This constraint is imposed in order to ensure a sufficiently accurate stress distribution in the vicinity of the weld. This constraint, however, holds only for plate thicknesses of up to 10mm.

For plates thicker than this, the maximum element size for the first ten elements adjacent to the weld remains 5mm in order to capture an accurate stress distribution.

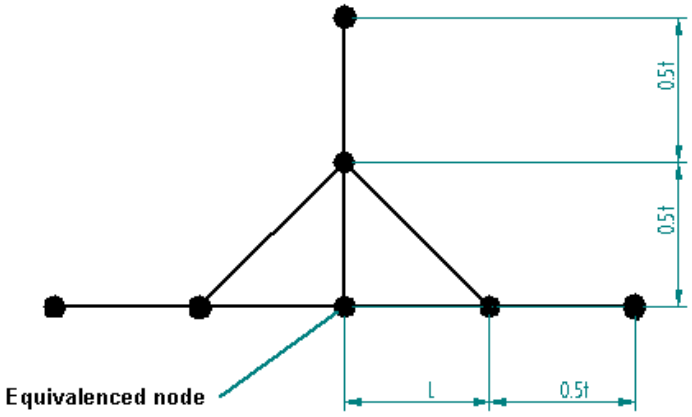

Figure 2.27: Full penetration weld modeling by means of shell elements.

At this point the question will be asked why the thickness of the inclined elements was chosen equal to the plate thickness. The thickness of the inclined element will determine the element's stiffness and consequently the stiffness of the weld representation as well. Since the stiffness of the element is determined by its thickness, it is reasonable to assume that an element with a high thickness will result in stiffness characteristics that tend towards a MPC, while a very low thickness will tend towards ordinary equivalencing. This notion is verified when figure 2.28 is studied which shows a close up view of the finite element results in bending for load case 1. The thickness of the inclined elements, i.e. the weld thickness were varied between 0.1 and 10 times the plate thickness and the stresses obtained compared to those obtained from the equivalenced models without weld representation as well as those containing MPCs.

From figure 2.28 it becomes clear that the model containing inclined elements with a thickness of 10 times the plate thickness yield the closest resemblance to the stresses obtained from the MPC model, while the model with inclined elements of a low thickness (0.1 times the plate thickness) tend towards the solution obtained from the model with no weld representation. When considering this trend it can be deduced that by varying the inclined elements' thicknesses, the results will always lie between the boundaries set by the two extreme cases, all of which were included in the previous analyses. When the previously obtained finite element results are studied it can further be noted that increasing the element thickness would yield more conservative results in some cases and thus tend towards MPC behavior (for example load case 1), while the same effect would be obtained in other cases when the thickness was decreased as can be seen from figure 2.22 (load case 4) where the model with no weld representation gave the highest stress values in the vicinity of the weld.

In view of the above fact it is concluded that setting the inclined elements' thickness equal to the plate thickness yields sufficient results to obtain good, conservative engineering solutions for the stress fields in the vicinity of the welds.

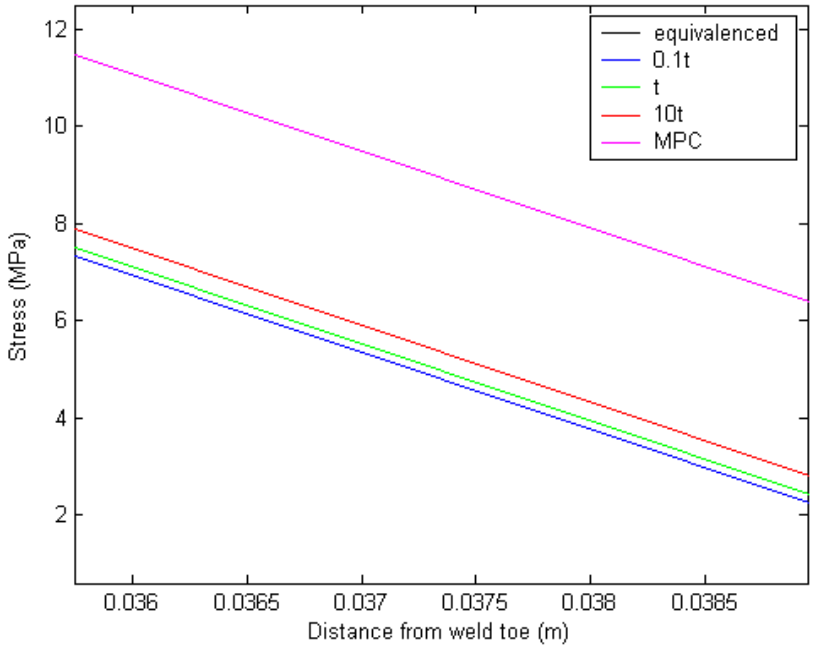

Figure 2.28: Finite element bending stress results for load case 1 with different thicknesses of the inclined elements representing the weld (3.535 kN).

Having a thickness equal to the plate thickness also allows faster and easier modeling procedures in the finite element packages since the properties of the elements representing the weld can be allocated together with the properties of the elements representing the associated members in the region.

The next step was to determine the manner and position where the nominal stress suitable for implementation with the nominal stress S-N curve must be extracted. As previously mentioned, the requirement for a stress parameter or value to be considered nominal was that it should not include any effects of the macro geometrical stress concentration due to the intersection formed by the joint or stress raising effects due to the notch formed by the weld toe. The extraction of nominal stress was found to be dependent on the loading mode. As can be seen by comparing figures 2.16 and 2.23, for instance, the position where nominal stress is reached differs considerably in the case of tension as opposed to bending. In the case of bending, irrespective of the boundary conditions or loading mode, the non-linear stress peak and macro geometrical stress concentration due to the weld disappeared at a distance of 25mm from the weld toe. This becomes clear when studying figure 2.29, which shows the bending stresses for load cases 1, 3, 5, 6, 7 and 8 on one graph. The stresses are those obtained by modeling with inclined shell elements.

For the case of tension the nominal stress (F/A) is only reached at a distance of 70mm from the weld toe for both the load carrying and non-load carrying cases. This becomes clear when figures 2.16, 2.17, 2.18, 2.21 and 2.22 are studied. The recommendation is thus to extract the stress value at a distance of 70mm from the weld toe in the case of tensile loading to obtain the nominal stress.

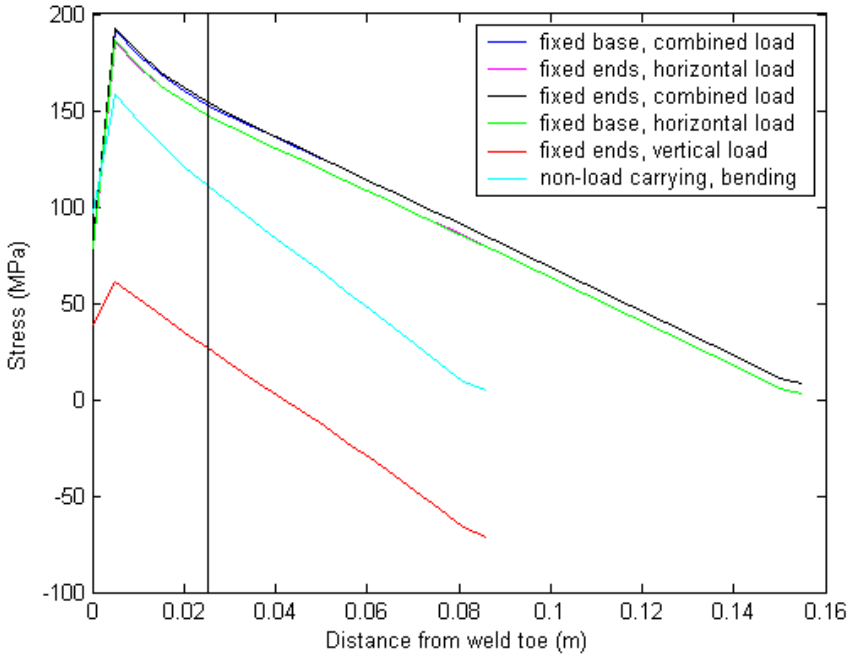

Figure 2.29: Finite element bending stresses for different load cases to illustrate the common geometrical position of the stress concentration due to the weld.

This is also the value of stress that must be used for nominal stress with the S-N curve as required by the various design codes implementing the nominal stress method such as the BS and the IIW. In the case of bending the stress should be extrapolated to obtain the value at the weld toe due to its linear distribution. The foremost point of extrapolation should be taken at a distance of 25mm from the weld toe to avoid including the stress peak due to the weld and the geometrical discontinuity. The second point can be taken at any point further away than 25mm from the weld toe, for instance at 40mm. Figure 2.30 shows an example of the procedure. The philosophy behind the extrapolation scheme and its compatibility with the design codes and procedures will be discussed in the subsequent sections.

To date the non-load carrying T-piece with a stiffener as shown in figure 2.31 has not been included in the investigation. It has already been established that the meshing configuration in figure 2.27 gives the best results in the case of T-piece configurations but an inclined element can, however, not be implemented in the case of a plate-stiffener configuration because the face of the inclined element and the stiffener will not be in the same plain. The only options that are left is thus ordinary equivalencing of the nodes at the intersection of the plate and stiffener or the implementation of MPCs. Figure 2.31 shows a finite element model of the plate-stiffener configuration with implementation of MPCs and a bending load. Finite element analyses were once again performed for both bending and tensile loading on the plate stiffener configuration, including models containing MPCs and ordinary equivalencing. The geometrical position where the stress response gets non-linear due to the stress raising effect of the intersection and weld toe was accordingly determined.

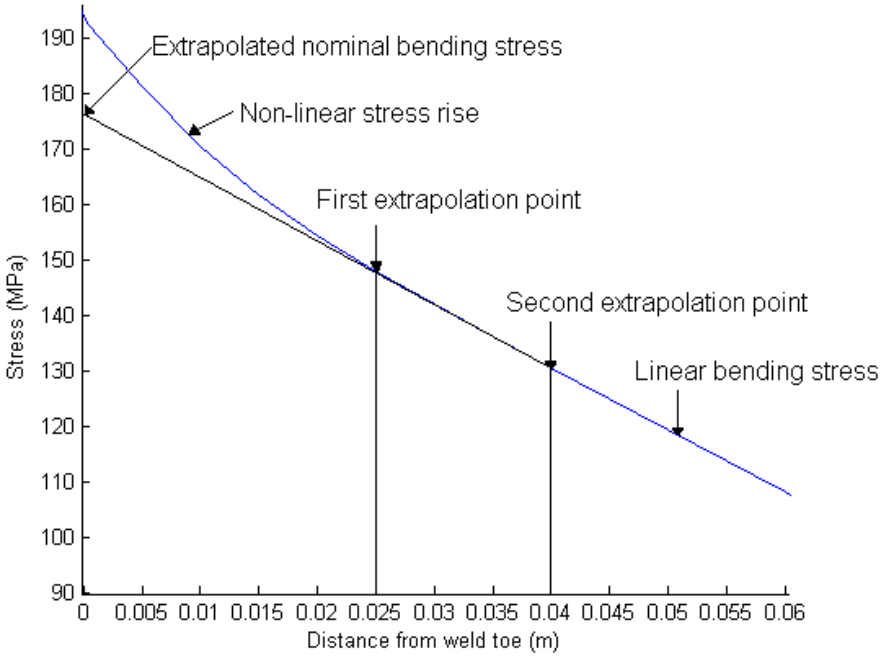

Figure 2.30: Linear extrapolation procedure for nominal bending stress extraction.

The finite element results are shown in figures 2.32 and 2.33. The origin of the graph once again represents the weld toe of the stiffener while the x-axis represents the geometrical distance from the weld toe along the longitudinal axis of the configuration. From the finite element analyses two deductions can be made.

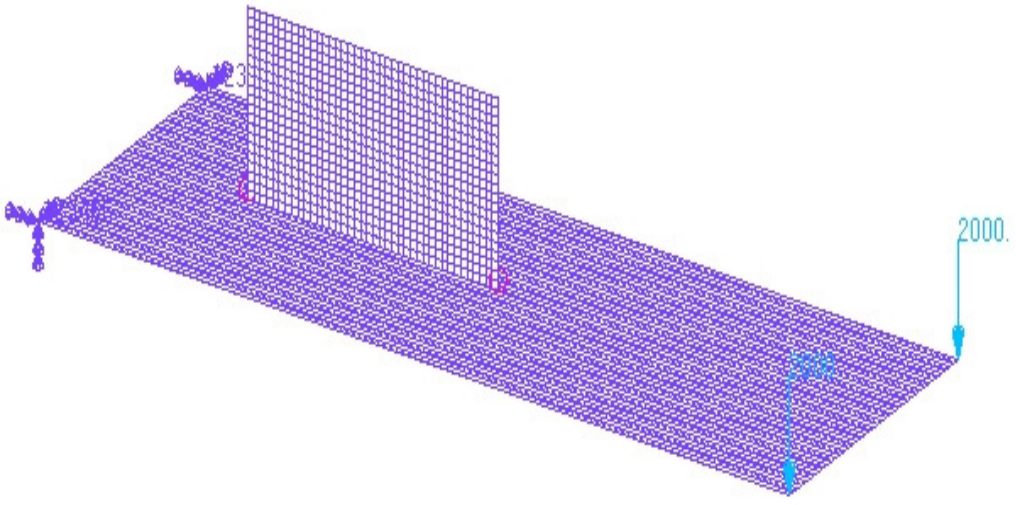

Figure 2.31: Finite element model with MPCs of a plate-stiffener configuration.

Firstly it can be seen that the MPC model predicts slightly higher far field stress values (in the order of 3%) than ordinary equivalencing, making them more conservative.

Secondly, it is clear that the position of the non-linear stress peak remains the same as the previously obtained results in the case of tensile loading, namely at a distance of 70mm from the weld toe but in the case of bending shifts to a distance of 50mm from the weld toe instead of 25mm as was previously determined for load and non-load carrying T-pieces. The nominal stress in the case of bending must thus be determined by extrapolation where the foremost point of extrapolation should be taken at a distance of 50mm from the weld toe to avoid including the stress peak due to the weld and structural discontinuity. This indicates that the position where the stress response gets non-linear is subject to the geometrical configuration of the weld category. The implication thereof is that the establishment of a generic stress extraction scheme is not viable and that each new category should be separately and independently analyzed.

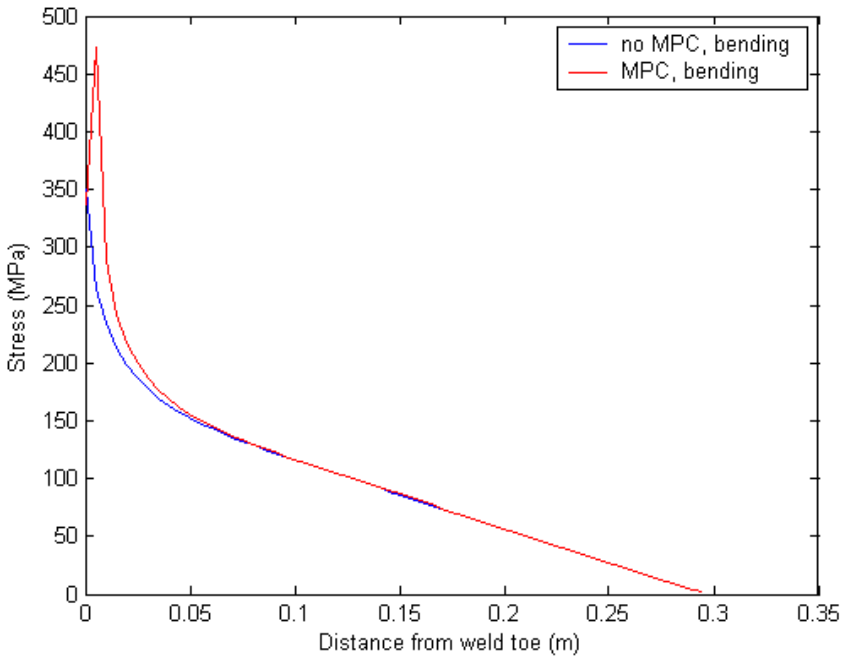

Figure 2.32: Finite element bending stress results along the longitudinal axis of the plate-stiffener configuration for the loading as shown in figure 2.31.

When the stiffener is welded in the same plane as the plate, i.e. a normal T-piece, such as is modeled in figure 2.14, but loaded in bending, the vertical member is not loaded while the horizontal member is in bending, i.e. the vertical member acts as the stiffener (load case 3). The results for such case stay the same as for a load carrying T-joint as can be seen in figure 2.19, i.e. the foremost point for extrapolation should be taken at a distance of 25mm from the weld toe in the case of bending. In the case of tension the problem corresponds with the load cases 2 and 4 analyzed earlier in this chapter. The results obtained for those cases indicated that the nominal stress

corresponding to the analytical tensile stress was reached at a distance of 70mm from the weld toe, similar to the load carrying case.

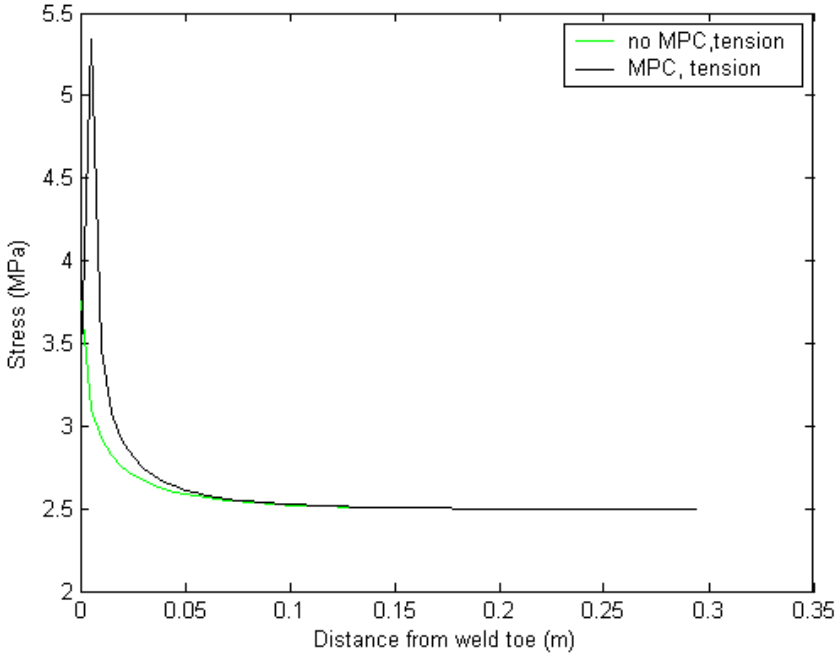

Figure 2.33: Finite element tensile stress results along the longitudinal axis of the plate-stiffener configuration.

2.4.3 Analyses of plate thickness dependence of the position of the non-linear stress rise

The following question that had to be addressed was whether the findings concerning the position for nominal stress extraction of the previous section are valid for thicker and thinner plates as well. The element size, however, was determined to be sufficient for convergence before the analyses were done. Consequently a further sensitivity analysis was done to investigate the above recommendations' dependence on plate thickness. The following variations on all of the load cases 1 to 8 were done:

- 20mm plate with 10mm weld size and 10mm element size
- 20mm plate with 10mm weld size and 5mm element size
- 6mm plate with 3mm weld size and 5mm element size
- 6mm plate with 3mm weld size and 3mm element size

It was mentioned earlier that the element size in the vicinity of the weld should be equal to half the plate thickness up to a plate thickness of 10mm in order to achieve convergence of stress. The reason why the 5mm element size was implemented in the 6mm model and the 10mm element size implemented in the 20mm model was purely to illustrate loss of accuracy if larger element sizes were used and consequently to motivate the relevance of the constraint on element size. Figure 2.34 shows the finite

element results for different plate thicknesses as analyzed for the load case 7, while figure 2.35 shows similar results in tension for load case 2.

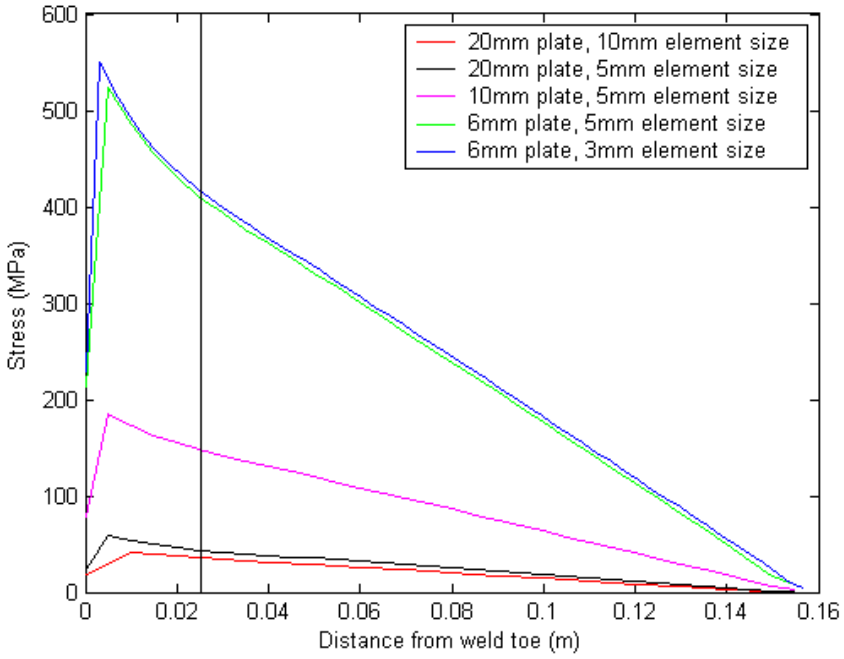

Figure 2.34: Finite element bending stress results for load case 7 for different plate thicknesses (1.246 kN).

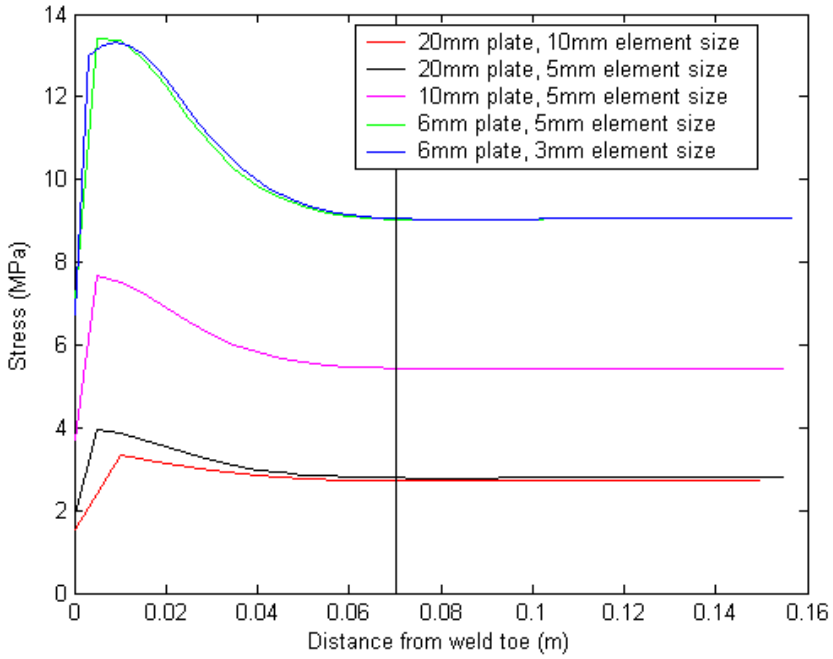

Figure 2.35: Finite element tensile stress results for load case 2 for different plate thicknesses (3.535 kN).

As can be seen from figure 2.34 and 2.35, the positions where the stress response gets non-linear and thus also the distance for nominal stress extraction are independent of plate thickness. This holds as long as the limitations on element size in terms of plate thickness are reached, i.e. that the weld is modeled with a leg length of 0.5 – 0.7 times the plate thickness and that the element size in the vicinity of the weld equals 0.5 times the plate thickness up to a plate thickness of 10mm. It can also be seen that the accuracy of the solutions decreases if the element sizes are larger than 0.5 times the plate thickness. These restrictions were mentioned earlier (section 2.4.2) and can now be seen to influence the resolution or accuracy of the stresses. It is therefore of utmost importance that convergence of stresses should always be ensured and verified by the analyst when other configurations are analyzed. The above results also held for the entire range of load cases 1 to 8 analyzed previously, although only two representative load cases are shown for the sake of clarity.

The plate thickness independence property of the position of the non-linear stress raise as shown above appears to be dissimilar to several statements in the literature where the position of the local stress peak is claimed to be a function of plate thickness. Dong (2001); Niemi (1995); Doerk et al. (2002) and Hobbacher (1996) all stated that the local stress peak due to the notch effect of the weld toe started at a distance of 0.4t in plate like structures where t equals the plate thickness. The IIW also gave such guidelines in their hot spot stress method described in their recommendations for fatigue design of welded joints and components (2004). The reason for such an ambiguity could however be accredited to the definition of the non-linear stress peak (N-LSP) as defined by the mentioned authors and the IIW as opposed to the definition of the non-linear stress rise referred to in this study. The N-LSP refers to the local notch effect of the weld toe only while the non-linear stress rise includes the macro geometrical stress concentration caused by the intersection of the plates as well as the local effect due to the weld toe.

The macro geometrical stress concentration could also be a property of the specific modeling technique (shell elements) implemented in this study since it should be kept in mind that the solutions obtained by shell elements in the vicinity of welds and plate intersections incorporates a mathematical discontinuity due to the sharp angles formed by the finite element mesh. The shell element solutions will consequently converge to the solutions prescribed by shell theory. This will become clear when the refined local finite element analyses of the following section (which do not show similar behavior) are presented.

The plate thickness independence of the non-linear stress rise relevant to the modeling technique implemented in this study is, however, an important property since it eliminates the necessity for consideration of plate thickness in nominal stress extraction and thus forms a universal, independent benchmark in the case of cruciform joints and T-pieces that can possibly be extended to other plate-like configurations. It should be noted, however, that the plate thickness independence is not necessarily true for actual welded joints in practice (as mentioned in the previous paragraph) but indeed for finite element results as obtained from shell element configurations.

As mentioned previously the philosophy behind the linear extrapolation scheme in the case of bending and its compatibility with the design codes and procedures will be discussed in the subsequent section.

2.4.4 Numerical verification of the integrity of the extrapolation procedure for nominal bending stress extraction

The recommendation for the extraction of nominal stress in the case of bending by means of extrapolation to obtain the linear value of bending stress at the weld toe in section 2.4.2 proceeds from the assumption that a bending stress distribution of such quantity causes a local stress situation at the weld toe similar to that caused by a nominal tensile stress of the same magnitude. The need for such equivalence arose due to the fact that the category S-N curves found in the fatigue codes and standards such as BS 7608 and the IIW recommendations were constructed from fatigue test results obtained by tensile loading of the relevant weld categories. No explicit results for bending thus exist in the fatigue design codes. Figure 2.36 shows a T-joint loaded in bending with the resulting linear stress distribution and bending stress, σ_b, as well as the assumed equivalent tensile stress σ_t on the same specimen. Note that $\sigma_b = \sigma_t$.

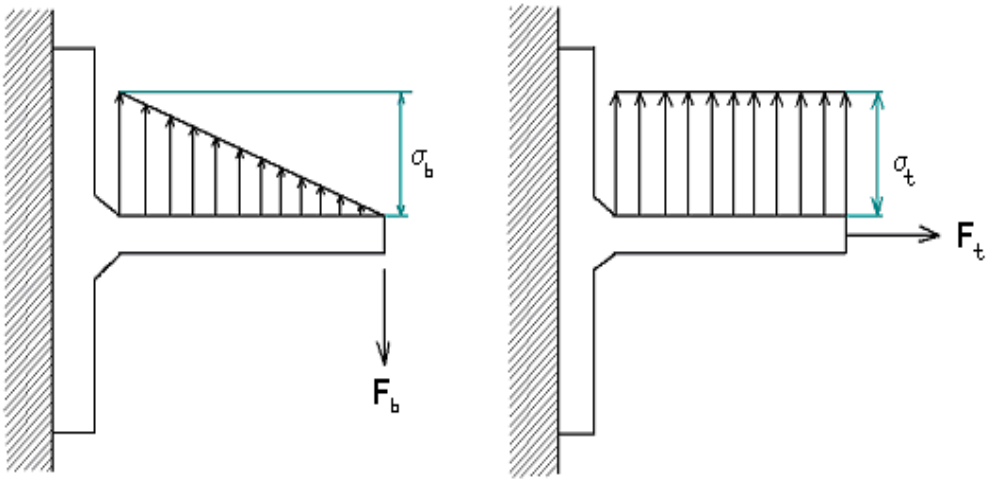

Figure 2.36: Bending stress on a clamped T-piece and the assumed equivalent tensile stress implied by the extrapolation technique.

In view of the above facts the need arose to ascertain that the linear bending stress at the weld toe, similar to the structural hot spot stress as defined by the IIW, obtained by the abovementioned procedure resulted in a local stress state around the weld toe of smaller or at least equal magnitude than that resulting from a uniform nominal tensile stress of the same value. This had to be established to ensure conservative results. To achieve this, two pairs of two-dimensional finite element models of the T-piece in figure 2.30 were created with a very fine mesh consisting of 2D quad8 shell elements – one pair had a fully clamped vertical member while the other had clamped in ends. The weld toe was modeled by means of a 3mm radius - similar to the effective notch stress method described by the IIW, to capture the notch effect at the weld toe accurately. Bending and tensile loading was imposed on the two pairs respectively, the forces F_t and F_b acting on the models being of such magnitude that

the linear bending stress (determined by extrapolation) at the weld toe due to F_b on the one model was equal to the uni-axial tensile stress at the weld toe due to F_t on the other model - comparable to the situation depicted in figure 2.36.

In order to establish whether the bending stress extraction method is viable and conservative, the local stress at the notch of the two models will be compared, since welding fatigue is in effect a local phenomenon, which is governed by local stresses in the vicinity of the weld toe. It is thus assumed that the bending stress extraction method will be viable if the local stresses due to F_b is smaller than or equal to those caused by F_t, since lower local stresses will result in better fatigue resistance. Figure 2.37 shows the finite element model loaded in bending together with a close up of the weld and mesh. Note the fine mesh as opposed to previous models as well as the modeling of the weld toe by means of an arc with a 3mm radius.

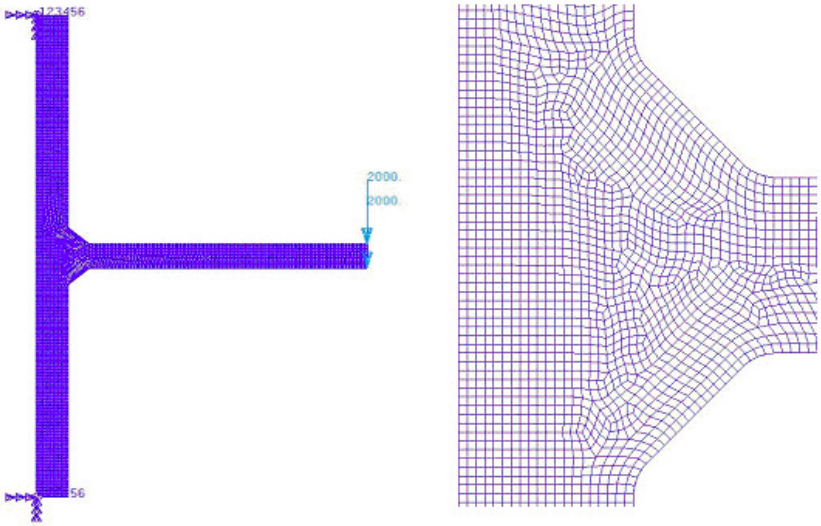

Figure 2.37: Two-dimensional finite element model of the T-piece with a 2 kN bending load.

The first analysis was done in bending with a load of 2 kN as shown in figure 2.37. The linear bending stress was extrapolated to the weld toe to obtain the nominal bending stress (excluding the stress peak), i.e. σ_b of figure 2.36. This stress was found to be 209.5 MPa for both the fully clamped and fixed end models. From this value, in turn, the tensile force needed to cause a nominal tensile stress, σ_t , of the same magnitude was found to be 104.75 kN. It was imposed on the models and a second pair of analyses, this time in tension, was done. The results are shown in figure 2.38.

The stress situation depicted in figure 2.38 is analogous to that shown in figure 2.36 except that local stresses at the weld toe are included. It is clear that the stress peak in the fully clamped case due to bending (290 MPa) is smaller than the one caused by tensile loading (337 MPa). The same holds for the fixed end models although the stress distribution in the tensile case differs from that obtained in the fully clamped model.

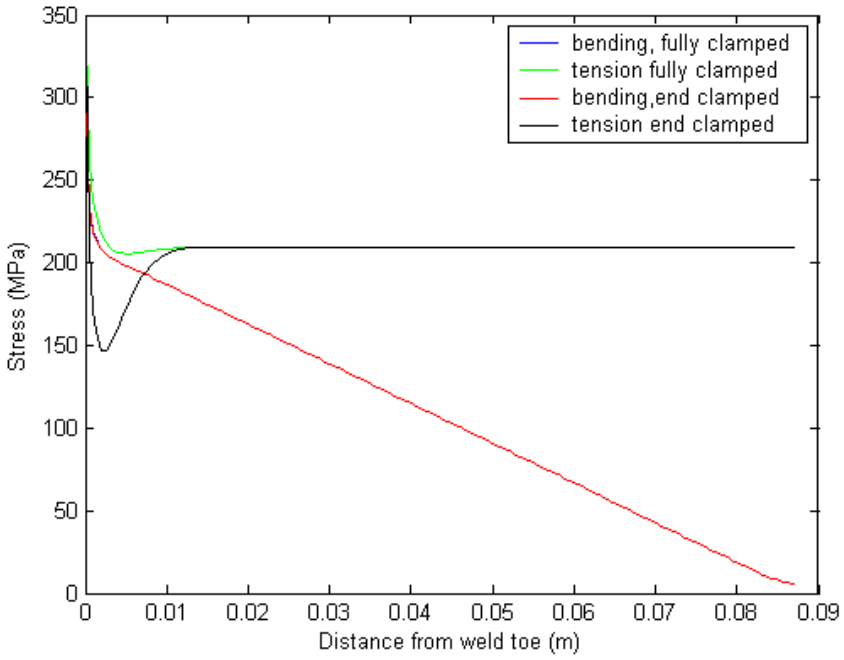

Figure 2.38: Finite element bending and tensile stress results obtained from the two dimensional shell model.

The difference in boundary conditions did not cause dissimilar stress distributions in the case of bending, however. It is consequently concluded that the bending stress extraction procedure by means of extrapolation to the weld toe as depicted in figure 2.30 is conservative and thus viable in practice. Finally the difference in the behavior of the non-linear stress rise between the two-dimensional model with local weld modeling and a very fine mesh and the ordinary shell models, implemented earlier should be noted. Firstly it is noted that the non-linear stress rise starts much closer to the weld toe (in the region of 4mm) than with the ordinary shell models. If the fact that the plate thickness of the two dimensional models above was once again equal to 10mm are considered, the non-linear stress rise at a distance of 4mm from the weld to (i.e. 0.4t) are in good correlation with the statements in the literature by Niemi, Dong, Doerk and Hobbacher, mentioned in section 2.4.3. The difference in stress response observed between the local and ordinary shell models also agrees with the arguments on shell element behavior concerning mathematical discontinuities at the weld toe, also discussed in section 2.4.3.

2.4.5 Nominal stress extraction under combined tension and bending

In view of the results, concerning nominal stress extraction, reached in section 2.4.2, it becomes clear that the position for nominal stress extraction is dependent on the type of load, i.e. tension or bending. Consequently, some sort of differentiation between bending and tensile stress needs to be made. Since the analyses in section 2.4.2 were all done for isolated cases of bending and tension respectively or for combined cases where the bending stress contribution were considerable higher than the tensile stress distribution, the question arose as to how the nominal stress should be extracted in the case of combined bending and tensile loading. This is essential

since in practice a considerable number of structural members in a complex structure experience a combination of bending and tension. Since the nominal stress should be extracted at a position of 70mm from the weld toe (both in load carrying and non load carrying cruciform joints) for pure tensile loading and at 25mm and 50mm respectively for cruciform joints, T-pieces and plate-stiffener configurations in the case of bending, the assumption is that some sort of relationship, combining the abovementioned positions should hold in the case of mutual bending and tension.

In order to quantify this relationship, finite element models of load carrying and non-load carrying cruciform joints were analyzed with different ratios of combined bending and tensile stress. The load carrying T-piece was analyzed first, implementing the following procedure: the finite element model was similar to the one shown in figure 2.7 with explicit weld modeling as stipulated in figure 2.27. The ends were clamped and a bending load of 1.246 kN was applied to the vertical member, causing an extrapolated nominal bending stress of 175 MPa at the weld toe. From this value a tensile load in the vertical direction that would cause the same nominal tensile stress was calculated as 114 kN. This load was then reduced to a fifth of its original size and applied to the finite element model in combination with the bending load, thus corresponding to load case 8 of section 2.4.1 The load was then increased linearly in five steps until the full load of 114 kN was reached. At this stage the nominal stress contribution of the bending and tension respectively was equal.

The resulting stress distribution in the vertical leg of the T-piece for all five load cases is shown in figure 2.39. The legend of the graph indicates the ratio of the tensile nominal stress to the bending nominal stress at the weld toe, while the vertical lines on the graph indicates the position at which the non-linear stress rise starts.

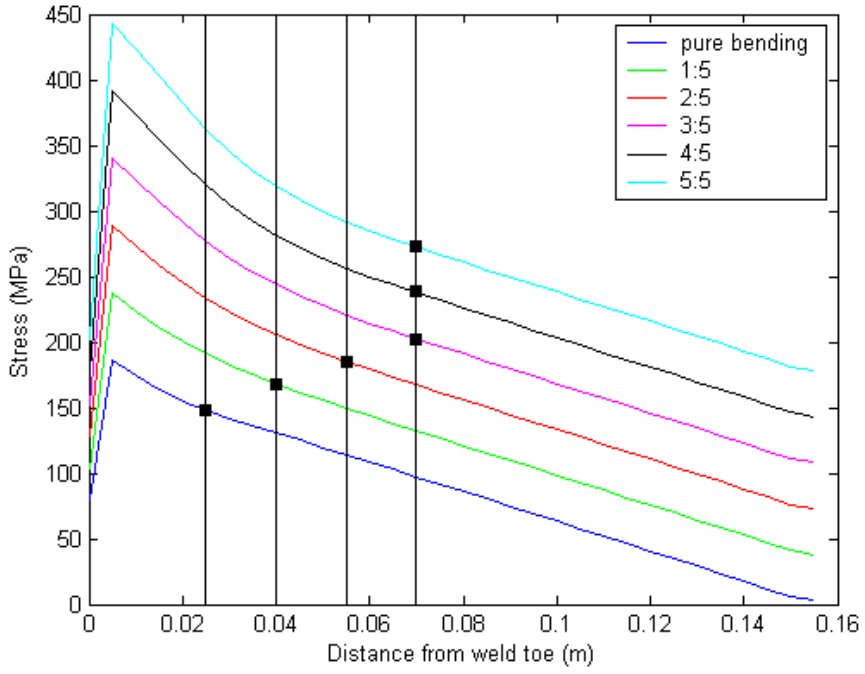

Figure 2.39: Finite element results and positions of the non-linear stress rise of the combined tensile and bending stresses in different ratios.

As can be seen from figure 2.39, the position of the stress concentration (indicated by the vertical lines) moves further away from the weld toe in a linear manner as the ratio of the tensile stress to the bending stress (hereafter referred to as the DOT – degree of tension) increases. This makes sense, since the stress concentration is further away from the weld toe in the case of tension than in bending, as shown earlier. This tendency holds up to a point of 70 mm from the weld toe and a DOT of 3:5 or 60%, after which the position of the non-linear stress rise remains the same. By considering the above information, an equation governing the position for nominal stress extraction in the case of combined tension and bending as a function of the DOT can be deduced by noting that:

- For a DOT of >3/5 or 0.6 the position stays at 70mm.
- For a DOT of 0 – 3/5 (0.6), the non-linear stress rise (N-LSR) starts at a position of 25mm (DOT = 0) to 70mm (DOT = 0.6).

Thus:

$$D = 70\,DOT + 25 \qquad [2.7]$$

where D is the distance of the foremost point of extrapolation from the weld toe (in mm). and DOT is the ratio of bending to tensile stress, expressed as a fraction.

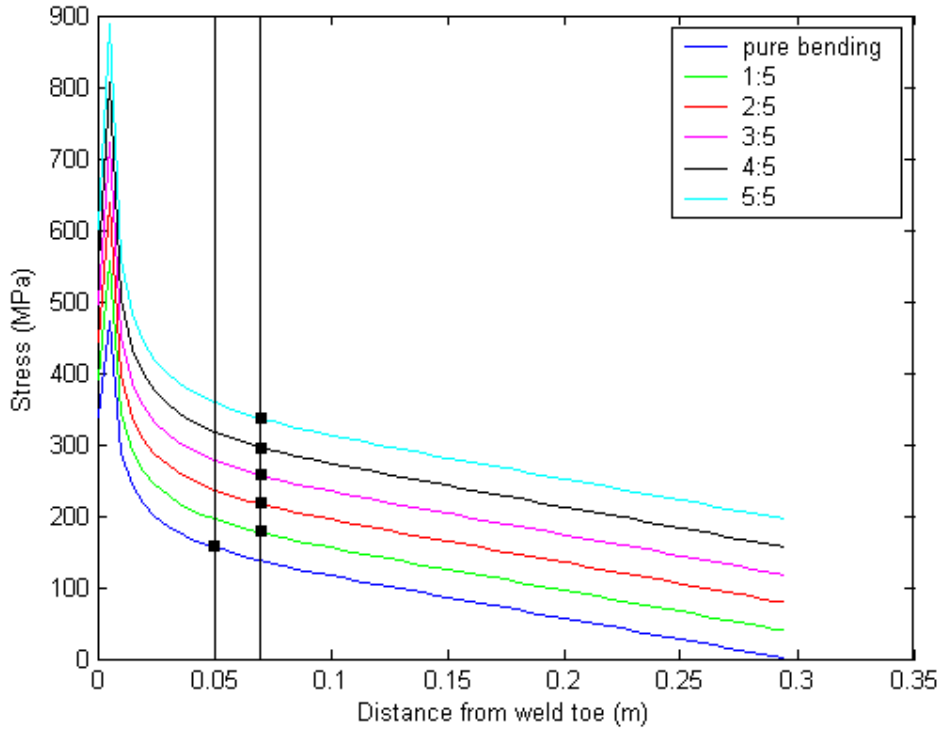

Figure 2.40: Finite element results and positions of the non-linear stress rise of the combined tensile and bending stresses in different ratios in a plate-stiffener setup.

The same procedure was repeated for the non-load carrying cruciform joint (plate-stiffener setup) similar to the one shown in figure 2.31. The limits were found to be

between 50mm (pure bending) and 70mm (DOT of 1:5 upwards). The results are shown in figure 2.40. Since the limits are so close to each other and the terminal distance of 70mm from the weld toe is reached with a DOT as small as 1:5 it is recommended that a fixed distance of 70mm for the foremost point of extrapolation is employed if any tension is present in a plate stiffener configuration.

2.4.6 Summary

At this point it is considered appropriate to give a short overview of the findings concerning the finite element modeling of welds in plate-like structures and the accompanying nominal stress extraction procedure developed in this study. A schematic representation of the finite element modeling and nominal stress extraction procedure for the different structural details and load cases considered in this chapter is presented below and will serve to provide the analyst with a summary of the findings in a compact manner and eliminate possible uncertainty that could arise due to the extensive nature of the work.

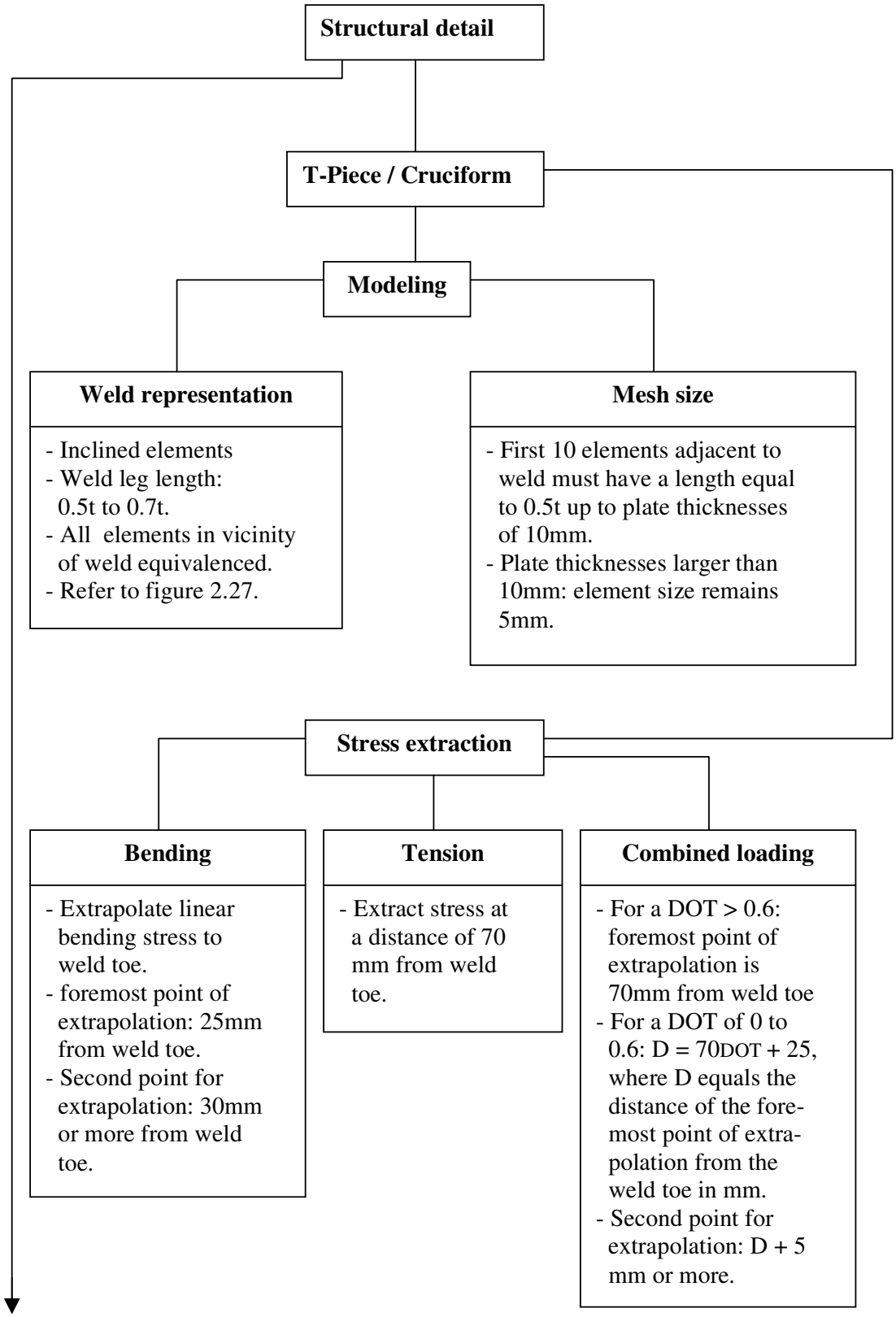
Structural detail
T-Piece / Cruciform
Modeling
Weld representation
- Inclined elements
- Weld leg length: 0.5t to 0.7t.
- All elements in vicinity of weld equivalenced.
- Refer to figure 2.27.
Mesh size
- First 10 elements adjacent to weld must have a length equal to 0.5t up to plate thicknesses of 10mm.
- Plate thicknesses larger than 10mm: element size remains 5mm.
Stress extraction
Bending
- Extrapolate linear bending stress to weld toe.
- foremost point of extrapolation: 25mm from weld toe.
- Second point for extrapolation: 30mm or more from weld toe.
Tension
- Extract stress at a distance of 70 mm from weld toe.
Combined loading
- For a DOT > 0.6: foremost point of extrapolation is 70mm from weld toe
- For a DOT of 0 to 0.6: D = 70DOT + 25, where D equals the distance of the fore-most point of extra-polation from the weld toe in mm.
- Second point for extrapolation: D + 5 mm or more.

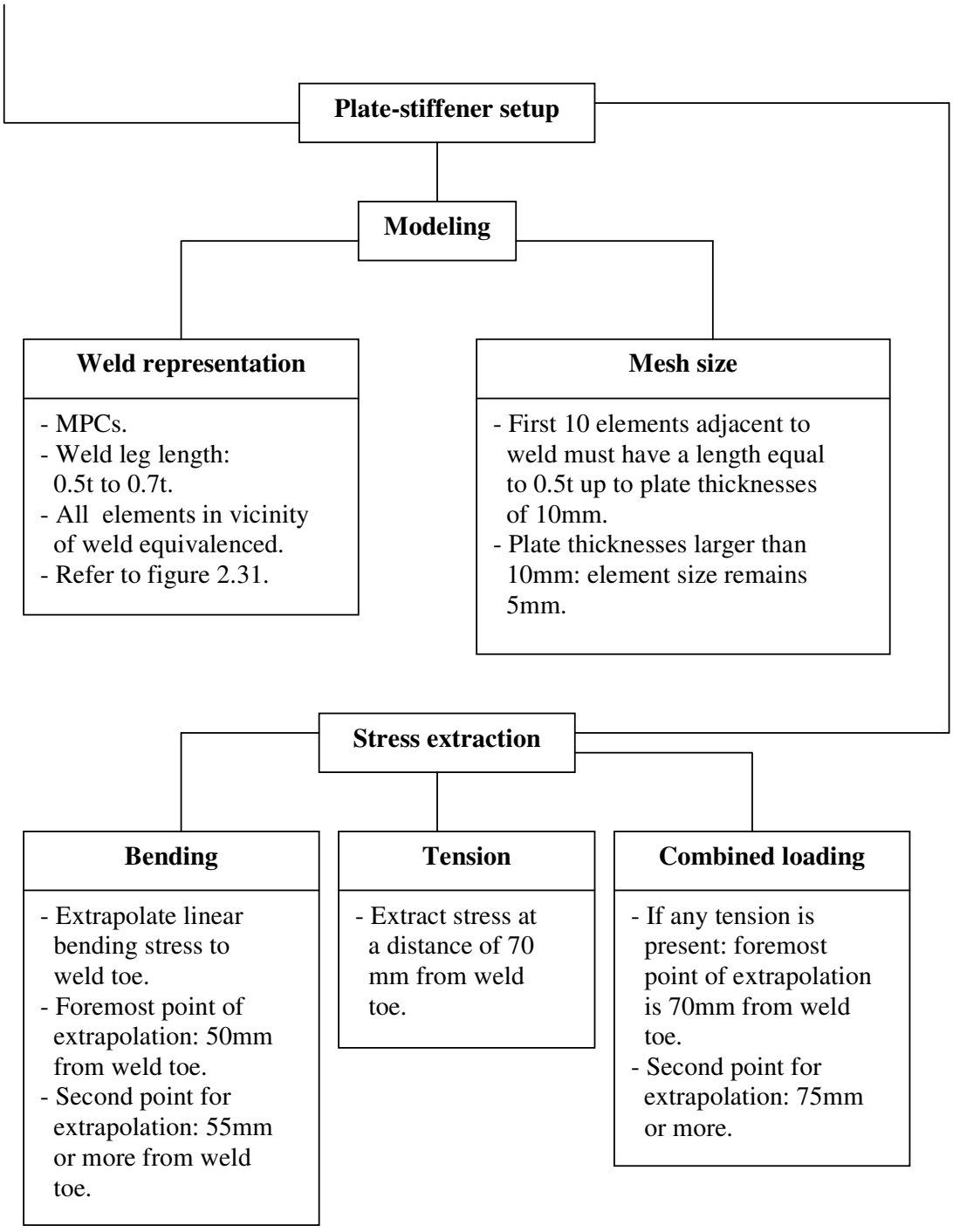

This concludes the section on finite element modeling and nominal stress extraction. The following step is thus to verify the developed procedure on a complex structure, which brings us to the design, setup and instrumentation of such a structure. This is addressed in the following chapter.

Chapter 3

3. Experimental setup for the verification of the meshing and stress extraction methodology by means of a complex structure

3.1 Nature of the test setup and procedure

The purpose of the experimental procedure is to design and manufacture a complex, plate-like structure with an H-frame-like geometry, containing a number of weld categories on which the finite element nominal fatigue design methodology can be verified. The outcome of the verification exercise is threefold. Firstly to establish that the meshing methodology, developed in the previous chapter, renders reliable results when extended to complex structures and configurations. This will be done by means of a static load test and strain gauge measurements on the structure, which will then be compared with the stresses obtained from a finite element model. The structure will be modeled according to the meshing recommendations developed in the previous chapter. The second purpose of the test rig is to establish the efficiency and reliability of the nominal stress extraction procedure, developed in chapter 2. This will be done by verifying a fatigue life prediction based on finite element results and experimental strain measurements. A life prediction based on the hot spot method will also be done by including a weld category assessable by the hot spot method in the structure. Thirdly the accuracy of the quasi-static fatigue life assessment methodology known as the fatigue equivalent static load (FESL) design methodology will be investigated. The FESL methodology is an equivalent static method for defining input loads in a finite element environment for a structure experiencing variable amplitude loading.

The structure will thus be excited by means of a stochastic signal of such nature that the response of the structure remains quasi-static. The excitation will be imposed by means of two servo-hydraulic actuators on opposite ends of the structure. The structure will simply be constrained in all other directions except the degrees of freedom taken up by the actuators. Due to the fact that there was no clamping in of the frame apart from the constraints to prevent free body motion, the stress response of the structure will solely be due to its acceleration as result of the imposed stochastic displacement and the associated inertial effects. The measured stress response of the

structure will then be used in conjunction with the results of a linear static finite element analysis in conjunction with an inertial load to determine a fatigue equivalent static load (FESL). This is an equivalent load (inertial or static) that can be imposed on the finite element model in order to determine the correct fatigue relevant stresses from which a life prediction can be made. The accuracy of the life prediction will serve as an indication of the integrity of the nominal stress extraction procedure. The relative accuracy of the hot spot versus the nominal approach can also be assessed.

In order for the above analysis to be possible the structure has to conform to certain design criteria relating to the distribution of the natural frequencies, the stiffness of the load carrying members and the nature of the weld categories. The abovementioned aspects will be discussed in the next section.

3.2 Design of the structure

3.2.1 Overall geometry and welding categories of the structure

The first step in the design procedure was to determine the geometry of the structure in such a way that the necessary weld categories could be included. The structure also had to be of such a weight that the reaction forces due to a 1g acceleration of the structure as a whole could be accommodated by the actuators imposing the displacement signals.

The preliminary design consisted of 100×10mm flat bar sheets welded in a rectangular configuration. A 40×400mm steel slab was supported in the centre by 100×10mm sheets with their longitudinal axes perpendicular to the rectangular frame. Several stiffeners as well as an additional member consisting of round tubing were included in the design. In order to create some exclusive significance for the hot spot stress method a configuration of stiffeners that are not included explicitly in the nominal stress codes were also included. Figures 3.1 and 3.2 show the geometry of the structure for the preliminary design as well as an example of each weld detail included in the structure.

The correlation of the weld details with the weld categories presented in the BS 7608:1993 and ECCS 6:1985 codes are also shown. The points numbered 1-4 on the structure correspond to the welding details shown in figure 3.2 while A and B are points where the input from the actuators are imposed on the frame (dimensions in mm). Point 5 is the part of the geometry suited for hot spot stress analysis.

The categorization is as follows:

[1]: 8.1 F - full penetration, butt-welded cruciform joint
[2]: 8.2 F2 - partial penetration, butt-welded cruciform joint
[3]: 5.3 F2 - weld toe / narrow attachment / stiffener, partial penetration
[4]: 9.6 W - hollow section welded onto plate, partial penetration

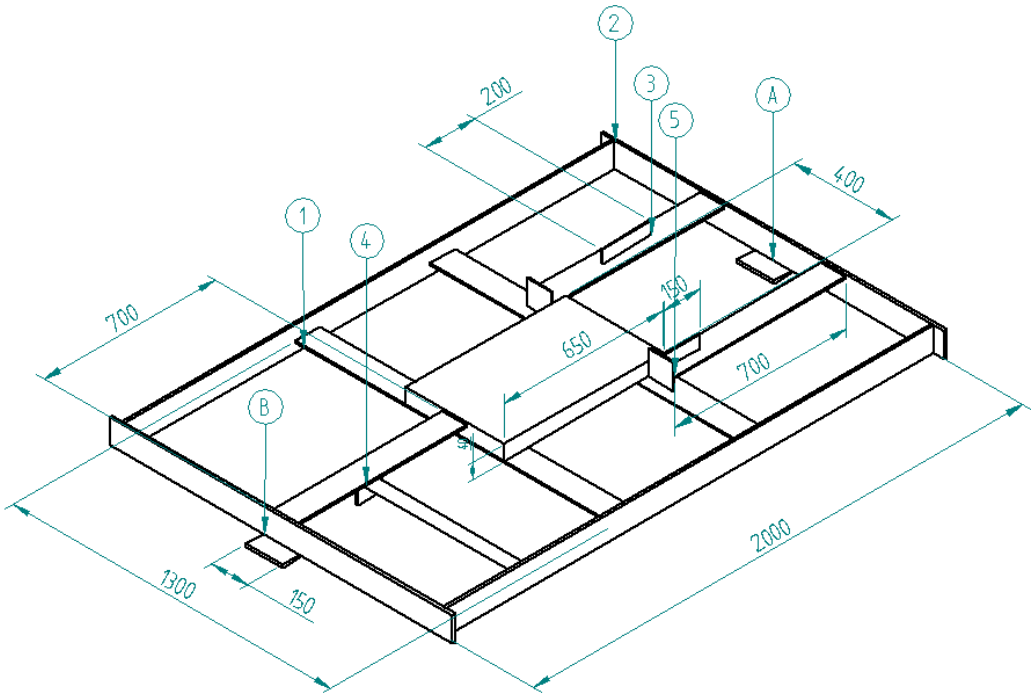

Figure 3.1: Geometry and setup of the preliminary design of the structure.

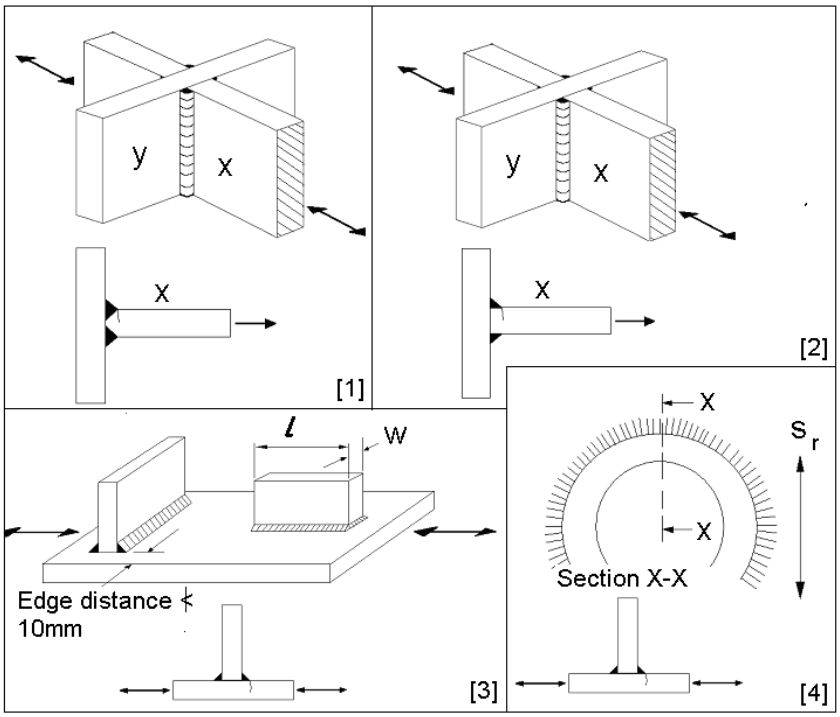

Figure 3.2: The four nominal stress assessable categories included in the structure (BS 7608:1993).

3.2.2 Finite element modeling

Once the preliminary design of the structure was established in such a way that the necessary welding categories were included and the geometrical constraints concerning weight and size satisfied, the second stage of the design was initiated. This dealt with the natural frequencies and stiffness (relating to the fatigue resistance under inertial loading) of the structure.

The first natural frequency had to be in the order of 7-10 Hz and also of such nature that it acted in the static deflection mode of the structure. This limitation was imposed simply to ensure that quasi-static response, assessable by means of the FESL methodology could be expected when a stochastic excitation signal with an energy content concentrated at 1-3 Hz was used as an input. This assumption originated from the rule of thumb that a structure's response will remain quasi-static provided that the excitation signal's primary/dominant energy content i.e. the peak of the power spectral density (PSD) plot is less than a third of the first natural frequency (Veltri & Bishop, 2003). The upper limit of 10 Hz was to ensure that the possibility existed to excite the structure into higher order modes with the available actuator capacity, should further study require it.

The stiffness of the structure, i.e. the thickness of the supporting beams, had to be of such a nature that it would be possible to perform a fatigue life test in a realistic and practical time. The stress response of the structure under stochastic loading would be entirely due to inertial effects since the structure is not clamped in as was mentioned in section 2.1. The rigidity of the beams supporting the centre mass as well as the centre mass' weight would then govern the fatigue resistance of the welds in a combined way since an increase in weight would cause greater inertial forces on the supporting beams while a decrease in beam stiffness would raise the bending stresses and consequently reduce the fatigue resistance of the structure.

The process of generating an input signal for the structure that will cause an ending fatigue life due to inertial effects, by numerical means, avoiding laborious and time consuming transient analyses, is iterative in nature and has to be accompanied by experimental feedback. The route that was decided on was to assume that the cycle counted stress response of the structure due to the stochastic input signal would be equal to the stress experienced by the structure under a uniform acceleration of 1g. This value was chosen since it was known from previous experience to be well within reach of the 40 kN actuators for structures of similar weight. This enabled the structure, for design purposes, to be analyzed by linear static finite element analysis with the implementation of an inertial load. The resulting stresses could then be entered into the category S-N curve of the weld that was expected to fail first and the expected life (in cycles) under constant amplitude loading determined. This value, in turn, could be compared with the actuators' frequency capability when initiating displacements causing 1g accelerations in previous, similar setups. Omitting the calculations for the reason that it is beyond the scope of this chapter, it could then be shown that the nominal stress in the beams supporting the centre mass had to be in the order of 70 MPa for a 1g load in order to ensure that fatigue failure would occur within 2 weeks.

The above analyses (normal mode analysis to determine the natural frequencies and the static inertial analysis) were performed on a finite element model representing the geometry in figure 3.1. The plates were modeled as surfaces and meshed with quad4 shell elements. The boundary conditions correlated with the intended constraints of the actual test setup. Several normal mode and static analyses were performed while the plate thicknesses and centre mass size were altered until the desired stress and frequency parameters were obtained. For a supporting plate thickness of 6mm and a centre weight size of 600x400x60mm the following parameters were obtained:

First natural frequency: 7.14 Hz
Second natural frequency: 11.02 Hz (lateral displacement)
Third natural frequency: 17.3 Hz
Fourth natural frequency: 23.94 Hz
Maximum stress in the vicinity of a weld due to a 1g inertial load: 85.5 MPa

Figure 3.3 shows the finite element model of the frame. The edges formed by the intersection of the actuator plates and the outer beams of the frame as indicated by points [A] and [B] are the constraints on the model relating to the actuators. They are both constrained in translation x, y and z since the actuators are clamped directly onto the test block. The only rotation that is constrained is rotation about the y-axis, due to the nature of the universal coupling connecting the actuator to the frame. Point [C] corresponds to the constraint imposed on the frame to avoid free body motion. Point [C] is constrained in rotation about the y- and z-axis as well as translation in the x-direction. The inertial load is applied in the y-direction. Points [1] and [2] indicates positions on the structure assessable by the hot-spot stress method.

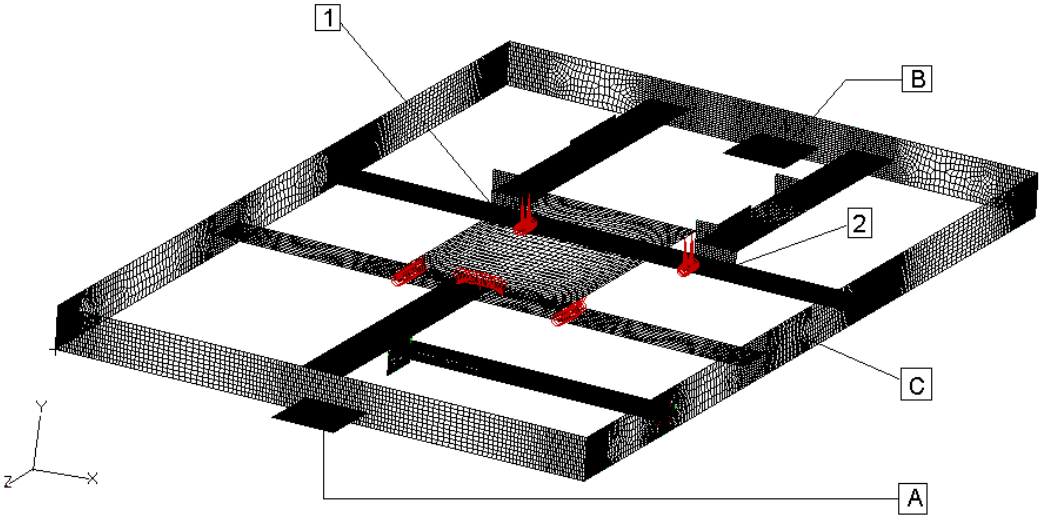

Figure 3.3: The finite element model and constraints of the structure.

Figure 3.4 illustrates the first natural frequency's mode shape. It is clear that this mode shape corresponds to the expected static deflection mode of the structure. Figures 3.5 and 3.6 show the third and fourth mode shape conforming to vertical displacements, i.e. no lateral resonance is present.

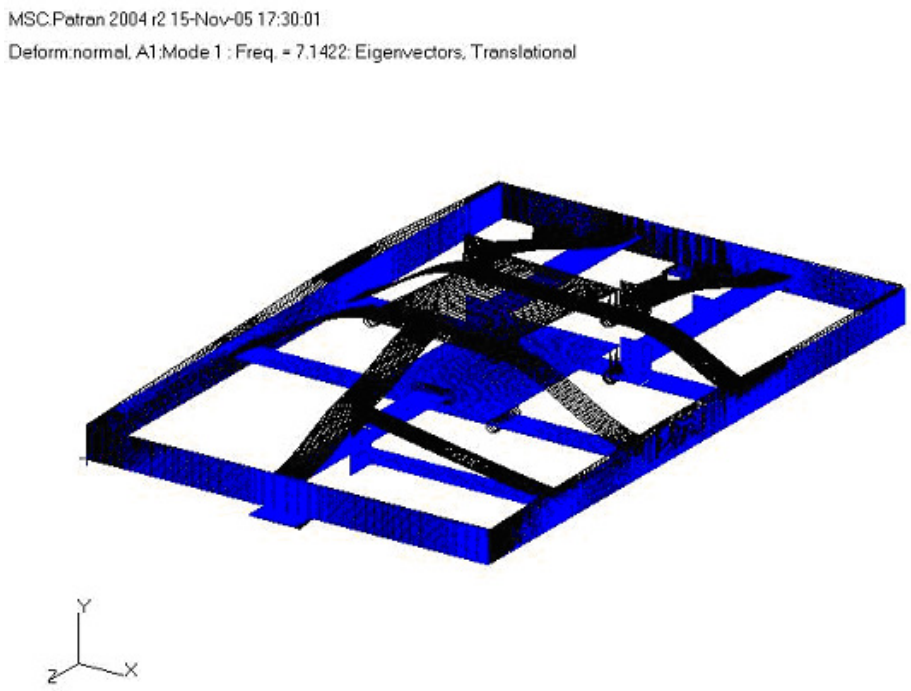

Figure 3.4: Finite element results showing the first natural frequency and its mode shape.

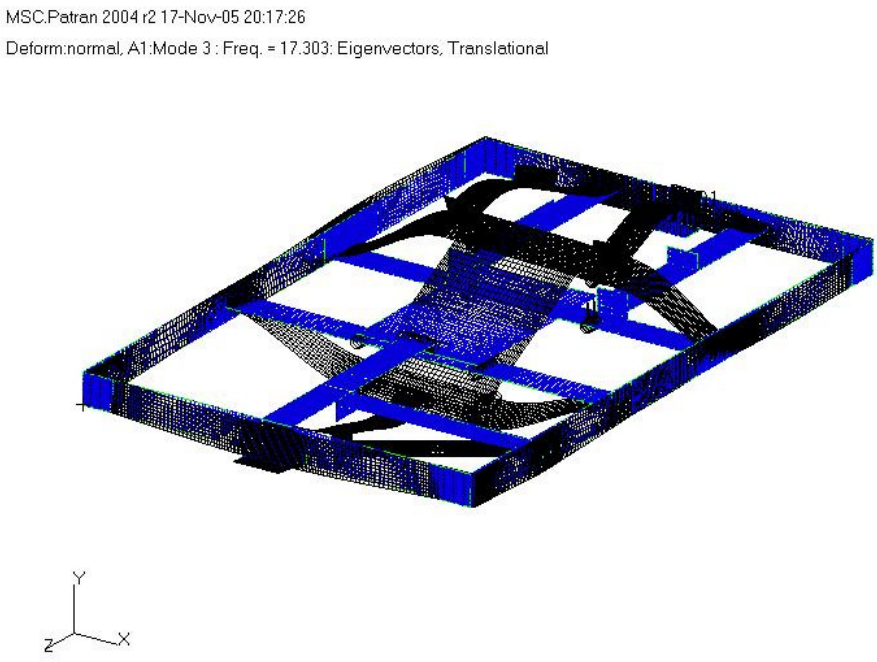

Figure 3.5: Finite element results showing the third natural frequency and its mode shape.

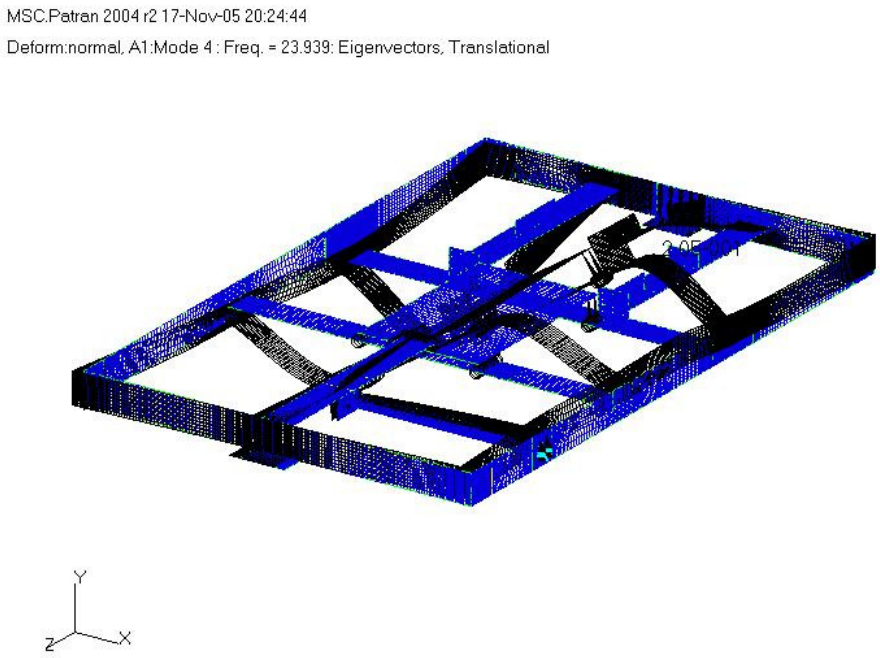

Figure 3.6: Finite element results showing the fourth natural frequency and its mode shape.

The meshing of the structure for preliminary design purposes did not include proper modeling of the welds. The intersection of two members was established solely by the equivalence of nodal points. The element size in the vicinity was taken to be 0.5 times the plate thickness of the supporting outer frame i.e. 5mm. The centre mass was connected to its supporting beams by means of multi-point constraints (MPCs). Figure 3.7 shows typical meshing in the vicinity of a plate intersection. The region indicated by point [2] on figure 3.3 is shown.

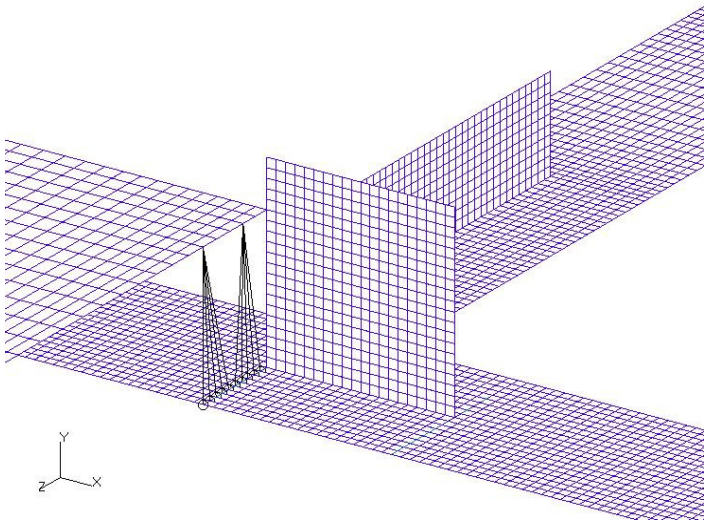

Figure 3.7: Meshing of detail [2], figure 3.3. Note the multipoint constraints connecting the beam and centre weight.

Figure 3.8 shows a contour plot of the stress response due to a 1g inertial load in the same region. The yellow band with a maximum of 85.5 MPa corresponds to the nominal stress referred to in this section.

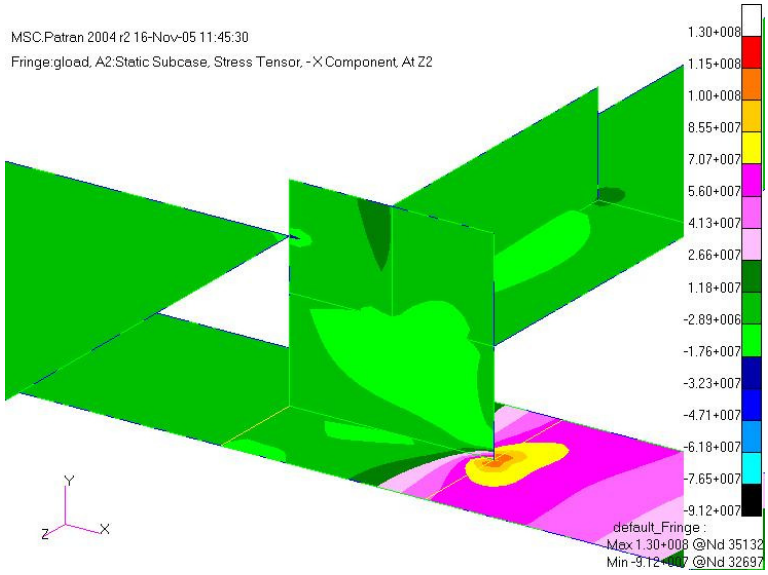

Figure 3.8: Finite element stress response of detail [2], figure 3.3.

3.2.3 Final design of the structure

After completion of the finite element analyses on the preliminary and altered designs, the final design of the structure was drafted and approved for manufacturing. The supporting members for the centre weight was 6×100mm flat bar while the outer frame was to be constructed of 10×100mm flat bar. The centre weight had dimensions of 60×400×650mm. The weld categories mentioned in section 3.2.1 were all included and a few small changes concerning geometry were made. Figure 3.9 shows the complete design of the structure as well as the nature of the welded joints and the plate thicknesses. The keys for the indicators on the drawing are as follows:

[1]: 100×10mm flat bar
[2]: 100×6mm flat bar
[3]: 42mm outer diameter, 2mm wall thickness round tubing
[a]: Full penetration welding, all round
[b]: Partial penetration welding, all round

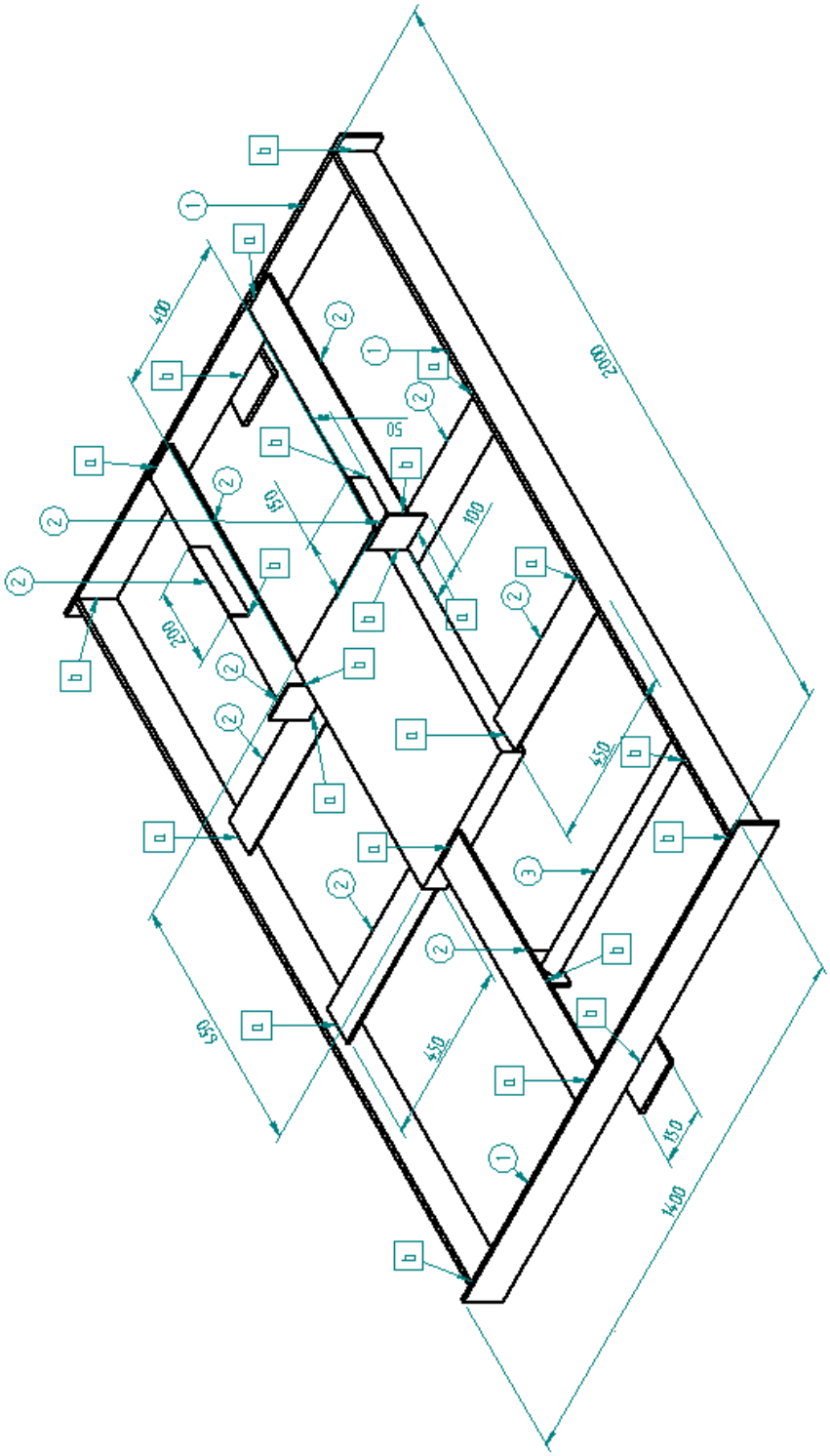

Figure 3.9: Final design of the H-frame including welding and plate properties.

3.3 Instrumentation and assembly of the test setup

3.3.1 Assembly of the structure onto the test block and actuators

After manufacturing the structure according to the design in figure 3.9 the assembly of the structure onto the test rig commenced. The frame was connected to two 40 kN actuators by means of the connection plates opposing ends with universal joints as interfaces. This was done in order to prevent the generation of cantilever bending moments in the structure and consequent strain on the actuator shafts and journal bearings due to out of phase excitation. The actuator bases, in turn, were connected directly to the test block by means of bolts. A stabilizer was connected to the frame in order to prevent free body motion and constrain the structure in its rotational degrees of freedom. Figures 3.10 and 3.11 show a schematic representation of the test setup.

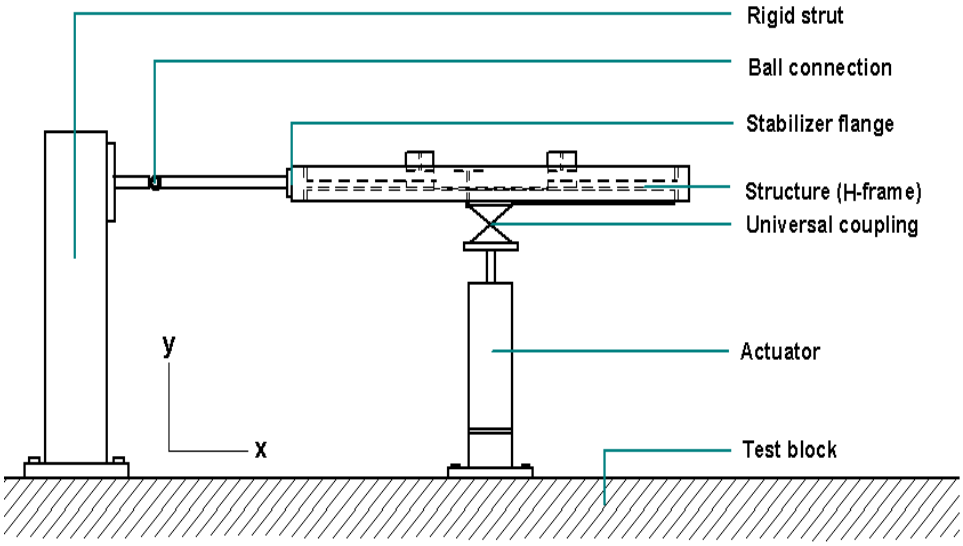

Figure 3.10: Front view of the test setup.

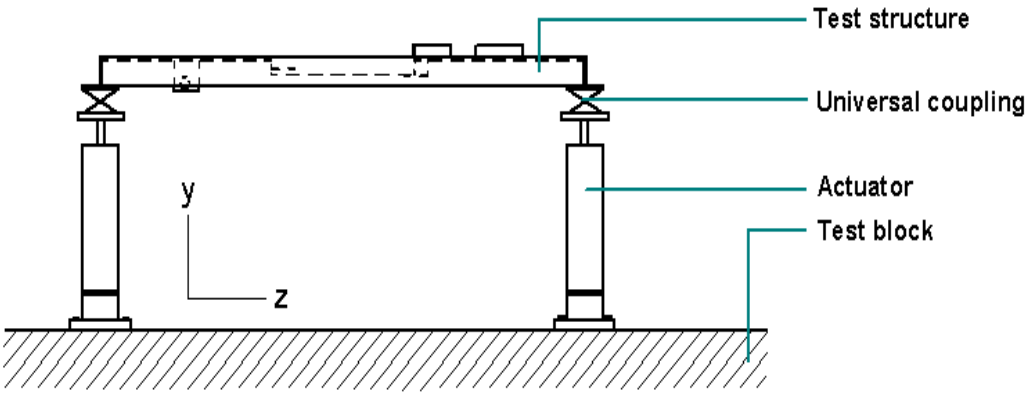

Figure 3.11: Side view of the test setup.

The stabilizer connected to the front of the structure (figure 3.11) constrains the structure in the z-direction in translation as well as rotation. The stabilizer on the side (figure 3.10) constrains the structure in the x-direction in translation as well as rotation about the z-and y-axis. The actuators constrain the structure in the y-direction (direction of excitation) as well as the x and z directions. It also prevents rotation about the y-axis. The boundary conditions on the finite element model were applied accordingly. Figure 3.12 shows an image of the structure, instrumented with strain gauges, mounted on the actuators and supported on the test block.

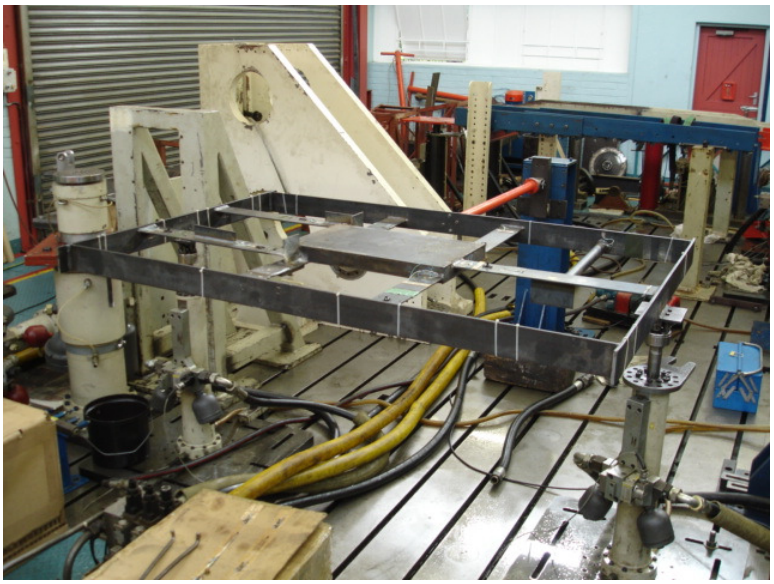

Figure 3.12: H-frame mounted on the test block with actuators, constraints and strain gauges.

3.3.2 Instrumentation

The finite element model pointed out the positions on the structure where the stress response was a maximum. These positions were selected for the application of strain gauges since the stresses in these areas were critical for fatigue analysis. Since the structure were to be loaded primarily in bending, the strain gauges were installed at a fixed distance of 25mm from the weld toe in the case of cruciform joints and at a distance of 50mm from the weld toe in the case of plate-stiffener configurations. This was done in order to extract stresses that did not include local and macro structural effects due to the weld geometry and the intersection. This arrangement resulted from the multiple numerical analyses of cruciform joints and plate-stiffener configurations performed in chapter 2, the incentive being the fact that the nominal stress method were to be used for the fatigue analysis.

The strain gauge in the vicinity of the structural detail, which was to be assessed using the hot spot method, was applied according to the regulations of the IIW fatigue design recommendations, XII-1965-03/XV-1127-03. The code prescribed the positioning of two strain gauges at 0.4t and 1.0t respectively from the weld toe for extrapolation purposes. Due to the size of the strain gauges and the relatively thin

plate thicknesses (6mm) the prescribed positions could not be matched. The alternative option of placement of the leading edge of the gauge at a distance of 0.3t from the weld toe and the second strain gauge at a distance of 1.5t was consequently implemented. Figure 3.13 shows the recommended positioning according to the IIW as well as the positioning for the capturing of nominal stress according to the recommendations developed in this dissertation (for T-joints). In the case of a plate stiffener configuration, the strain gauge should be placed at a distance of 50mm from the weld toe instead of 25mm. Figure 3.14 shows a top view of the test structure with the strain gauges numbered from 1 to 10. Later reference to strain gauge positions will be consistent with this numbering.

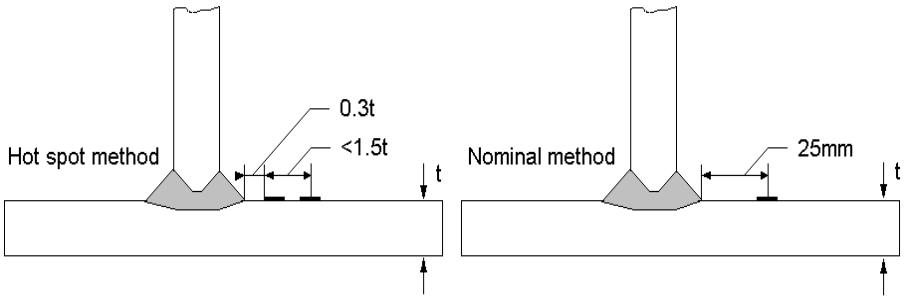

Figure 3.13: Recommended placement of the strain gauges for the hot spot and nominal stress methods respectively.

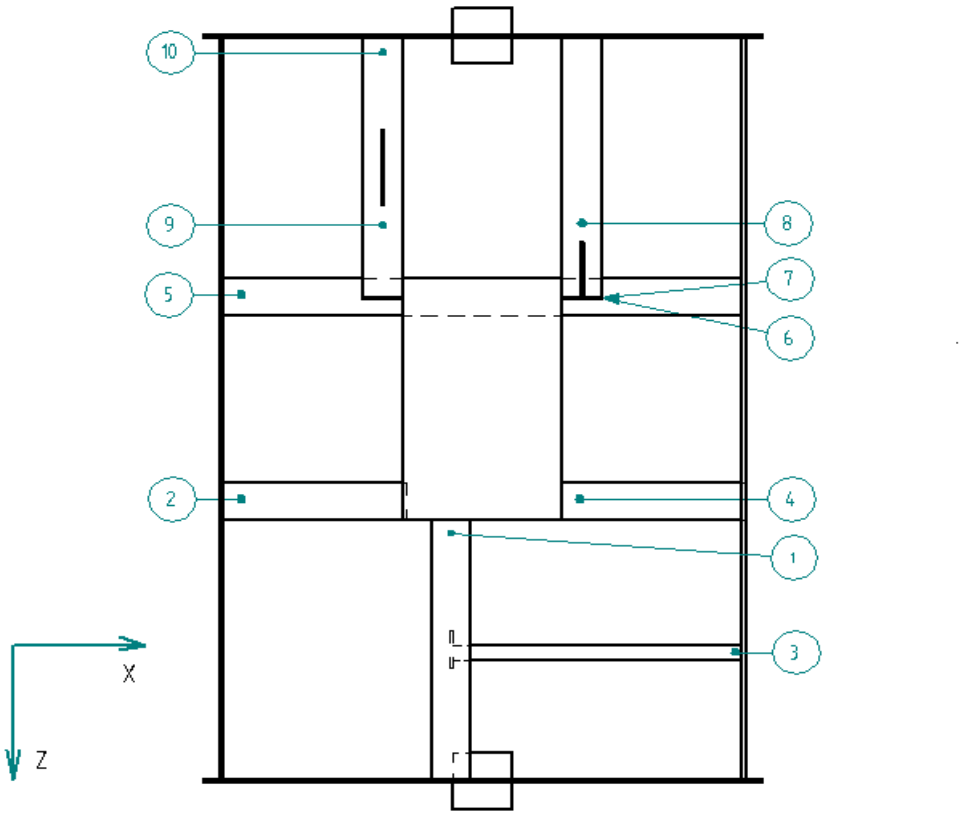

Figure 3.14: Top view of the H-frame showing strain gauge positions.

The strain gauges were of a 0º-90º configuration, connected in a half bridge arrangement. The data acquisitioning were done by means of the Spider 8 bridge connector. Figures 3.15 and 3.16 show the adhered strain gauges at the respective welding categories included in the structure. The strain gauges in figure 3.15 are positioned at 25mm and 50mm from the weld toe for the T-joint (8.1-F) and stiffener (5.4-F2) respectively.

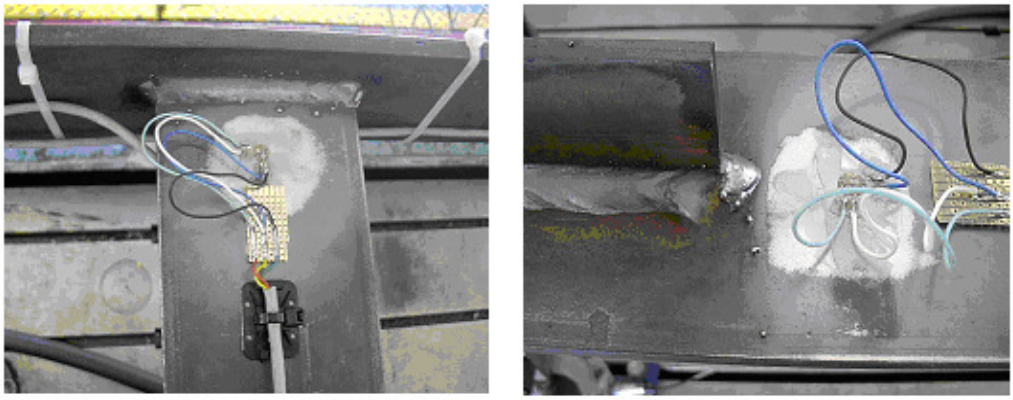

Figure 3.15: Cruciform joint and a plate stiffener configuration instrumented with strain gauges.

The strain gauges in figure 3.16 are positioned at 4mm and 9mm from the weld toe for the hot spot stress assessable detail according to the IIW regulations. The strain gauge on the hollow section was also placed at a distance of 25mm from the weld toe although guidelines for this particular category were not established in chapter 2.

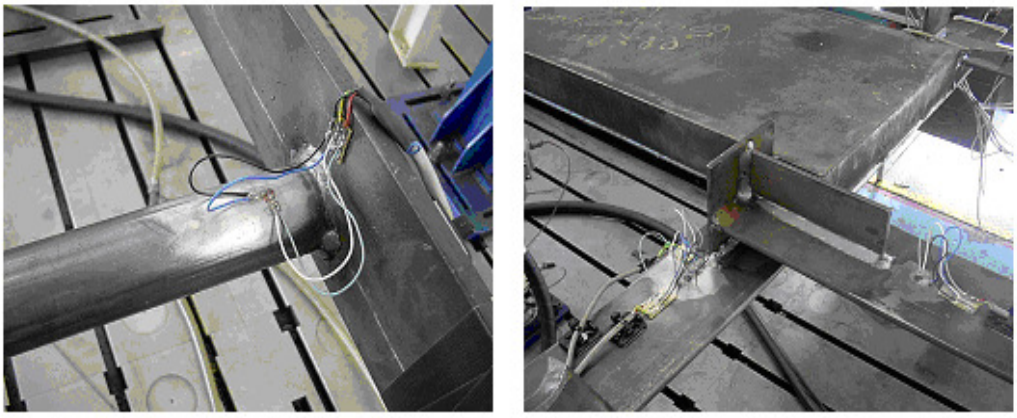

Figure 3.16: 9.6 W hollow section and the hot spot assessable detail equipped with strain gauges.

Once the structure was instrumented the following step was to perform a static and dynamic stress verification, fatigue life prediction and fatigue testing. All of these procedures are addressed in the following chapter.

Chapter 4

4. Static and dynamic stress verification, fatigue life prediction and testing

4.1 Static stress analysis and verification

4.1.1 Finite element model and test procedure

Once the structure was assembled onto the test block and instrumented, the first step was to investigate the integrity of the finite element meshing methodology as developed in chapter 2. The emphasis was laid on the stresses in the vicinity of the welds due to their relevance to fatigue resistance, and for the application of the nominal stress approach.

Firstly, the structure was re-meshed according to the developed meshing methodology, i.e. the welds were represented with adjacent, inclined elements as shown in figure 2.27. The element size in the vicinity of the weld was set at either 3mm or 5mm, depending on the plate thickness, which alternated between 6mm and 10mm. The welds that formed part of plate-stiffener configurations were modeled with rigid links (MPCs), similar to those shown in figure 2.8, while the element sizes still equaled half the plate thicknesses. Figure 4.1 shows the meshing in the vicinity of the weld associated with strain gauge 2 of figure 3.14, which is representative of the meshing of the structure as a whole. The implementation of a fine mesh and inclined elements to represent the weld is clear.

Once the structure was re-meshed, the 0°-90° strain gauges at all the positions mentioned in figure 2.14 were connected into a half bridge configuration and calibrated according to the same procedure as the half bridge strain gauges in the first round of testing of the T-piece specimen, described in chapter 2. The next step was to apply a static load at some central point of the structure and capture the strain gauge readings for comparison with the finite element results under the same loading. The application of an accurate static load on the H-frame was done by means of known weights, positioned in the centre of the centre mass of the structure.

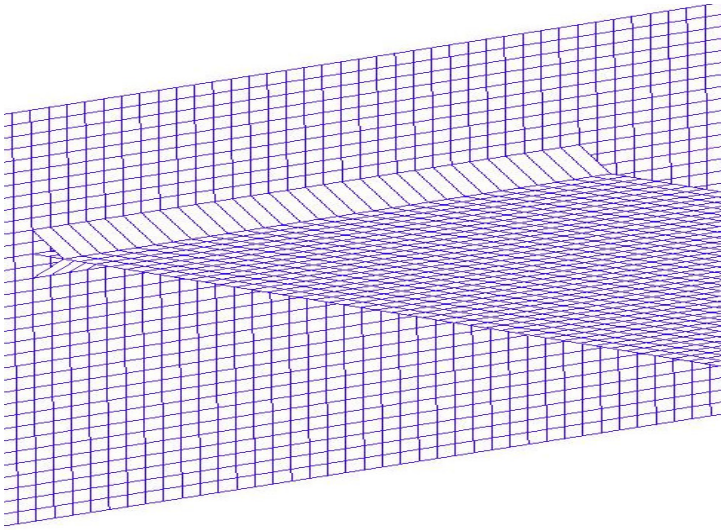

Figure 4.1: Meshing of the cruciform joint and weld at position 2 of the structure in figure 2.14.

The measuring procedure was the same as that for the T-piece, i.e. every strain gauge was connected into a half bridge configuration on a separate channel. It should be noted that the zero or tared position for the strain gauge readings was before any external weight was applied but with the deformation due to the centre mass and the weight of the strain gauge cables included. This initial deformation, however, is considered as irrelevant since the structure remains in its linear elastic range, causing the zero point of measurement to be extraneous.

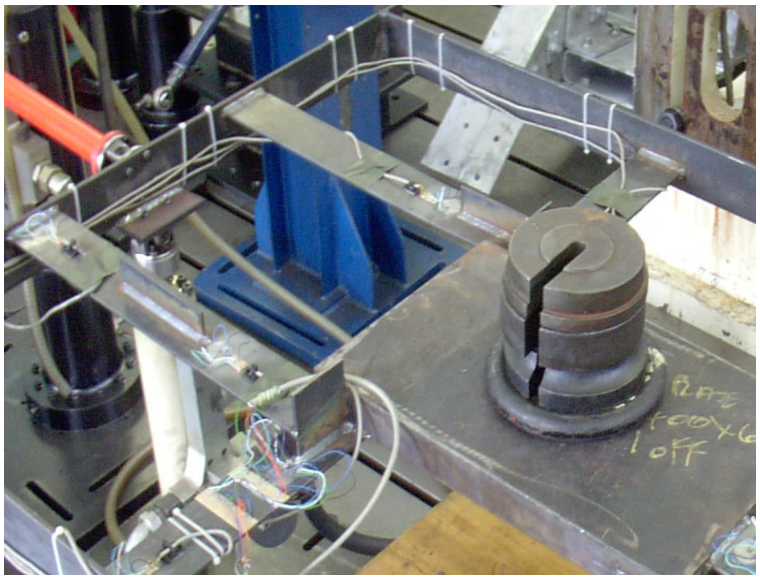

Figure 4.2: Static loading of the H-frame by means of weights during strain gauge measurements for static stress verification.

The weight was applied in steps of ± 100 N, depending on the size of the available weights, up to a final load of 405.3 N. Strain gauge measurements were taken at each interval. The load was then removed in the same increments and the measurements repeated in order to ensure that the strain gauges operated linearly. Figure 4.2 shows an image of the structure under full loading during the measuring process.

4.1.2 Test results, data processing and conclusions

The combined 0°-90° strains, $\varepsilon_{measured}$, was processed to stresses in exactly the same manner as described in section 2.2.3, i.e. by assuming a uni-axial stress state in the beams of the structure where the strain gauges were positioned. This assumption implied that $\varepsilon_x = -\nu\varepsilon_z$, by which the longitudinal stress could then be obtained by dividing the measured strain, $\varepsilon_{measured}$, by $(1+\nu)$, as was outlined in section 2.2.3.

After completion of the experimental stress determination, the finite element simulation was done with a total load of 405.3N applied to the centre mass of the structure. The application region was circular with dimensions corresponding to those of the bottom weight in the experimental setup. The boundary conditions on the model corresponded to those in the actual test setup as discussed in section 3.2.2. By completion of the analysis the stresses along the longitudinal axis of the beams were extracted from the finite element model at the exact points corresponding to the strain gauge positions for unambiguous comparison. Table 4.1 stipulates the 0°-90° strain gauge and finite element results for the positions indicated in figure 3.14. Note that the longitudinal axis of the beams in the structure can be oriented along either the x-axis or the z-axis of the global coordinate system in figure 3.14. The stresses under consideration are those along the longitudinal axis and will be identified as either σ_x or σ_z, depending on the orientation of the beam.

Table 4.1: Comparison of 0°-90° strain gauge results with results obtained from the finite element analysis.

Strain gauge position	Direction of longitudinal axis	Measured stress (MPa)	FEA stress (MPa)	Percentage error
1.	z	-16.2	-21.3	23.9%
2.	x	10.1	11.4	11.4%
3.	x	0.8	2.6	69.2%
4.	x	-18.0	-20.5	12.2%
5.	x	11.0	16.5	33.3%
6.	x	-26.7	-36.3	26.4%
7.	x	-19.4	-23.3	16.7%
8.	z	-7.7	-8.3	7.2%
9.	z	-4.5	-2.8	37.8%
10.	z	7.5	9.3	19.4%

From table 4.1 it is clear that the correlation is extremely poor – with an error of up to 37.8%, especially if it is kept in mind that the measurements were taken under laboratory conditions and that a refined finite element model with realistic constraints was used. The source of the error could thus lie with one of two possibilities: either

the finite element model or the measurements. The finite element model could have faulty load and boundary condition application or did not account explicitly for misalignment that could be present in the test structure. A sensitivity analysis performed on the finite element model, however, confirmed that the combined effect of the misalignment and deviation in load/boundary condition application could answer for a 5% deviation in stress at the critical points at the most. The problem consequently had to lie within the measuring technique or data processing procedure.

The structure experiences, due to the fact that its supporting beams are oriented in two directions (x and z), deflection and stresses in both the x and z direction. The integrity of the uni-axial assumption, implemented in the processing of the 0°-90° strain gauge data is consequently under suspicion. It was thus questioned whether ε_x was indeed equal to $-\nu\varepsilon_z$, for if it was not the case, the value $\varepsilon_{measured}$, would still be accurate but the extraction of the strains ε_x and ε_z and consequently the stresses along the longitudinal axes of the various beams, σ_x and σ_z, would be erroneous. This could be easily seen if equations 2.3 to 2.5 were considered. The only way to confirm such a notion would be by implementation of independent measuring channels in the 0° and 90° directions at the critical positions in order to determine the longitudinal axis -and transverse strains autonomously and accurately.

Since comprehensive knowledge of the complete stress state (including shear- and principal stresses) at the critical points would be advantageous for life prediction and would also provide a better understanding of the stress response of the structure, it was decided to apply rosette strain gauges at a few critical positions. This would enable separate measuring channels for strain verification and validation of the abovementioned notion concerning the assumed uni-axial stress state in the structure. It would also provide means to quantify the complete stress state for it cannot be obtained from 0°-90° strains only since the strains along the 45° directions relative to the longitudinal axis are also needed.

The structure was consequently equipped with four rosette gauges at the positions indicated in figure 4.3. Gauge A is positioned for stress verification purposes. Gauge B is placed at the expected position of failure, assessable by the nominal stress method while gauge C and D are positioned at the location where failure assessable by the hot spot stress method is expected – similar to the 0°-90° gauges placed at position 6 and 7 in figure 3.14. The incentive behind the placement of gauges B, C and D will be discussed later in this chapter when the fatigue life prediction is addressed. Finally the original 0° and 90° degree measuring grids of the 0°-90° strain gauge at position 1 of figures 3.14 and 4.3 were uncoupled and connected into two separate channels by implementation of passive strain gauges. For the purpose of stress verification the following gauges with associated measuring channels were thus implemented: gauge A (0°, 45° and 90°), gauge B (0°, 45° and 90°), and gauge 1 (0° and 90°). Note that the 0° measuring grid is always aligned with the longitudinal axis of the member on which the gauge is installed.

The test procedure was repeated for the same load as the initial 0°-90° test with 8 channels for the two rosette gauges and the uncoupled 0°-90° gauge. The bridge was completed for each channel by a passive measuring grid connected in a half bridge

configuration together with the active measuring grid into the bridge connector / data acquisitioning system.

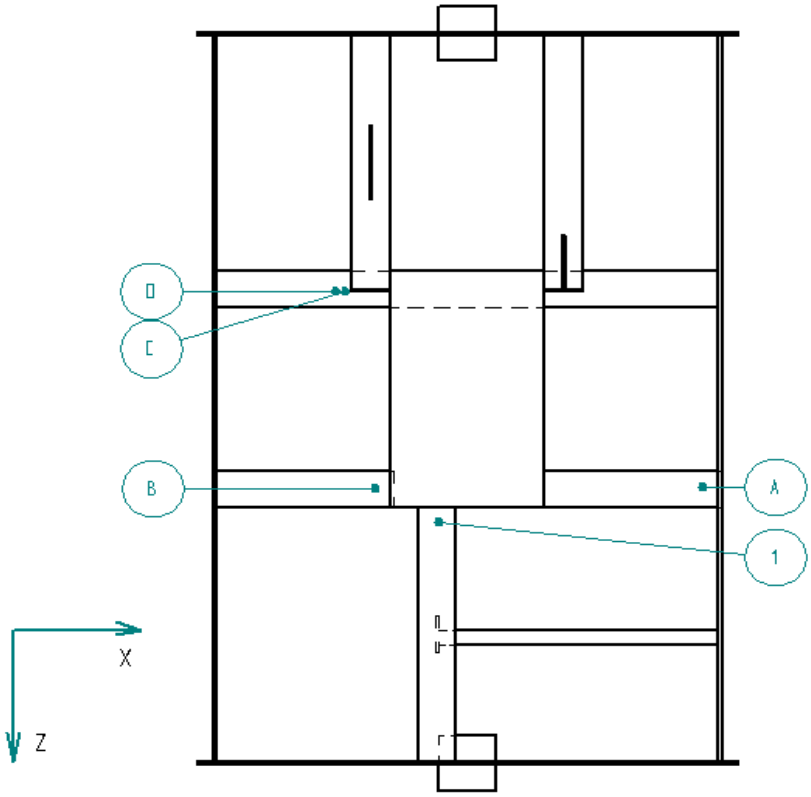

Figure 4.3: Position of the rosette strain gauges for stress verification and life prediction on the structure.

The value, $\varepsilon_{measured}$, obtained for each channel was thus the actual strain in the particular direction for the associated measuring grid. The stresses in the longitudinal and transverse direction for each measuring point are then obtained by implementation of Hooke's law for plane stress (equations 4.1 and 4.2):

$$\sigma_x = E/(1-\upsilon^2)[\varepsilon_x - \upsilon\varepsilon_z] \qquad [4.1]$$

$$\sigma_z = E/(1-\upsilon^2)[\varepsilon_z - \upsilon\varepsilon_x] \qquad [4.2]$$

Finally the 0° and 90° grids of two rosette gauges' as well as the 0°-90° gauge at position 1 were connected into a half bridge configuration, thus forming three measurement channels. The same load was applied again, the measurements taken and the data processed to stresses, assuming uni-axial stress states in the beams, as was done in the original 0°-90° measurements.

Tables 4.2 – 4.4 summarize the results obtained from the two rosette gauges and the 0°-90° gauge with independent measuring grids (stresses calculated from equation 4.1 and 4.2) as compared to the stresses obtained from the 0°-90° measurements together with the uni-axial assumption. The finite element results and relevant, measured

strains are also included to illustrate the measuring error if a uni-axial stress state is assumed. The strain gauge numbers correspond to those in figure 4.3

Table 4.2: Rosette, 0°-90° and finite element results for strain gauge A.

(A)	FEM (MPa)	Measured (Rosette) (MPa)	% Error (FEM vs. rosette)	Measured (0°-90°) (MPa)	% Error (FEM vs. 0°-90°)	% Error (rosette vs.0°-90°)
σ_x	18.72	17.27	7.65%	12.25	34.53%	27.61%
σ_z	4.47	4.55	1.76%	0	Inf.	Inf.
ε_x	-	7.66×10^{-6}	-	5.95×10^{-5}	-	22.34%
ε_z	-	-5.59×10^{-6}	-	-1.96×10^{-5}	-	71.51%

Table 4.3: Rosette, 0°-90° and finite element results for strain gauge B.

(B)	FEM (MPa)	Measured (rosette) (MPa)	% Error (FEM vs. rosette)	Measured (0°-90°) (MPa)	% Error (FEM vs. 0°-90°)	% Error (rosette vs.0°-90°)
σ_x	-20.9	-21.22	1.51%	-14.83	29.18%	30.25
σ_z	-5.71	-5.85	2.56%	0	Inf.	Inf.
ε_x	-	-9.37×10^{-5}	-	-7.21×10^{-5}	-	23.05%
ε_z	-	5.62×10^{-6}	-	2.40×10^{-5}	-	76.6%

Table 4.4: Rosette, 0°-90° and finite element results for strain gauge 1.

(1)	FEM (MPa)	Measured (rosette) (MPa)	% Error (FEM vs. rosette)	Measured (0°-90°) (MPa)	% Error (FEM vs. 0°-90°)	% Error (rosette vs.0°-90°)
σ_z	-21.30	-22.78	6.50%	-16.21	23.94%	28.88%
σ_x	-6.19	-6.33	2.21%	0	Inf.	Inf.
ε_z	-	-1.0×10^{-4}	-	-7.87×10^{-5}	-	21.30%
ε_x	-	5.77×10^{-6}	-	2.60×10^{-5}	-	78.08%

From tables 4.2 to 4.4 it becomes apparent that there exists a good correlation between the finite element results and the results obtained from the rosette strain gauges with errors ranging from 1.51% to 7.65 %. The 0°-90° results, however, is poor as was already established from the results presented in table 4.1. The reason for

the poor 0°-90° strain gauge results becomes clear when the rosette strains are investigated. If the value of $\varepsilon_z/\varepsilon_x$ for strain gauge B is determined, for example, a value of -0.06 is obtained which is not even close to a Poisson's ratio of –0.33 which is expected in pure bending. The reason for this phenomenon was discovered after a more thorough investigation of the stress and strain distribution in the beams of the structure. Since the measuring points or strain gauge positions are close to the welds and the intersection points of the structure, the fundamental conditions for the Poisson effect to take place is not satisfied. This is because the beam cannot contract in the transverse direction to the longitudinal axis due to the displacement constraint imposed on it by the intersection. This explains the reason for the ratio of $\varepsilon_z/\varepsilon_x$ for strain gauge B to be so small – since ε_z is constrained by the intersection as previously explained.

The uni-axial assumption, however, still holds in the centre of the beams, since the constraints due to the end effects is not prominent any more. This becomes clear when figure 4.4, which is a graph of the ratio of ε_x to ε_z (obtained from FEA as a function of distance from the weld) is considered. The last point on the graph corresponds to the mid span of the beam. The particular beam is the one containing strain gauge B. Note the discontinuity and deviation from the value of -0.33 at the weld while the value tends towards -0.33 as the midspan of the beam is approached.

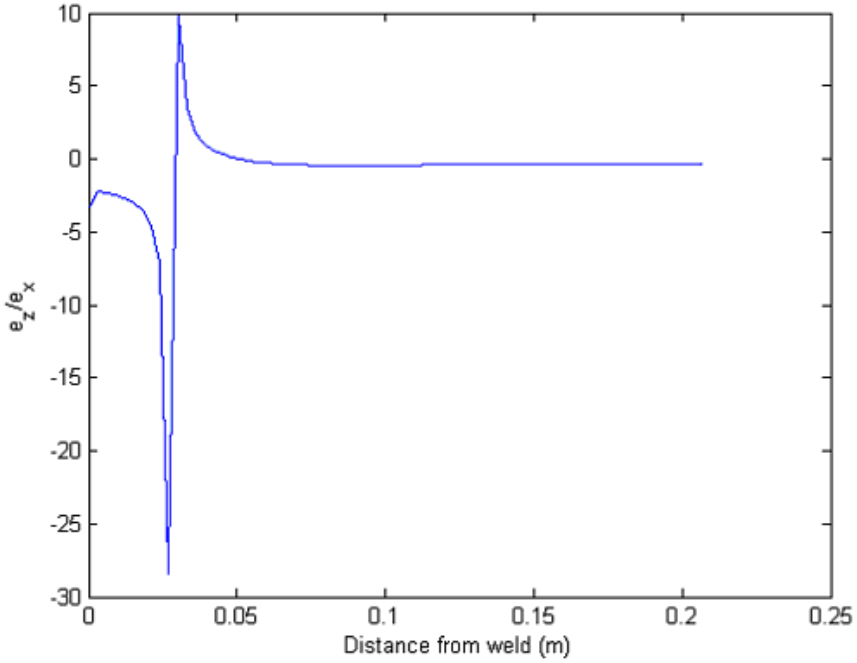

Figure 4.4: The ratio $\varepsilon_z/\varepsilon_x$ obtained from finite element analysis for the beam containing strain gauge B.

The application of 0°-90° strain gauges for input loading quantification such as will be performed later in this chapter is thus viable, as long as multi-axial loading is not present in the particular member and the measurement point is well clear of end effects. For stress quantification in the vicinity of welds with the intention of life prediction, the implementation of rosette gauges with independent measuring grids is

indispensable, particularly when principal stresses are also needed. This will become clear in the section on the actual fatigue life prediction of the structure.

4.2 Dynamic stress analysis and verification

4.2.1 Numerical analysis

Since the test structure will be excited by means of stochastic loading, the need arose to verify numerically whether the response to the chosen input signal will be suitable for quasi-static analysis. This was done by means of transient finite element analyses, employing the proposed excitation signal. The input signal was an imposed displacement on the structure at the connecting points to the actuators by means of the actuators (points A and B in figure 3.3). The term quasi-static implies that the structure does not respond dynamically to the excitation, i.e. the natural modes of the structure is not excited and does not contribute to the stress response of the structure.

As was mentioned in chapter 3, section 3.2.2, the first natural frequency of the structure was determined to be 7.14Hz. The mode shape at this frequency corresponded to the expected static deflection mode of the structure, as can be seen in figure 3.4. The general rule of thumb (mentioned in section 3.2.2) to maintain quasi-static response requires that the excitation signal's dominant energy content is less than a third of the first natural frequency.

Two equivalent stochastic excitation signals as a function of time were consequently created, by prescribing a PSD with its peak at 1Hz.

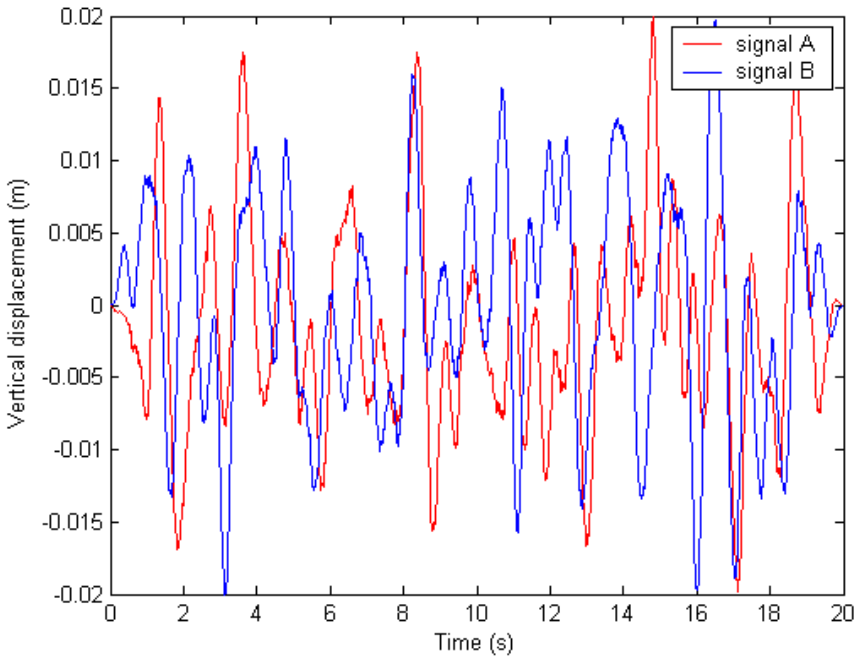

Figure 4.5: Excitation/input signals for the transient analyses (vertical displacement vs. time).

After the signals were generated, a PSD analysis of the signals were once again performed to verify that the dominant energy content of the signals were situated at a frequency of less than a third of the first natural frequency of the structure, as required to avoid dynamic response.

Figures 4.5 and 4.6 show the excitation/input signals and an accompanying PSD plot. From figure 4.6 it can clearly be seen that the energy content is concentrated between 0.5Hz and 2Hz, which is well less than a third of the first natural frequency of the structure (7.14Hz). The excitation signals were consequently accepted as suitable to impose on the finite element model for the transient FEA which, if the obtained response was satisfactory, could then be imposed on the structure for fatigue testing accompanied by a quasi-static life prediction procedure.

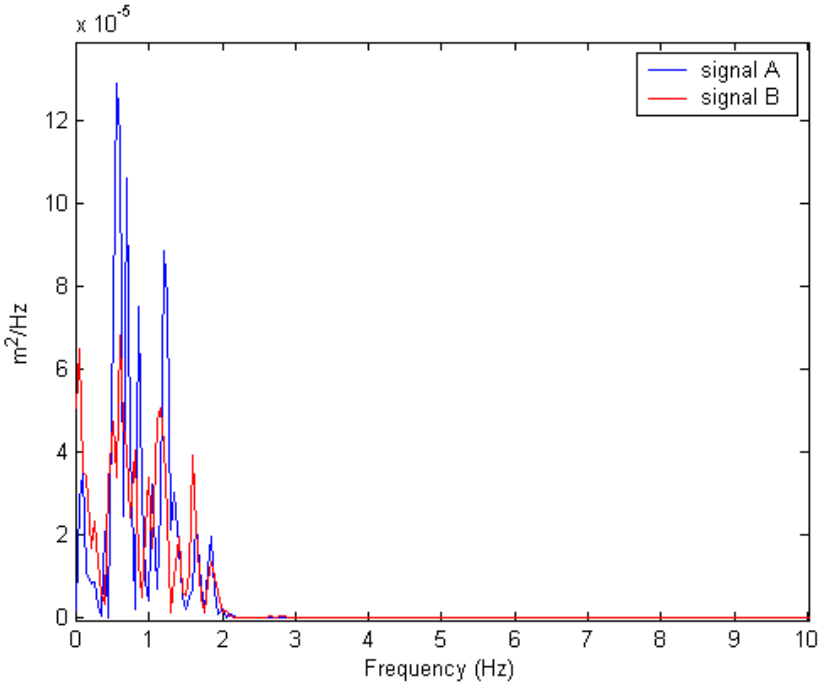

Figure 4.6: PSD of the excitation/input signal (signal A) showing the energy distribution of the signal as a function of frequency.

At this point the structural damping coefficient was not yet determined since it had to be determined experimentally. Typical values for lightly damped structures are in the order of 0.03. Since an estimation of the structural damping coefficient was needed for the transient analyses a value of 0.03 was assumed. It was, however, not clear whether such an estimation would provide sufficient damping for the finite element model in order to obtain a useful approximation of the structure's response. The question was addressed by imposing a pure sinusoidal displacement signal with a frequency of 0.75 Hz on the structure. Two transient simulations, one with structural damping corresponding to the assumed value of 0.03 and one without structural damping were performed. Figure 4.7 shows a PSD plot of the structure's response for both the damped and undamped cases.

When studying the two PSDs of the respective analyses shown in figure 4.7, it can be seen that the response of the undamped case is situated around 7 Hz with a very high energy content. This indicates resonance, while the damped case has almost no energy around 7 Hz, with the majority concentrated at 0.75 Hz which is the excitation frequency of the sinusoidal signal. From this it can be deduced that the damping coefficient implemented in the FEA was realistic and will be sufficient for the purposes of preliminary transient analysis and to investigate the nature of the structure's response.

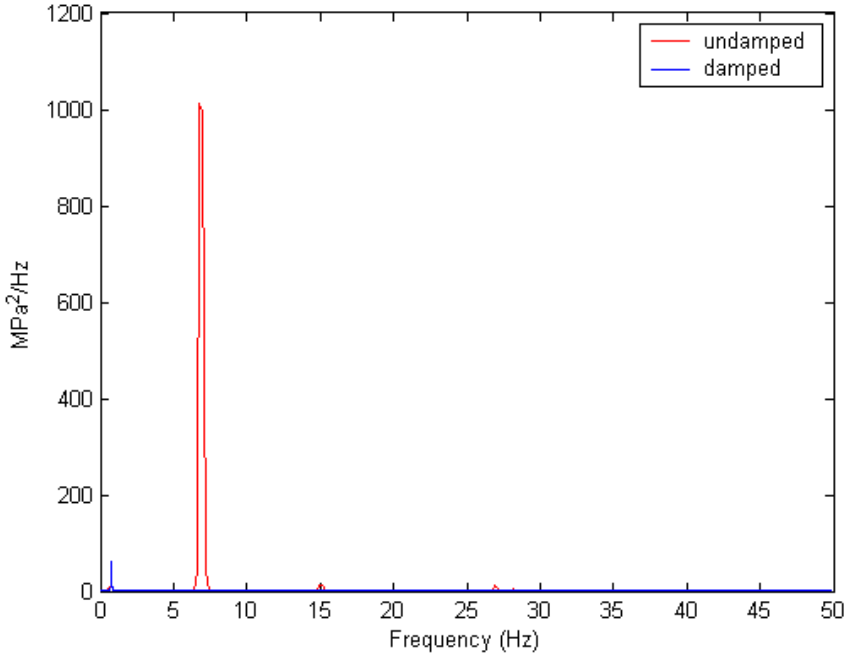

Figure 4.7: PSD of the stress response of the structure under sinusoidal loading for damped and undamped cases.

The following step was to perform two transient finite element analyses on the structure using the original finite element model with boundary conditions as indicated in figure 3.3 together with the excitation signals A and B. The only difference is that the constraints due to the actuators (A and B) were now modified to accommodate the excitation signal in the y-direction instead of a static constraint. The aim of the transient analyses with imposition of stochastic excitation signals was to analyze the structure's suitability for fatigue analysis by means of quasi-static analysis, in particular the fatigue equivalent static load (FESL) fatigue assessment methodology.

The philosophy behind the approach and the requirements concerning the response of the structure will be outlined and discussed in the following section in order to clarify the relevance of the two transient finite element analysis procedures applied to the structure in the section thereafter.

4.2.2 The fatigue equivalent static load (FESL) methodology

The following is an outline of the quasi-static, fatigue equivalent static load, fatigue assessment procedure for complex structures under stochastic loading based on the method given by Wannenburg (1998). Wannenburg proposed this method as a means of quantifying variable amplitude input loads in such a manner that it can be implemented in a static finite element analysis. This will enable a substantial reduction of required analysis time since laborious and time consuming transient analyses can hence be replaced with equivalent static finite element analyses. In his paper he shows how this method is applied to fuel tankers and compared to comprehensive fatigue design based on measured dynamic inputs. He also showed the correlation of the method with the design rules stipulated in trailer design codes such as the South African Bureau of Standards (SABS), among others.

The first step is to perform strain gauge measurements of a typical operating cycle of the structure under consideration to obtain the stress history. Strain gauges should be placed away from stress concentrations to measure nominal stresses sensitive to global bending and tensile and shear stresses due vertical, longitudinal and lateral loading.

Once the stress response at a point is determined the following step is to perform a Rainflow cycle counting procedure on the measured stress response to partition the stochastic stress response into discrete stress ranges $\Delta\sigma_i$, and accompanying cycle quantities for each stress range, n_i.

The number of cycles to failure, N_i, for each stress range $\Delta\sigma_i$ can then be calculated from the material S-N curve or that of the particular weld category under consideration. Equation 4.3 describes the S-N curve as presented in the BS 7608: 1993 fatigue design code:

$$N_i = C_d / (\Delta\sigma_i)^m \qquad [4.3]$$

where C_d is a constant relating to the particular S-N curve and m is the inverse slope of curve (m=3 in the case of welds).

The total damage, D, due to all of the stress ranges can then be calculated using Miner's linear damage summation rule:

$$D = \sum \frac{n_i}{N_i} \qquad [4.4]$$

It is now assumed that there exists a constant sinusoidal stress range $\Delta\sigma_e$ which will cause the same total damage, D_e, over N cycles where:

$$N = \sum n_i \qquad [4.5]$$

And

$$D_e = \frac{N}{N_e} \qquad [4.6]$$

where N_e is the life associated with $\Delta\sigma_e$. Note that N can be any value convenient for the analyst but will be defined as such throughout the coming analyses for consistency.

By considering equation 4.3, N_e can be expressed in terms of $\Delta\sigma_e$ as follows:

$$N_e = C_d / (\Delta\sigma_e)^m \qquad [4.7]$$

If the damage D_e, due to $\Delta\sigma_e$ is now equated to the damage D due to the variable loading, $\Delta\sigma_e$ can be expressed as a function of $\Delta\sigma_i$, n_i and N:

$$\Delta\sigma_e = \left[\sum \frac{\Delta\sigma_i{}^m n_i}{N} \right]^{\frac{1}{m}} \qquad [4.8]$$

The next step is to define the FESL. This requires a linear static finite element analysis of the structure under consideration by means of a unit load. This unit load can either be a 1g acceleration or a 1N force. This study will make use of a 1g inertial load. Once the finite element analysis is completed the static stress due to the unit inertial load is determined at the same location as the measured stress response. The FESL is then defined by:

$$FESL = \frac{\Delta\sigma_e}{\sigma_{gload}} \qquad [4.9]$$

The FESL can thus be seen to be a factor by which the unit load is scaled in order to implement in the linear static finite element analysis. This scaled inertial load will serve as a means to reproduce the stress condition, as caused by the actual input loading, throughout the structure. This method can be applied to any structure or loading mode, provided that the ratios of the stresses in the structure relative to each other during the dynamic or stochastic loading is the same as during the static deflection of the structure. In order for this requirement to be met, it has to be ensured that the response of the structure under the operational loading remains quasi-static.

This is the aim of the following section in which the structure's response to the input signals generated in the previous section (section 4.2.1) will be numerically investigated. Special attention will be given to the response of the structure in terms of the requirements for quasi-static analysis, i.e. the ratios of the stresses throughout the structure relative to each other and those obtained from linear static analyses will be investigated

4.2.3 Transient finite element analyses

As mentioned previously, two transient finite element analyses accompanied by a critical assessment of the stress response of the structure will be performed in this section. This is done in order to verify the structure's suitability for quasi-static analysis under excitation by means of signals A and B generated in section 4.2.1.

The first analysis was done with the first excitation signal (signal A shown in figure 4.5) imposed at points A and B of figure 3.3. Points A and B thus experienced in-phase loading. A structural damping coefficient of 0.03, as verified to be sufficient for the particular structure, was introduced in the FEA.

The longitudinal stresses at all 10 strain gauge positions (figure 3.14) were recorded. Figure 4.8 shows the stress history, σ_z, at position 1 for the duration of the excitation, as obtained from the transient finite element analysis with signal A imposed at points A and B. It appears, from inspection, that the stress response follow signal A but there is substantial higher frequency response present, i.e. stress response at a frequency of higher than 2 Hz, This becomes clear when the PSD plot of the stress response is considered, as shown in figure 4.9.

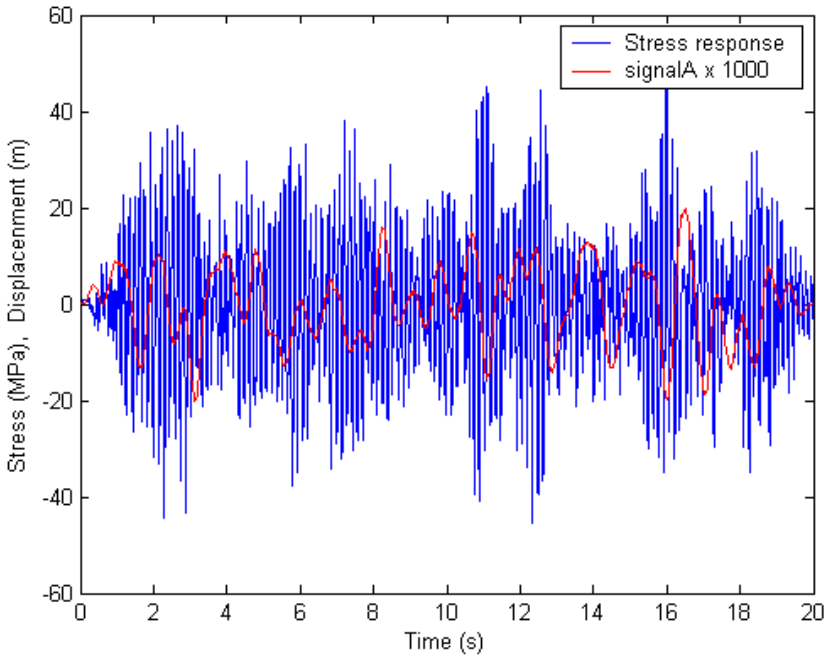

Figure 4.8: Stress response, σ_z, at strain gauge position 1 for in-phase loading with signal A.

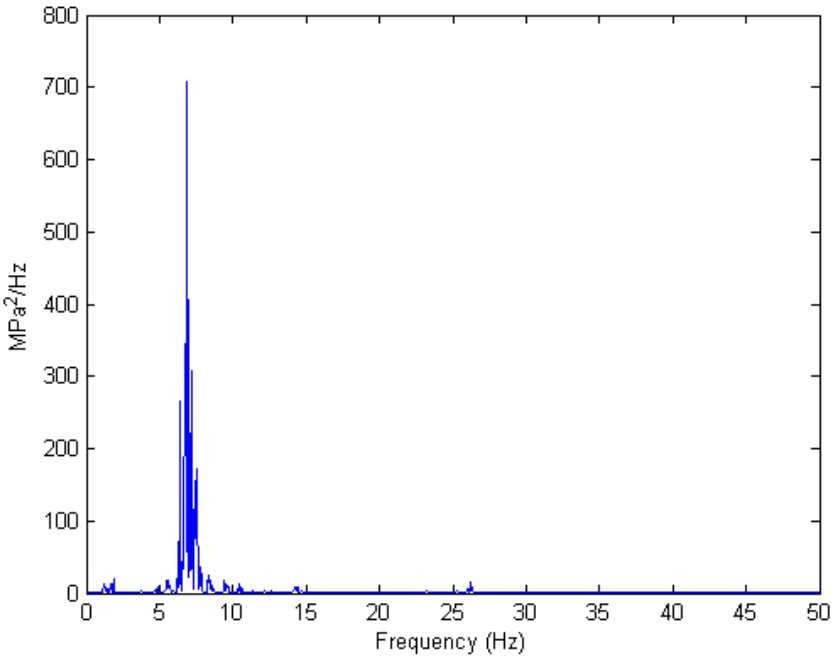

Figure 4.9: PSD of the stress response for strain gauge position 1.

The peak of the PSD lies at 7 Hz, which corresponds with the first natural frequency of the structure as obtained from FEA. This is reason for some concern since it is an indication of the presence of the first mode in the response. The relevance thereof will be dealt with shortly, when the relative ratios of the stresses are determined.

The second analysis was done with out of phase loading, i.e. signal A imposed on point A and signal B imposed on point B. The results of the stress response and PSD characteristics were similar to that obtained with in-phase loading. Since it became clear that some sort of resonant behavior takes place in both in-phase and out of phase loading, the question arose as to whether the quasi-static and FESL technique was viable in practice. The following step was thus to process the measured stress results by means of cycle counting, an additional inertial static analysis and the determination of a fatigue equivalent static load (FESL) factor at each of the 10 strain gauge positions in the same way a measured stress response would be handled.

The outcome of the analysis would be twofold. Firstly the question as to whether the response of the structure will allow quasi-static analysis would be resolved. This would be confirmed if it could be shown that the ratios of the stresses relative to each other during dynamic loading were the same as the relative ratios during static deflection. Secondly the above question would also be clarified in the case of out of phase loading, since deflections in the form of the second vertical mode (if a cantilevered beam was taken as an example) is possible in the case of out of phase loading.

If the FESLs were calculated for each point on the structure and the values were comparable within a certain range, it would thus serve as a confirmation that the ratios of the stresses relative to each other was the same during static and dynamic loading

for the chosen input signals. This would, in turn, indicate that the response of the structure was quasi-static in nature and that the quasi-static fatigue analysis procedure would be viable for the test structure. The obtained stress values due to the inertial loading (σ_{gload}), the equivalent dynamic stresses $\Delta\sigma_e$, obtained from the transient analyses and the resulting FESL factors for each strain gauge position is shown in table 4.5 for both in-phase and out of phase loading. Units of stress are in MPa.

Table 4.5: Transient, inertial and FESL results for in- and out of phase loading.

σ_{gload} (MPa)	Strain gauge position	$\Delta\sigma_e$: In-phase (MPa)	FESL	$\Delta\sigma_e$: Out of phase (MPa)	FESL
65.32	1.	38.29	0.59	27.45	0.42
42.51	2.	25.16	0.59	17.65	0.42
8.63	3.	4.52	0.53	3.24	0.38
60.52	4.	34.04	0.56	24.08	0.38
49.29	5.	26.58	0.54	19.88	0.40
94.31	6.	49.57	0.53	35.81	0.38
69.01	7.	36.26	0.53	26.12	0.38
25.78	8.	13.16	0.51	12.21	0.47
11.34	9.	5.65	0.50	6.83	0.6
24.80	10.	12.26	0.49	13.44	0.54

It is thus clear that certain positions correlate very well with each other such as positions 1 to 7 and thus point to quasi-static response. Some concern is, however, caused by positions 8, 9 and10, which differ by up to 30% from 1 to 7 in both the in-phase and out of phase cases. The integrity of these values will be confirmed, once the FESL values are experimentally determined and compared to the numerically obtained values. The numerical results and FESL values for positions 1 to 7 are acceptable and show that the relative ratios between the stresses are the same during dynamic and static loading.

Returning to the presence of resonance in the structure as indicated by the large energy content in the region of the first natural frequency when figure 4.9 is studied, the question can be asked why the structure remains suitable for quasi-static analysis as shown above. The answer lies in the fact that the first mode shape corresponds to the static deflection mode of the structure. Excitation of the first mode shape will thus yield relative stress ratios corresponding to those obtained from static deflection.

Finally it is deduced that the response of the structure regarding its viability for quasi-static analysis is comparable in both in-phase and out-of-phase loading when the FESL values are considered. This is expected since the formation of deflections corresponding to the third mode shape (second vertical mode) in figure 3.5 due to out of phase loading is in fact not possible due to the structure's boundary conditions at the actuators (universal couplings), which do not allow end moments. Since deflection in the second vertical mode shape under static or quasi-static conditions requires end moments, only deflections conforming to the first mode shape will result. This, however, do not hold for higher frequency excitation which could still cause higher order modes, regardless of the boundary conditions at the actuators.

4.2.4 Experimental investigation of the structure's response to stochastic loading

The numerical results obtained in the previous section concerning the structure's response to a stochastic excitation were verified on the actual structure by means of strain gauge measurements at strain gauge positions 1 to 10. These positions corresponded with the positions on the numerical analysis. The input signal was created by means of a PSD with a prescribed energy content at 2 Hz as shown in figure 4.11. The amplitude of the input signal was selected in order to create stresses in the structure with a range in the vicinity of 140 MPa. This was to ensure that the input signal was of the same magnitude, causing damage of the same order as the signal that would be used for the final fatigue test. The amplitude of the signal was determined by measurement with the rosette gauge at position B in figure 4.3, which is a typical position at which failure could be expected on the structure. The quantification and scaling of the input signal, as well as the failure analysis will be discussed in the section on life prediction, later in this chapter. The experimental excitation was also out of phase since it was determined in the previous section that the FESL methodology could be implemented for out of phase loading in the case of this structure. The excitation signals for actuators A and B and their PSDs to illustrate the energy distribution of the signals are shown in figures 4.10 and 4.11 respectively.

Once the input signal was finalized, the 0°-90° strain gauges at the 10 positions in figure 3.14 were connected into a half-bridge configuration. The structure was then

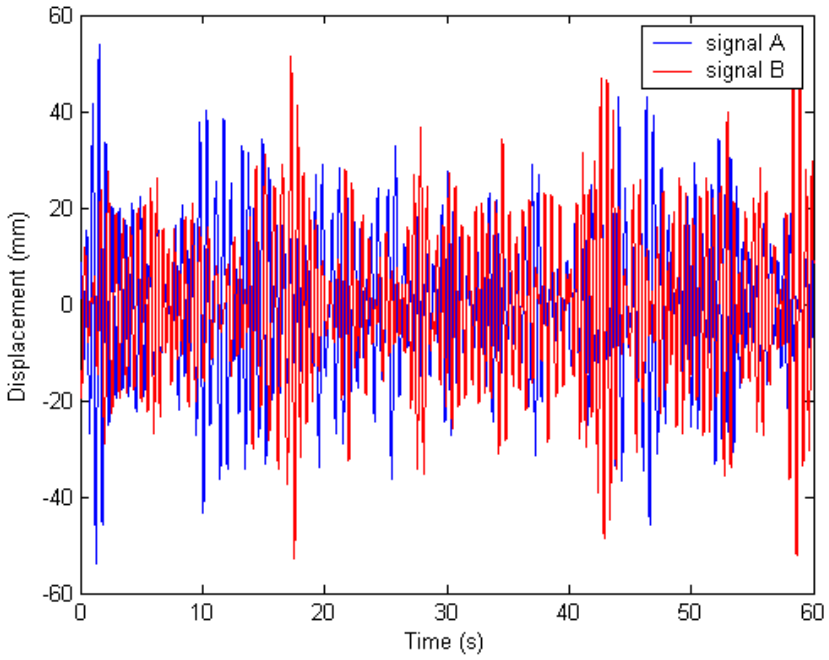

Figure 4.10: Displacement vs. time for the two positions A and B as imposed on the structure by the actuators.

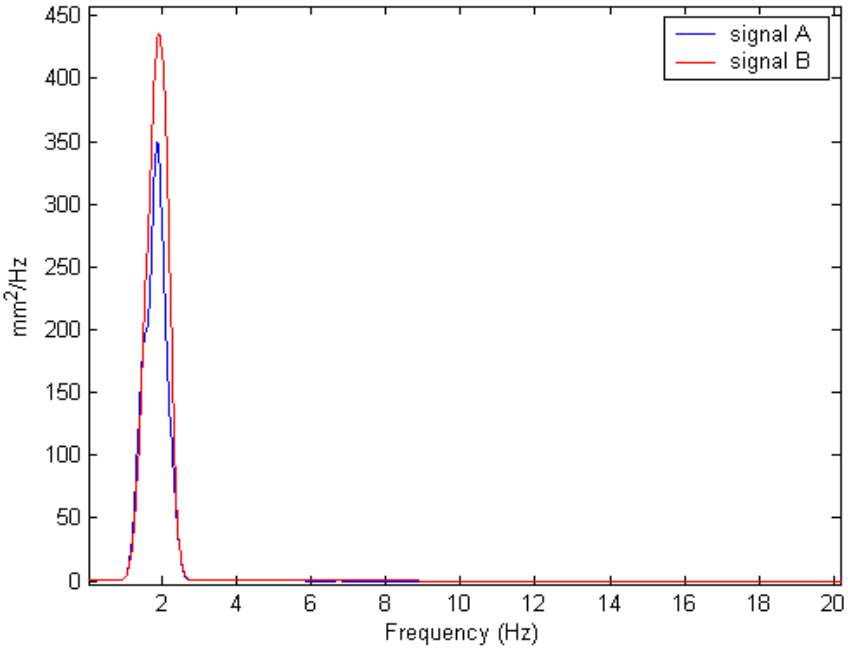

Figure 4.11: PSD of the displacement response of signal A and signal B.

excited and the bridge disturbances were recorded for all 10 positions for the duration of one block of 60 seconds. The bridge disturbances were then converted to strains in the relevant longitudinal directions similar to the procedure followed in section 2.2.3.

The measured longitudinal stress σ_z, or σ_z was then determined for each strain gauge position by multiplying with Young's modulus:

$$\sigma_{x/z} = E\varepsilon_{x/z} \qquad [4.10]$$

For further insight into the response of the structure PSD plots of the stress response of the ten strain gauges were created. Figure 4.12 shows the PSD plot for strain gauge 1. Note that the other nine strain gauges yielded a similar response to strain gauge 1. The two distinct peaks at 2Hz (excitation frequency) and 7Hz (first natural frequency) respectively are clearly visible in figure 4.12. It thus shows good correlation with the normal mode analysis performed in chapter 3 which indicated that the first natural frequency of the structure is situated at 7.14Hz. The fact that the majority of energy is present at 2Hz is also a good indication of the absence of resonance and that quasi-static analysis can be performed with confidence. Note that the relative values of the peaks of the PSD plots at 2Hz and 7Hz differ from those obtained from the transient analysis. This have to be attributed to the damping coefficient implemented in the transient analysis, although it appeared to be sufficient as was shown in section 4.2.1.

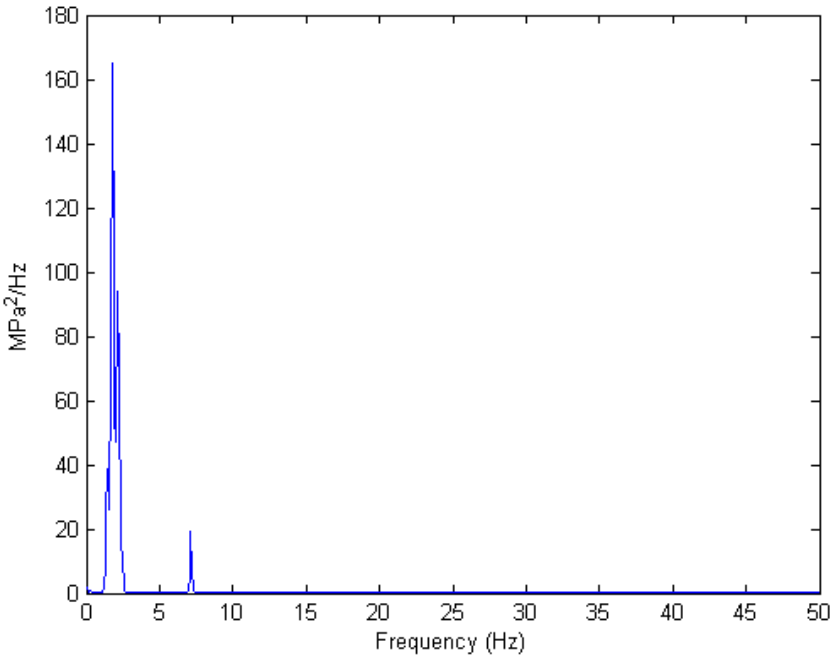

Figure 4.12: PSD of the measured stress response, σ_z for strain gauge position 1.

The following step was to perform Rainflow cycle counting on the measured stresses and to determine a fatigue equivalent stress range, $\Delta\sigma_{measured\_e}$ in the same manner, using equation 4.8, as described in the section 4.2.2. The last step was to determine the FESL factor for each of the strain gauge positions by implementing equation 4.9 and the values of $\Delta\sigma_{measured\_e}$ for each strain gauge. In this manner a longitudinal stress quantity, which gives a partial representation of the stress state in the structure, was defined without going through laborious rosette analysis as was done during the static stress verification. Such a parameter as σ_x, or σ_z would be sufficient for the experimental verification of the structure's viability to FESL analysis, since during FESL analysis it is in fact not just a fatigue relevant stress that is scaled but a complete stress state. This is due to the linearity of the procedure and the FEA. Agreement of the FESL factors for the ten strain gauge positions, determined using the longitudinal stresses obtained through half-bridge analysis instead of the fatigue relevant stresses, would thus be wholly sufficient to verify the amenability of the structure to FESL analysis. Table 4.6 shows the obtained stress values and the FESL factors obtained from the measured response.

Table 4.6: Measured, Inertial and FESL results for out of phase loading.

Strain gauge position	σ_{gload} **(MPa)**	$\Delta\sigma_{measured\_e}$ **(MPa)**	**FESL**
1.	65.32	27.45	0.38
2.	42.51	17.65	0.38
3.	8.63	3.24	0.37
4.	60.52	24.08	0.43

5.	49.29	19.88	0.43
6.	94.31	35.81	0.44
7.	69.01	26.12	0.43
8.	25.78	12.21	0.55
9.	11.34	6.83	0.61
10.	24.80	13.44	0.56

Once again it can be seen that certain positions give reason for concern. In this case it are positions 8, 9 and 10 that yield FESL factors that differ significantly from the other factors. The reason for this has to lie somewhere within the dynamics of the structure since it cannot be allocated to modeling issues, as was the case with the FESL obtained from the numerical analysis. The notion is that the presence of the first mode in the response does indeed affect the relative ratios of the stresses in some way, although the mode shape corresponds to the static deflection of the structure. The second possibility is that there does exist some difference between the static deflection mode and the deflection mode due to the stochastic excitation. It is, however, interesting to note that the problematic positions all lie in the same third of the structure i.e. close to actuator A and also corresponds to the problematic positions indicated by the transient analysis. The implication of the FESL values as listed in table 4.5 are that accurate fatigue life predictions will be made if the failure location and the scaling strain gauge are both located in the region of strain gauges 1 to 7, excluding the round tubing. The FESL life prediction will consequently proceed in such a manner since the failure locations and the scaling rosette strain gauge are both in the region of strain gauges 1 to 7.

When the FESL method is implemented in practice, care should be taken, however, to ensure that the requirements for proper FESL analysis are met. This is, as was already mentioned, that no higher order modes take part in the response of the structure and that the actual response of the structure does indeed correlate with the static deflection mode of the structure. The correlation between the response of a structure and its static deflection mode must also be carefully considered in practice. A more detailed analysis of the structure's response to unearth the reason for the deviations of FESL values 1 to 3 is, however, beyond the scope of this research.

Once the suitability of the structure for quasi-static analysis was assessed the next step was to quantify the input signals and perform the actual fatigue life prediction and test on the structure. This is addressed in the following section.

4.3 Fatigue life prediction and testing

4.3.1 Scaling and quantification of the input signal

The reason for the scaling of the amplitude of the input signals (signal A and B) is to ascertain that the fatigue damage on the structure due to one block of excitation will be sufficient to cause fatigue failure within a practical and attainable time. The fatigue analysis will concern two points on the structure namely point B and D in figure 4.13. As mentioned in the scope of research, a nominal stress analysis (point B) as well as a hot spot stress analysis (point D) will be performed. Point B and point D was

recognized as the points expected to fail first in their respective categories by means of a static finite element analysis employing an inertial load. Since point D experiences the highest stresses and also corresponds to a weld category with a lower fatigue resistance, it will be the first position on the structure to fail and will be assessed by the hot spot method. Point B will be the second position on the structure bound for failure and will be assessed by means of the nominal stress method.

The input signals A and B shown in figure 4.10 were scaled to reach a stress range of more or less 140 MPa point B. This was done in order to ensure that the time limit for the fatigue test was imposed on the location expected to require the most cycles to failure. As mentioned, position D experiences higher stresses than position B and can also be correlated to a category with lower fatigue resistance. Note that position D does not belong to an actual category in the BS code, hence the assessment by the hot spot stress method. Finite life would thus be ensured for point B as well as point D. The scaling procedure was as follows:

- Connect the rosette gauge at position B, measuring three independent channels (0°, 45° and 90°) similar to the static stress verification described in section 4.1.2.
- Impose signal A and B (1 block of 60s) on the structure, starting at a low maximum displacement value (in the order of $1/10^{th}$ of the signal used for the dynamic stress verification) and determine the measured stress response for the x -and z-directions by implementation of equations 4.1 and 4.2.
- Perform Rainflow cycle counting on the relevant measured stress history (σ_z) and determine a fatigue equivalent stress range $\Delta\sigma_e$ from the cycle counted ranges by implementation of equation 4.8.
- Determine the damage caused to the structure by one block of excitation by implementation of the S-N curve for the particular category (category F, BS7608: 1993).
- Repeat the procedure until the desired damage is caused by one block of excitation. In this case it was required that the damage should be of sufficient magnitude to cause failure after two weeks' continuous repetition of the loading history

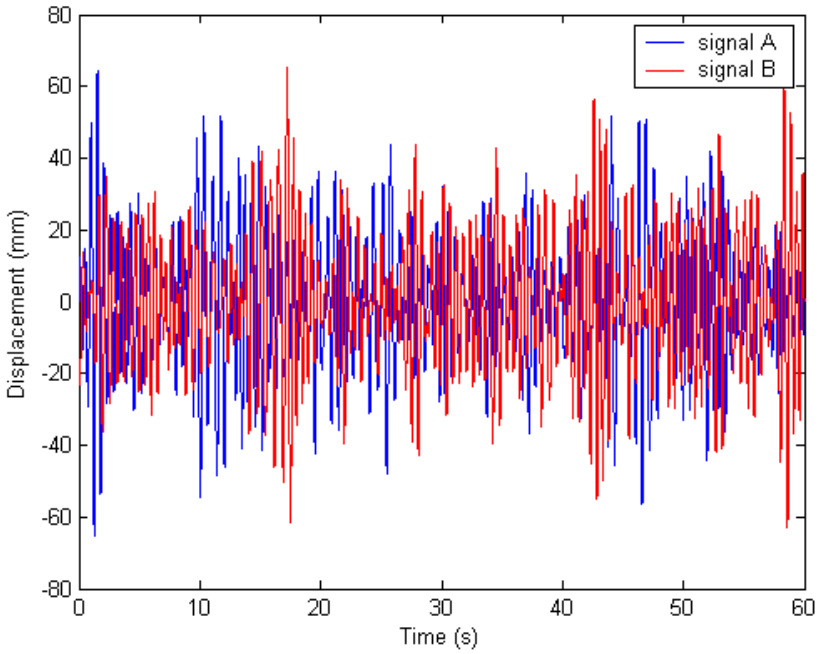

Figure 4.13: Displacement versus time characteristics of the final drive signals as imposed on the structure by the actuators.

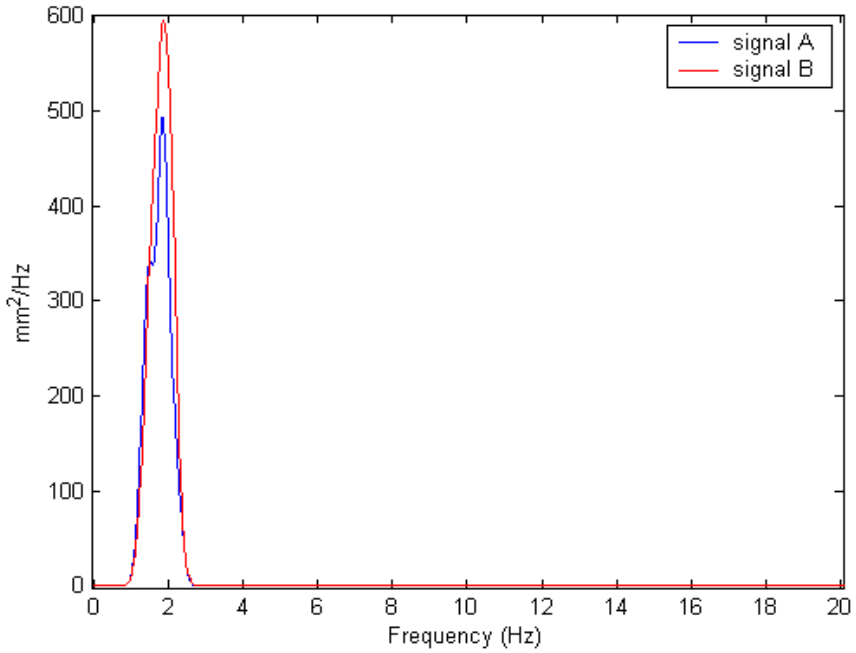

Figure 4.14: PSD of the displacement response of signals A and B.

The final drive signals for actuators A and B, causing sufficient damage, are shown together with a PSD plot in figures 4.13 and 4.14 respectively. These are the input signals that will be employed in the endurance test of the structure. A delay of 20 seconds will be introduced between the excitation blocks during the actual endurance

test to allow sufficient differentiation between the subsequent blocks. The corresponding stress response will be used in the fatigue analysis of the nominal and hot spot positions (points B and D respectively).

4.3.2 Fatigue life prediction by means of the nominal stress method

Position B on figure 4.3 will be assessed by means of the nominal stress method and falls within category F of the BS 7608: 1993 fatigue design code. According to the IIW recommendations the principal stresses at a failure location should also be included in the fatigue analysis, providing that the direction of the largest principal stress is within 60° of the longitudinal axis of the member. The nominal stress fatigue life prediction procedure will consequently proceed from the measured stress response along the longitudinal axis of the member, σ_x, as well as the algebraically larger of the two principal stresses, σ_1 or σ_2, should they act within 60° of the longitudinal axis of the member. The recommendations concerning the position for nominal stress extraction, developed in chapter 2 will also be implemented in the analysis.

The principal stresses are defined as the maximum tensile stresses occurring in a member due to the combination of tensile and shear stresses acting along the x and z directions of a stressed member. These stresses coincide with the x- and z-axis in the case of pure bending and tension but are oriented at other angles if shear stresses are present. The principal stresses, σ_1 and σ_2, always act perpendicular relative to each other. The IIW recommendations stipulating the inclusion of principal stresses in fatigue analysis makes sense since their magnitude exceeds that of the uni-axial stresses when shear stresses are present. Neglecting them can thus lead to non-conservative life predictions.

The first step in the life prediction was to obtain the rosette strain gauge measurements at position B for one block of excitation. The strains were then converted to stresses σ_x, σ_z and τ_{xz} by means of equations 4.1 and 4.2, as was done in section 4.1.2. The calculation of σ_1 and σ_2, proceeded by means of equation 4.10:

$$\sigma_{1,2} = \frac{\sigma_x + \sigma_z}{2} \pm \sqrt{\left(\frac{\sigma_x - \sigma_z}{2}\right)^2 + {\tau_{xz}}^2} \qquad [4.10]$$

After the larger of these stresses was determined (a process that had to be repeated for each measured entry of the stress response caused by a block of excitation), it was verified that it acted within 60º of the longitudinal axis of the member by calculating the angle θ at which it occurred. The smaller principal stress's accompanying angle was also determined and checked for perpendicularity to verify the correctness of the larger principal stress.

After the relevant longitudinal and principal stresses were determined, the next step was to determine the expected number of blocks to failure of point B, based on the measured stress response. The nominal stresses suited for implementation with the S-N curve were obtained by linear extrapolation of the longitudinal stress σ_x, and the principal stress σ_1, to the weld toe. The extrapolated stresses were denoted as σ_{x_nom},

and σ_{prins_nom} respectively. The procedure corresponded with the recommendations developed in section 2.4.2.

The extrapolated stress response is shown in figure 4.15 for both the longitudinal and principal stresses. Note that the longitudinal stresses and the principal stresses are almost similar in magnitude since a condition of pure pending is approached in the member accommodating point B.

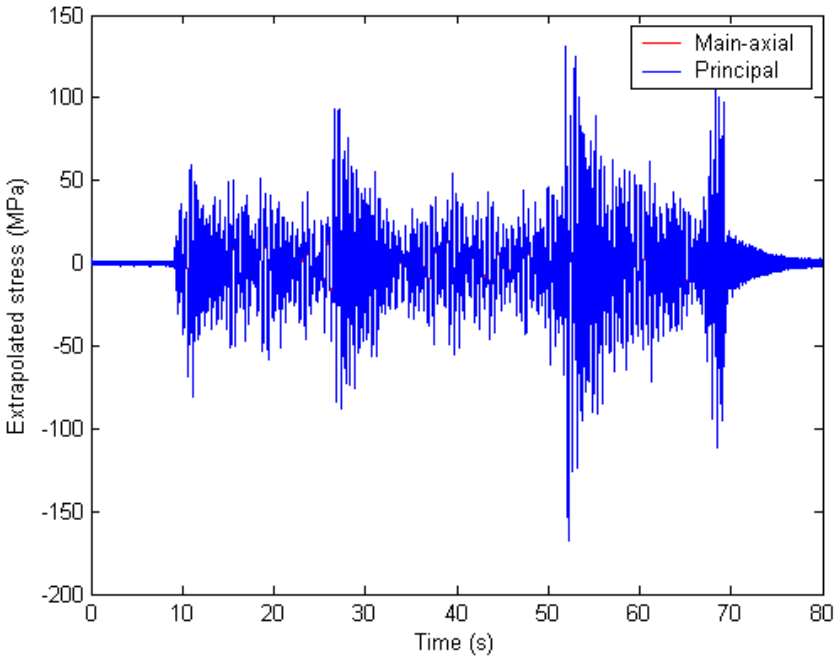

Figure 4.15: Extrapolated nominal stress obtained from strain gauge measurements (point B) for one block of excitation.

Figure 4.16 shows the stress response over one second for greater clarity. It should also be noted that the duration of the stress response is 80s and not 60s since a 20s delay is introduced between the excitation blocks as mentioned in the previous section. The little difference that exists is caused by shear stresses resulting from torsion in the member due to slight misalignment caused by the welding process.

The next step was to determine the fatigue equivalent stress range $\Delta\sigma_e$ for one block of excitation over 80s and N cycles (where N equals the sum of the discrete cycles isolated by the Rainflow algorithm for one block of excitation) for the stress response σ_{x_nom}, and σ_{prins_nom} respectively. This was done by implementation of equation 4.8. The following values for $\Delta\sigma_e$ were obtained for the longitudinal and principal stresses respectively:

$\Delta\sigma_e$ (longitudinal) = 52.2 MPa
$\Delta\sigma_e$ (principal) = 52.3 MPa

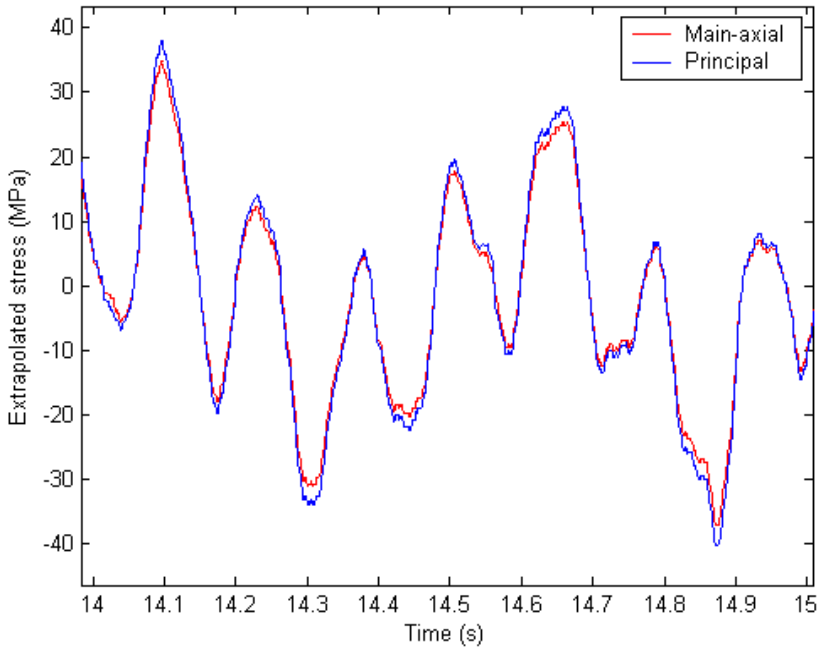

Figure 4.16: Extrapolated nominal stress obtained from the strain gauge measurements (point B) for one second of excitation.

The next step was to determine the fatigue damage caused by the input loading. Firstly the expected life N_e under sinusoidal loading with a stress range equal to $\Delta\sigma_e$ was determined for both the longitudinal and principal equivalent stresses by substitution of $\Delta\sigma_e$ into the relevant S-N curve of the weld category:

$$N_e = C_d / (\Delta\sigma_e)^m \qquad [4.11]$$

where $C_d = C_o = 1.726\times10^{12}$.

The value of the constant C_d was taken as C_o in order to implement the 50% probability of failure curve instead of the design curve ($C_d = C_2$), which lies two standard deviations below the mean curve. This was to ensure realistic, instead of over conservative predictions since implementation of the design S-N curve would result in much shorter life predictions. The damage caused by one block could then be calculated from equation 4.6 for both the longitudinal and principal stresses and was respectively found to be:

$D_{longitudinal} = 9.89\times10^{-5}$
$D_{principal} = 9.93\times10^{-5}$

The number of blocks to failure was then determined by calculating the reciprocal of the damage:

Number of blocks to failure using longitudinal stress = $1/D$ = 10110.
Number of blocks to failure using principal stress = $1/D$ = 10070.

It thus becomes clear that implementation of principal stresses does not have a significant influence on the life prediction in this particular case but must not be overlooked when greater shear stresses are present. The extrapolation procedure, however, is crucial in all cases, since non-conservative predictions would be made if an uninformed choice of stress were used in the case of bending, since the extrapolation procedure would be omitted, resulting in the extraction of lower stresses. The following section will deal with the fatigue life prediction of point D by means of the hot spot stress method.

4.3.3 Fatigue life prediction by means of the hot spot stress method

Point D in figure 4.3 will be assessed by the means of the hot spot stress method, since the specific welding detail is not categorized in the BS code. As mentioned earlier, point D also experiences the highest stress among similar details in the structure during stochastic loading and is thus expected to fail first. The stress extraction will proceeded in the same manner as with point B, except that the extrapolation procedure is prescribed by the IIW in their fatigue design recommendations for welded joints and components.

The prescribed stress extrapolation procedure gave rise to the installation of two rosette gauges at positions C and D as can be seen on figure 4.3. The foremost point of the measuring grid of the first gauge was placed at position C at distance of 0.3t from the weld toe, i.e. 1.8 mm, while the second strain gauge's grid centre point was positioned at position C at a distance of 9mm from the weld toe, which corresponded to the IIW requirement of a distance of 1.5t from the weld toe. Figure 3.13 shows the recommended placement of the strain gauges.

The stress extraction proceeded in the same manner as was described for the nominal category in the previous section , except that the extrapolated hot spot stress, σ_{hs} along the longitudinal axis of the member obtained from the two strain gauges was processed by the Rainflow algorithm instead of the nominal stress, σ_{x_nom} as was done in the previous section. Equation 4.8 was used to determine a fatigue equivalent stress $\Delta\sigma_e$ from which the life prediction could be made. The principal stresses were once again determined for the two strain gauges from where the hot spot stress based on the extrapolation of the principal stresses at the two strain gauge positions, σ_{hs_prins}, were determined. The hot spot stress ranges at point D for the principal and longitudinal stresses are shown in figure 4.17. The following values of $\Delta\sigma_e$ in terms of longitudinal and principal hot spot stresses were obtained:

$\Delta\sigma_e$ (longitudinal) = 134 MPa.
$\Delta\sigma_e$ (principal) = 134.3 MPa.

It is once again clear that there exist very small differences between the longitudinal and principal hot spot stresses due to the absence of significant shear stresses in the member containing points C and D.

The expected life N_e of the joint under constant sinusoidal loading with $\Delta\sigma_e$ was determined by substitution of $\Delta\sigma_e$ (obtained from the longitudinal and principal hot spot stresses respectively) into the relevant hot spot S-N curve of the weld category.

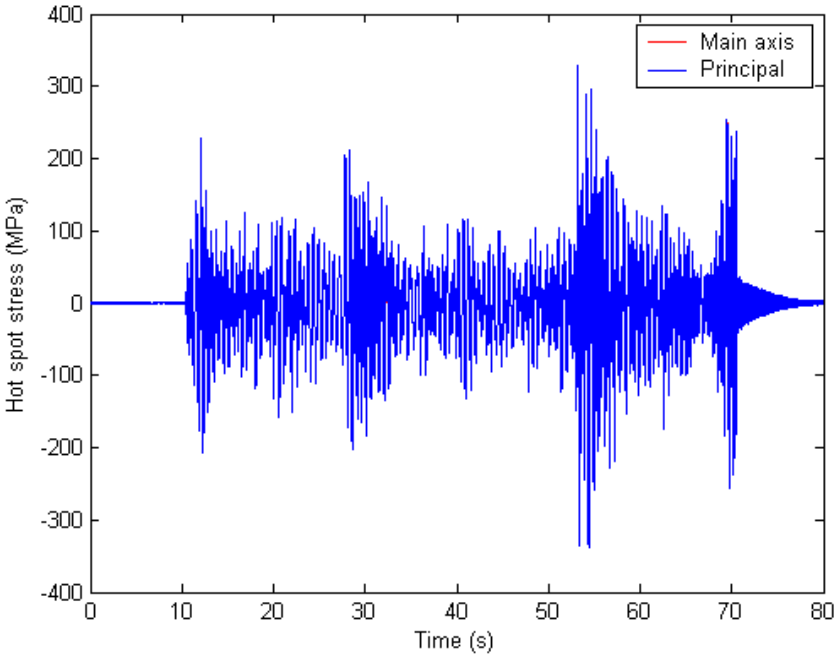

Figure 4.17: Hot spot stresses obtained from the strain gauge measurements at point C and D for one block of excitation.

The applicable hot spot S-N curve fell under category 1 of the IIW recommendations, with a FAT value of 100 MPa.

$$N_e = C_d / (\Delta\sigma_e)^m \qquad [4.12]$$

where $C_d = C_o = 5.715\times10^{12}$.

The damage caused by one block could then be calculated from equation 4.6 for both stress parameters and was found to be:

$D_{longitudinal} = 5.061\times10^{-4}$.
$D_{principal} = 5.086\times10^{-4}$.

The number of blocks to failure was consequently determined by the reciprocal of the damage:

Number of blocks to failure using longitudinal stress = $1/D$ = 1976.
Number of blocks to failure using principal stress = $1/D$ = 1966.

The final step of the fatigue life analysis concerns the finite element prediction, implementing the FESL methodology. The analysis will implement both the nominal and hot spot methods and will once again focus on point B and point D. The finite element analysis, response measurement and FESL supported life prediction for the two points will be dealt with in the subsequent section.

4.3.4 Nominal and hot spot fatigue life predictions supported by FEA and the FESL methodology

In the case where a complex structure is analyzed in practice the probability of applying strain gauges at the correct failure locations are very low due to the vastness of the structure as well as the fact that some critical points are not accessible for strain gauge application. In such cases the FESL methodology will be implemented to obtain the stress response of the whole structure by utilization of the stress response captured at one point by a single strain gauge as well as a complete finite element model of the structure. This could only be done if the response of the structure met the requirements as outlined in section 4.2.1.

It has already been verified by computation of the FESL values at the 10 half-bridge strain gauge positions that the structure's response is quasi-static in nature at the possible failure locations (section 4.2.3). The following step is a fatigue analysis based on the FESL methodology and the final finite element model constructed according to the meshing regulations developed in chapter 2. The results will be compared to the life predictions obtained from the direct strain gauge measurements in section 4.3.2 and 4.3.3. The incentive is to illustrate the effectiveness of the method and also to verify its reliability.

The fatigue assessment procedure (as outlined in section 4.2.2) was as follows. The strain gauge for which the strain response due to than 1 block of loading was determined was strain gauge A in figure 4.3 (rosette gauge). The longitudinal stresses at position A was determined by means of equation 4.1. The following step was to determine the fatigue equivalent sinusoidal stress $\Delta\sigma_e$ by means of Rainflow cycle counting of the longitudinal stress response (which was exactly similar to the stress response on other parts of the structure such as shown in figure 4.15 and 4.17, except for magnitude differences). Equation 4.8. was implemented to determine the value of $\Delta\sigma_e$ at position A as 47.94 MPa. The stress due to the inertial load of 1g was next determined from the finite element model at the position on the model corresponding to position A as 59.5 MPa. From this the FESL value could be determined from equation 4.9 as follows: FESL = 47.94/59.5 = 0.81.

Consequently an inertial load of 0.81g was imposed on the finite element model. The stress response at the points B and D of figure 4.3 (the two possible failure locations) is shown in figures 4.18 and 4.19. Note that the MPCs connecting the two members are not visible in the contour plot. The reason for implementation of MPCs instead of inclined elements is due to the difference in thickness of the two members and the fact that only the centrelines are modelled by the shell elements.

The static stress values due to the inertial load could now be extracted from the finite element model at the two expected failure locations (point B and D). At point D the stresses were to be extracted at the prescribed positions of 0.4t and 1.0t from the weld toe. This corresponded to distances of 4mm and 6mm. The stress values were then linearly extrapolated to the weld toe according to the hot spot stress procedure as stipulated by the IIW:

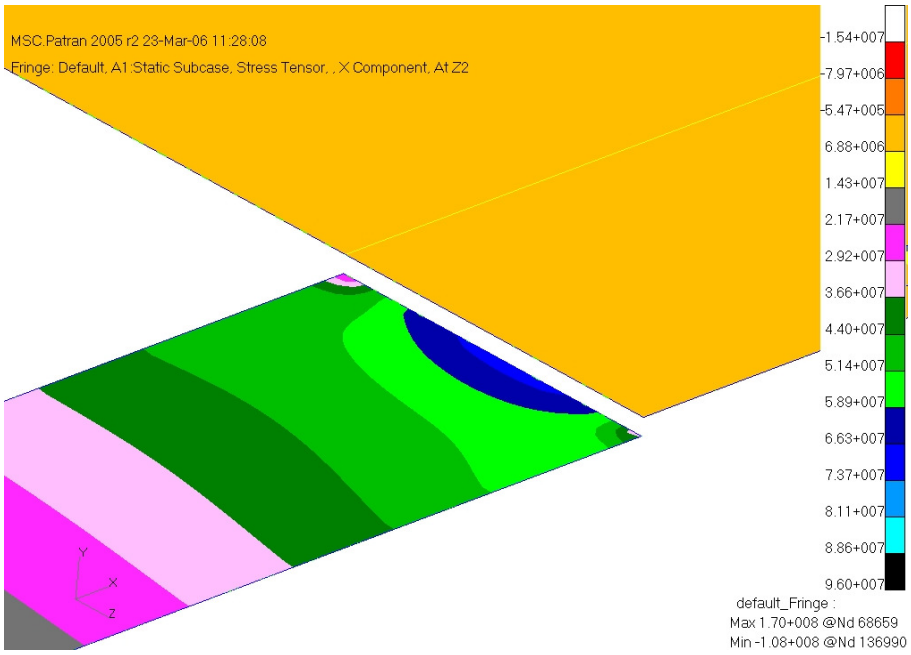

Figure 4.18: Stress response of point B of figure 4.3 due to the fatigue equivalent inertial load of 0.81g.

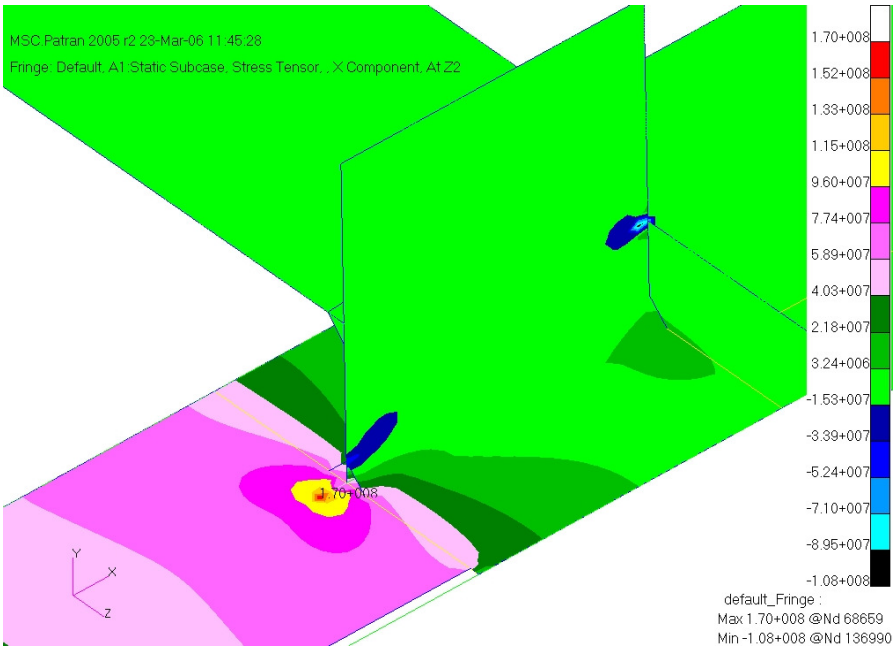

Figure 4.19: Stress response at point D of figure 4.3 due to the fatigue equivalent inertial load of 0.81g.

$$\sigma_{hs} = 1.67\sigma_{0.4t} - 0.67\ \sigma_{1.0t} \qquad [4.13]$$

At point B the stress value 25mm away from the weld toe was to be taken as the foremost point of extrapolation while the stress value 40mm away from the weld toe was taken as the second point.

The following values for nominal stress range (position B) and hot spot stress range (position D) were determined from the finite element model by implementation of the above procedure:

σ_{nom} = 60.2 MPa
σ_{hs} = 179.5 MPa

The above values (longitudinal) were then substituted into the relevant S-N curves for the nominal and hot spot stress methods (equation 4.11 and 4.12) and the expected life N_e under constant sinusoidal loading with σ_{nom} and σ_{hs} determined for the two positions respectively. From there the damage was calculated from equation 4.6 where N was taken as the sum of the discrete cycles obtained from the Rainflow procedure performed on the measured stresses used to scale the FESL input (after equation 4.5). From there the number of blocks to failure was calculated as the reciprocal of the damage. The following predictions were obtained:

Point B: Number of blocks to failure: 6730
Point D: Number of blocks to failure: 822

At this point the question could be asked why the stresses and life predictions obtained from the FESL procedure are more conservative than the actual measurements. In the first place, point B will be considered. It is clear from tables 4.2 and 4.3 that position B undergoes a higher absolute value of stress under static loading than point A (20.9 MPa vs. 18.7 MPa). Such a ratio of stresses will consequently also exist during inertial analysis due to the linear nature of the finite element analyses. The ratio of the fatigue equivalent stresses $\Delta\sigma_e$ obtained from the strain gauge measurements and the procedure outlined in section 4.2.4 for the two positions is, however, close to 1. This causes a higher stress state to be extracted at position B in the finite element analysis with the fatigue equivalent inertial load imposed on the structure, which in turn accompanies a shorter predicted life. This is once again due to the linear nature of the scaling process.

This phenomenon illustrates the purpose of the analyses performed in section 4.2.3 and 4.2.4 where the relative ratios of the stresses in the structure due to dynamic and static loading were investigated. Conservative results were thus obtained for point B due to the fact that its stress ratio relative to point A during static loading was higher than during dynamic loading. The situation could, however, have been different. This would obviously have lead to non-conservative results – a situation which should be kept in mind in practice.

The same could be said for position D, but there is another factor that also has an influence, namely the sharp stress concentration in the region where the stresses are extracted. It has previously been shown that for a detail similar to the one assessed at point D, the non-linear stress response is already reached 50mm away from the weld toe. It is also clear that the stress concentration is very sharp. Although the IIW recommendations for hot spot stress extraction does include the macro geometrical

stress concentration or non-linear stress rise, the non-linear stress peak (figure 1.2) is not included. By contemplation of figure 2.32, however, it is clear that stresses extracted at a distance of 4mm and 9mm are well within the non-linear stress peak. The finite element extraction of hot spot stresses are thus believed to be very conservative, in comparison with strain gauge measurements, since the difference in measured and calculated stresses at points C and D is much higher than could be accredited to response non-linearities of the structure, as was the case with point B.

Figure 4.20 shows a graph of the stress response in the region of points C and D to illustrate the sharp non-linear stress rise near the weld toe. The origin of the x-axis marks the weld toe.

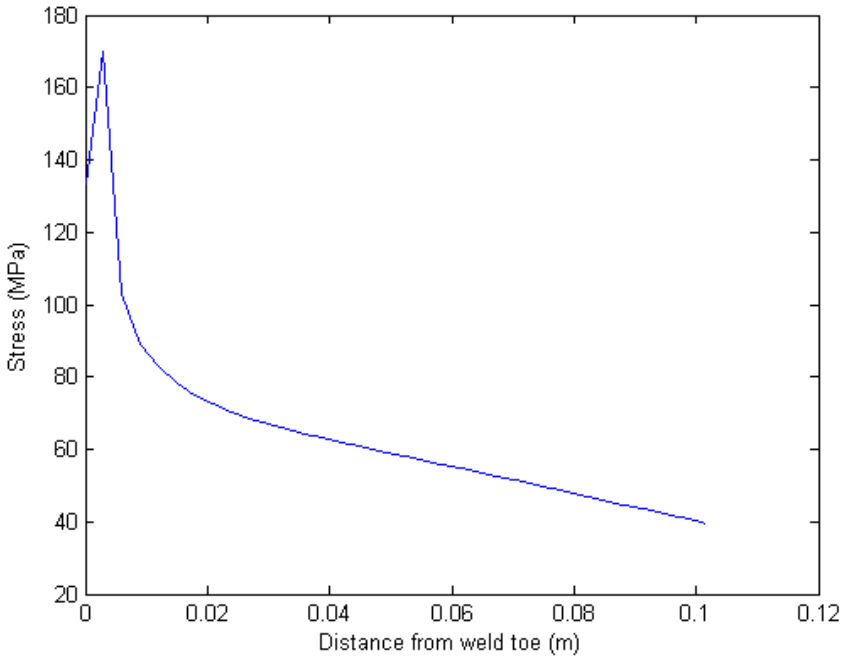

Figure 4.20: Stress distribution in the region of points C and D.

In this case it is clear that the non-linear stress peak starts at 25mm from the weld toe, as opposed to the 50mm distance seen in figure 2.32. It could be due to the fact that the stiffener configuration is different and that the support and boundary condition of the joint also differs from the details assessed in section 2.4.2. The relevance of the observed difference of the start of the non-linear stress rise will later be discussed.

The final part of the verification of the proposed nominal stress extraction methodology is the actual endurance test which will serve to corroborate the preceding fatigue life analysis. The fatigue test procedure and actual fatigue life results are discussed in the following section.

4.3.5 Fatigue testing and results

The final step of the investigation was to perform the actual fatigue test on the structure to verify the integrity of the life predictions performed in section 4.3.2 to 4.3.4. The test setup is shown in figures 3.10 to 3.12, except that the strain gauge leads were removed since the relevant measurements were completed. The excitation signals shown in figure 4.13 were imposed on the structure by means of the Matlab based Dura and Qantim fatigue testing and signal generation software packages. The blocks of excitation imposed on the structure were logged until failure was detected. At locations B and D failure is defined as the observation of a through wall crack by the IIW, since it is a big structure. On component level, failure is defined as complete rupture according to the IIW.

The test was run until a through wall crack was identified at the first failure location. Point D failed first (after 8050 blocks) and was consequently welded up to allow failure at point B to commence. Point B did not fail after after 18000 blocks of excitation and the test were consequently discontinued due to practical considerations, since the test was approaching a duration of almost one month. Another factor influencing the decision to stop the test was the fact that failure could even occur after 40000 blocks due to the huge amount of scatter in the S-N curves as mentioned in the literature survey. An idea of the magnitude of the data scatter for a typical fatigue test can be formed when figure 1.12 is considered. It can clearly be seen that for a specific stress, the values for life lie within a scatter band and can differ with up to a factor of 5 on both sides of the mean (for the hot spot stress method). Hobbacher (2003) also illustrated that scatter bands containing data that differed up to a factor of 10 on both sides of the mean, i.e. containing total differences of up to a factor 100 was typical for nominal stress curves. A factor of four, as was obtained from at point D thus gave a good indication as to what could be expected at point B. The results obtained are shown in table 4.6.

Table 4.6: Fatigue test results

Location	Predicted life (measured, longitudinal)	Predicted life (measured, principal)	Predicted life (FESL + FEA, longitudinal)	Actual life
Point D	1976	1966	822	8050
Point B	10110	10070	6730	>18000

Figure 4.19 shows the geometry in the vicinity of point D as well as a close up image to observe the cracks at the weld toe for point D. Note that the crack started at the weld toe and propagated through the beam until a through thickness state was reached (indicated by the arrows), which was taken as failure.

The completion of the endurance tests marked the end of the verification procedure and also the experimental work concerning the structure. The interpretation of the fatigue results as well as the conclusions and recommendations concerning the study as a whole are addressed in the following chapter.

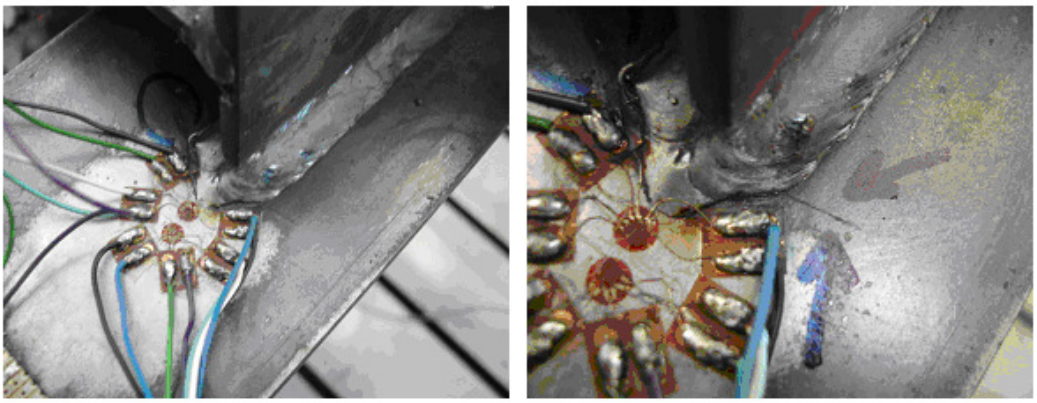

Figure 4.19: Geometry and position of the cracks at the hot spot failure location (point D).

5. Recommendations and conclusions

The primary aim of this study was to develop and validate an economic finite element meshing and nominal stress extraction scheme for the assessment of the fatigue life of welds in complex plate-like structures. The need for such a study arose due to the absence of explicit guidelines for nominal stress determination by means of finite element modeling in the BS 7608:1993, ECCS 6:1985 design codes and the IIW:XIII-1965-03 fatigue design recommendations.

Guidelines for the correct representation of a weld in plate-like structures and subsequent meshing in the vicinity of the weld were developed in chapter 2. The weld categories that were covered were basically load carrying and non-load carrying variations of simple cruciform joints and T-pieces as well as a few plate-stiffener configurations. The experimental establishment of the 20-node solid element as a benchmark by which other element configurations could be validated and assessed laid the foundation for the numerical work. It was found throughout that modeling of the weld by means of adjacent inclined elements as shown in figure 2.27 gave the closest or at least a conservative resemblance to the solid element configuration. From there an extensive study into the nature and position of the non-linear stress rise (hereafter referred to as the N-LSR) resulting from the notch effect of the weld toe and the macro structural stress raising effect of the plate intersections was done on the cruciform joint, T-piece and plate-stiffener configurations. A variety of load cases and geometrical variations were numerically investigated from which the stress extraction procedure as outlined in section 2.4.1 –2.4.6 was developed. Three very important points emerged from this investigation:

1. The start of the N-LSR appears at fixed distances from the weld toe of a cruciform joint, T-piece or plate-stiffener setup, irrespective of the plate thickness or boundary condition.
2. The position of the N-LSR is, however, dependent on the loading mode of the connection. This resulted in different positions for the start of the N-LSR under bending and tensile loading. When a combination of bending and tensile loading acted on a member, the position of the N-LSR was governed according to the relative stress contributions of the loading modes.
3. The position of the N-LSR was found to be category specific, especially in the case of bending. This was established due to the fact that the N-LSR appeared at different positions for T-joint and the plate-stiffener configurations.

The three abovementioned points have the following implications as concerned to the application of the developed procedure in industry. Firstly it was surprising to found that the position of the N-LSR was independent of plate thickness since it is claimed by several authors in the literature to be a function of plate thickness (Dong, 2001; Niemi, 1995; Doerk et al., 2002 and Hobbacher, 1996). As previously mentioned, the reason for such an ambiguity could, however, be accredited to the definition of the non-linear stress peak (N-LSP) as defined by the mentioned authors and the IIW as opposed to the definition of the non-linear stress rise (N-LSR) referred to in this study. The N-LSP refers to the local notch effect of the weld toe only while the N-

LSR includes the macro geometrical stress concentration caused by the intersection of the plates as well as the local effect due to the weld toe.

This gets clear when the numerical work based on a local analysis with proper weld geometry modeling with a fine mesh in section 2.4.4 is considered, since it can be clearly seen from figure 2.33 that the N-LSP starts at a distance of more or less 4mm from the weld toe for a plate thickness of 10mm. This, to the contrary, is in good correlation with the literature, which states that the N-LSP appears at a distance of 0.4t from the weld toe (t=plate thickness).

The second point relates to the fact that the position of the N-LSR or macro structural stress concentration was dependent on the loading mode and in combined cases dependent on the relative stress contribution of possible bending and tensile loads. This trend led to the development of a parametric equation for the position of stress extraction in terms of the degree of tension (equation 2.7). The question can, however, be asked as to how such a degree of tension should be determined in the case of a complex structure. This is because it can be extremely difficult to differentiate between the bending and tensile stress contributions at a certain point. In the case of symmetrical structural elements the answer is to determine the tensile stress simply as the difference between the stresses on the top and bottom extremities because pure bending has a symmetrical stress distribution with opposite signs on the extremities according to Euler beam theory. The determined difference would thus be the superimposed tensile stress in the structural element. In the case of uncertainty or where the tensile stress cannot be quantified it is recommended that the foremost point for extrapolation simply be taken as 70mm from the weld toe, since all stress raising effects will then be excluded. Note that the specific parametric equation and above recommendations only covers the structural details that were investigated in sections 2.4.1 to 2.4.6. This brings us to the third point.

The fact that the position of the N-LSR was found to be category specific indicates a need to extend the findings to other welding categories in order to obtain a more complete set of meshing and stress extraction guidelines. However, if a structure that needs to be analyzed contains categories that have not been investigated yet, the recommendation is that a graph of the stress in the structure in the vicinity of the specific category is constructed, starting at the weld toe. In this manner, a good indication of the nature of stress response of the specific category as well as the position of the N-LSR can be obtained. Stresses should then be extrapolated to the weld toe with the point marking the end of the linear stress distribution taken as the foremost point of extrapolation in the case of bending. In this way the N-LSR should be excluded from the extracted nominal stress. In the case of tension, the position where the stress field gets uniform should be used for the nominal stress. In the case where a category is included in the structure which is not covered by the nominal stress method, it is strongly recommended that the hot spot stress method as outlined in the IIW fatigue recommendations should be implemented due to its clear and well outlined procedure. The method is more universal in nature and thus suited to accommodate new geometries or structural details.

A number of conclusions were also reached from the experimental strain analyses. From section 2.3 it should be recalled that the 0°-90° strain gauge measurements with half-bridge configurations gave poor results due to the eccentricity of the specimen,

hence the implementation of a full bridge configuration. It is, however, true that there will always exist some sort of misalignment or eccentricity in actual components and it has to be accounted for. It is thus recommended to stay clear of half bridge measurements when pure tension or bending needs to be extracted, even if the loading mode is unambiguous and apparent absence of eccentricity or misalignment exists. In cases where pure bending or tension needs to be extracted the use of full bridge configurations is suggested.

The same situation (poor measurement results due to implementation of half-bridge configurations) was encountered when the static stress verification on the complex structure was performed. This time the reason is the fact that even if a situation of pure bending or tension is encountered, one can not always be sure that the ratio of the strains in the transverse and longitudinal directions relative to each other will have a ratio equal to Poisson's ratio for the specific material as illustrated in section 4.1.2. It is thus recommended that rosette strain gauges with independent measuring grids should be implemented when stress determination on complex structures are done. The incentive behind it is threefold:

Firstly it is important to determine the correct fatigue relevant longitudinal stresses in the vicinity of the weld. Application of strain gauges at such positions will consequently always be necessary when fatigue analyses by means of direct measurements are performed. As explained in section 4.1.2 the Poisson effect is not always possible at welds due to the geometric constraints of the intersection (refer to figure 4.4), even if a uni-axial stress state is present.

Secondly, in the multi-axial situation, the application of rosette strain gauges enable the determination of principal stresses, which can be significantly higher than the longitudinal stresses if shear stresses are present. The fatigue design codes such as BS 7608 and the IIW recommendations state that cracks will propagate perpendicular to the direction of the highest principal stress and that fatigue life predictions consequently have to be based on principal stresses. Neglecting the principal stresses could thus lead to grave underestimations.

Thirdly, strain gauge measurements are utilized to quantify input loading when the FESL methodology (implemented in section 4.3.4) are used. Consequently, if the stress response at the position of such a strain gauge is incorrectly measured (such as could happen with 0°-90° strain gauges and faulty assumptions), the input loading will be erroneously quantified, leading to finite element stresses throughout the whole structure that are inaccurate. In this study the implementation of 0°-90° strain gauges gave non-conservative results, which, in practice, could have lead to premature failures. The only scenario where 0°-90° gauges could be safely implemented for input load quantification is when positioned at points in the structure, experiencing pure bending or tension or a combination thereof that are far away from structural discontinuities, i.e. at the centre of a long beam.

The results obtained from the FESL analysis gave reason for some concern. When table 4.6 is considered, it becomes clear that the structural response as a whole is not quasi-static for the given input displacement. This is due to the deviation of the FESL values at points 8, 9 and 10 although positions 1, 2, 3, 4, 5, 6 and 7 showed good correlation with the static results as concerned to relative stress ratios. The reason for

such a variation remains unclear since the structure's boundary conditions were correct and the input signal's energy content was well beneath the first natural frequency of the structure. The integrity of the finite element model was ensured since excellent correlation between measurements and measured response was obtained as far as the static stresses and the first natural frequency of the structure are concerned.

It is thus clear that implementation of the FESL technique could present some difficulties, as was illustrated in section 4.3.4 when overly conservative life predictions were obtained. As already mentioned it is also possible that the predictions could be non-conservative. In view of the FESL analysis results, it is recommended that some further research or verification be done concerning the constraints of a quasi-static analysis. Among the questions that should be addressed are those that arose in this study like the requirements on input loading frequency content and relative stress ratios in a structure during dynamic excitation as compared to static loading. Furthermore it is recommended that in the event of a quasi-static analysis being performed in industry an additional strain gauge being applied on the most probable failure location, which should be determined from the finite element model with the FESL imposed on it. Although this is not always possible due to geometrical and logistic constraints, which actually formed part of the incentive for the development of the FESL technique) the application of such a gauge should verify the predicted stress response and also ensure reliable life prediction. Secondly it would serve as an indication of the validity of the FESL analysis on the specific structure.

The hot spot- and nominal stress fatigue life predictions gave very pleasing results if the actual obtained lives of the two failure locations on the structure are considered. The hot spot stress method as implemented in conjunction with the finite element method, however, gave extremely conservative results. As previously discussed, these conservative results are attributed to the early appearance of the N-LSR with implementation of course shell meshes, as opposed to the accepted position of the N-LSP as reported by the IIW, which forms the basis of the hot spot stress approach. The hot spot stress prediction, based on actual measurements gave far more realistic results, as can be seen from table 4.6. It is consequently concluded that the numerical application as prescribed by the IIW is effective and very conservative which, from a design point of view, is reassuring. Table 4.6 also indicates that the nominal stress prediction gave conservative results. The FESL prediction was very conservative, for reasons that could once again be attributed to the response of the structure, as discussed in section 4.3.4.

When the predicted lives are compared to the actual lives it is seen that in the case of the hot spot stress analysis, the actual fatigue life of the weld exceeded the predicted life by a factor of four while the nominal detail exceeded the predicted life by at least a factor of two, although failure was not reached. The question then immediately arises as to how the prediction can be claimed as accurate when a deviation of up to four times the predicted life exists? Firstly the nature of the S-N curve should be considered. As mentioned in the literature survey, the S-N curve stays but a curve fit through a collection of fatigue data with a huge amount of scatter due to the complex nature of welding fatigue. As Hobbacher (2003) put it: "The printed fatigue classes in tables of structural details and the clear and undoubted FAT values sometimes give rise to the illusion that these numbers are accurate". An idea of the magnitude of the

data scatter for a typical fatigue test can be formed when figure 1.12 is considered. It can clearly be seen that for a specific stress, the values for life lie within a scatter band and can differ with up to a factor of 5 on both sides of the mean (for the hot spot stress method). Hobbacher (2003) also illustrated scatter bands containing data that differed up to a factor of 10 on both sides of the mean, i.e. total differences of up to a factor 100 was typical for nominal stress curves. Taking into account the fact that the welding of the structure was of utmost quality, as well as the uncertainties introduced by the stochastic loading and linear damage accumulation procedure, a factor four and two deviation respectively (on the safe side) of fatigue life is considered acceptable.

In view of the above discussion it is concluded that the goals of the study was reached and that an effective, economic and conservative finite element meshing scheme and nominal stress extraction procedure was developed and successfully validated on a test structure subjected to stochastic loading such as could typically be expected in industry.

References

Atzori, B., Meneghetti, G. (2001). Fatigue strength of fillet welded structural steels: finite elements, strain gauges and reality. *International Journal of Fatigue*; 23: 713-721.

BS 7608. (1993). Code of practice for fatigue design and assessment of welded structures.

Conle, F.A., Chu, C.C. (1998). Fatigue analysis and the local stress-strain approach in complex vehicular structures. *International Journal of Fatigue*;19 (Suppl. 1): S317-23.

Conle, F.A., Mousseau, C.W. (1991). Using vehicle dynamics simulations and finite element results to generate fatigue life contours for chassis components. *International Journal of Fatigue*; 13 (3):195-205.

David, P.K., Sarkanit, S. (1997). Thickness effect on the fatigue strength of welded steel cruciforms. *International Journal of Fatigue*;19(1):311–6.

Dickens, J.M., Nakagawa, J.M.,Wittbrodt, M.J. (1997). A critique of mode acceleration and modal truncation augmentation methods for modal response analysis. *Computers & Structures*; 62:6: 985-998.

Doerk, O., Fricke, W. (2004). Fatigue analysis of fillet welds around stiffener and bracket toes. IIW doc. XIII-2034/XV-1170-04.

Doerk, O., Fricke, W., Weissenborn, C. (2003). Comparison of different calculation methods for structural stresses at welded joints. *International Journal of Fatigue*; 25: 359-369.

Dong, P. A. (2001). Structural stress definition and numerical implementation for the fatigue analysis of welded joints. *International Journal of Fatigue*;23:865-876.

Dong, P., Hong, J.K. (2004). The master S-N curve approach to fatigue of piping and vessel welds.IIW doc. XI-777-03. *Welding in the World*;.48, 1/2: 28-36.

Dong, P., Hong, J.K., Cao, Z. (2003). Stresses and stress intensities at notches: “anomalous crack growth” revisited. *International Journal of Fatigue*; 25: 811-825.

Dowling, E. (1999). Mechanical behavior of materials. Prentice-Hall.

ECCS, Technical committee 6. (1985). Recommendations for fatigue design of steel structures, first edition.

Fayard, J.L., Bignonnet, A., Dang Van K. (1996). Fatigue design criterion for welded structures. *Fatigue and Fracture of Engineering Materials and Structures*;19(6):723–9.

Fermér, M., Andréasson, M., Frodin, B. (1998). Fatigue life prediction of MAG-welded thin sheet structures. Volvo Car Corporation, SAE 982311.

Fermér, M., Svenson, H. (2001). Industrial Experiences of FE-based fatigue life predictions of welded automotive structures. Volvo Car Corporation. Fatigue and Fracture of Engineering Materials and Structures; 24; 489-500.

Fricke, W. Fatigue. (2003) Analyses of welded joints: state of development. *Marine Structures*;16:185-200.

Fricke, W., Paetzhold, H. (1995). Fatigue strength of scallops - an example for the application of nominal and local approaches. *Marine structures*;8:423-447.

Gere, M. (2001). Mechanics of materials, fifth edition. Brookes/Cole.

Hobbacher, A. (2003). Comparison of methods for fatigue analysis at an example of cruciform fillet welded joints. Metal structures-Design, Fabrication, Economy, Jarmai & Farkas (eds), ISBN 90-77017-75-5.

Hobbacher, A. (1996). Recommendations for fatigue strength of welded components. Cambridge; Abington Publishing.

Hobbacher, A. (2004). Recommendations for fatigue design of welded joints and components. IIW doc XIII-1965-03 / XV-1127-03.

Lazzarin, P., Tovo, R. (1998). A notch intensity factor approach to the stress analysis of welds. *Fatigue and Fracture of Engineering Materials and Structures*; 21(9):1089–104.

Li, X.Y., Partanen, T., Nykänen, T., Björk T. (2001). Finite element analysis of effect of geometry and load condition on fatigue strength of lap joint. *International Journal of Pressure Vessels and Piping*;78 :591-597.

Lie, S.T., Lan, S. (1998). A boundary element analysis of misaligned load-carrying cruciform welded joints. *International Journal of Fatigue*;20(6):433–9.

Mackerie, J. (2002). Finite element analysis and simulation of welding - an addendum: a bibliography (1996-2001). *Modeling Simul.Mater.Sci.Eng.*;10:295-318.

Mercer, I., Malton, G., Draper, J. (2003). The effect of user decisions on the accuracy of fatigue analyses from FEA. ABAQUS users' conference.

Niemi, E. (1995). Stress determination for fatigue analysis of welded components. IIS/IIW 1221-93. Cambridge, Abington Publishing.

Niemi, E. (2001). Structural stress approach to fatigue analysis of welded components- Designers guide - Final Draft. IIW Doc. XIII-1819-00.

Niemi, E., Marquis, G.B. (2003). Structural hot spot stress method for fatigue analysis of welded components. Metal structures-Design, Fabrication, Economy. Jarmai & Farkas (eds), ISBN 90-77017-75-5.

Partanan, T., Niemi, E. (1996). Hot spot stress approach to fatigue strength analysis of welded components: fatigue test data for steel plate thicknesses up to 10 mm. *Fatigue and Fracture of Engineering Materials and Structures*;19:709-22.

Petterson, G. (2002). Fatigue analysis of a welded component based on different methods. IIW doc. XIII-1949-02, *Welding in the World*; 46, 9/10: 41-51.

Poutiainen, I., Marquis, G. (2004). A single point structural stress assessment procedure for load carrying fillet welds. IIW docXIII-2012-04 XV-1174-04.

Radaj, D. (1996). Review of fatigue assessment of non-welded and welded structures based on local approaches. *International Journal of Fatigue*; 18,(3):153-170.

Radaj, D., Sonsino, C., Flade, D. (1998). Prediction of service fatigue strength of a welded tubular joint on the basis of the notch strain approach. *International Journal of Fatigue*;20(6):471-80.

Ryu, J.,Kim, H., Wang,S. (1997). A method of improving dynamic stress computation for fatigue life prediction of vehicle structures. SAE 971534.

Sanders,J.R., Tesar,D. (1978). The analytical and experimental investigation of vibration oscilations. ASME 78-DE-1.

Sarkani, S., Michaelov, G., Kihl, D. (2001). Stochastic fatigue damage accumulation in a T-welded joint accounting for residual stress fields. International *Journal of Fatigue*; 23:71-78.

Savaides, G., Vormwald, M. (2000). Hot spot stress evaluation of fatigue in welded structural connections supported by finite element analysis. *International Journal of Fatigue*; 22:85-91.

Shrikantan, S., Yerrapalli, S., Keshtkar, H. (2000). Durability design process for track body structures. *International. Journal of vehicle Design*; 23(1/2):94-108.

Taylor, D., Barret, N., Lucano, G. (2002). Some new methods for predicting fatigue in welded joints. *International Journal of Fatigue*;24:509-518.

Taylor, D. (1999). Geometrical effects in fatigue: a unifying theoretical model. *International Journal of Fatigue*; 21:413–20.

Teng, T., Fung, C., Chang P. (2002). Effect of weld geometry and residual stresses on fatigue in butt welded joints. *International journal of pressure vessels and piping*;79:467-482.

Tebbe, J.C., Mathers, M.D. (1995). Multiple load input sensitivity technique for finite element-based durability evaluation. SAE 951099.

Tovo, R., Lazzarin, P. (1999). Relationships between local and structural stress in the evaluation of the weld toe stress distribution. *International Journal of Fatigue*;21: 1063-1078.

Wannenburg, J. (1998). The applicability of static equivalent design criteria for fatigue design of dynamically loaded structures. Proceedings of the fifth international colloquium on ageing of materials and methods and methods for the assessment of lifetimes of engineering plants. Edited by Penny R.K., Chameleon press Ltd.

Van Tonder, F., Wannenburg, J., Heyns, P.S. (2006). Numerical verification of a proposed dynamic fatigue design methodology. *9th International congress on fatigue,* Atlanta, Georgia, May 2006.

Veltri, M., Bishop, N.W.M. (2003). Fatigue analysis of dynamically sensitive systems using FEA. Engineering Analyses and Design, Hutton Roof, Eglinton Road, Tilford, Farnham, Surrey, GU10 2DH, UK.

Xu, H. (1998). An introduction of a modal scaling technique: an alternative and supplement to quasi-static g loading technique with application in structural analysis. SAE 982810.